UNIVERSITÀ DELLA CALABRIA

UNIVERSITA' DELLA CALABRIA

Dipartimento di Farmacia e Scienze della Salute e della Nutrizione

Dottorato di Ricerca in

MEDICINA TRASLAZIONALE

CICLO XXXII

Chemical Modifications of Polyphenols for the Development of new Molecules and Functional Foods for the Treatment of Metabolic Disorders

Settore Scientifico Disciplinare CHIM/08

Coordinatore: Ch.mo Prof. Sebastiano Andò

Firma

Firma oscurata in base alle linee guida del Garante della privacy

Supervisore/Tutor: Ch.ma Dott.ssa Francesca Aiello

Firma

Firma oscurata in base alle linee guida del Garante della privacy

Dottorando: Dott. Gabriele Carullo

Firma

Firma oscurata in base alle linee guida del Garante della privacy

INDEX

	Pages
List of Abbreviations	**4**
Introduction	6
FOOD CHEMISTRY SECTION	**4**
Chapter 1: Wine and Grape Pomaces as source for the development of functional foods	8
Winemaking process and waste production	8
Materials & Methods	**10**
Chemicals	10
Preparation of the Arvino grape pomace extracts	10
Preparation of Mantonico, Pecorello and Sangiovese grape pomace extracts	11
Disposable phenolic groups by Folin–Ciocalteu procedure	11
Determination of total antioxidant activity	12
Determination of scavenging activity on DPPH radicals	12
Determination of scavenging effect on the ABTS radical cation	13
NMR analysis	13
Mass spectrometry analysis	14
Synthesis of pectin conjugates with **MSS**, **PSS**, **MBS**, **PBS**	14
Preparation of kefir	14
Cell culture	14
Measurement of trans-epithelial electric resistance	15
Paracellular Permeability Assay	16
Animals	16
Preparation of rat aortic rings	16
Effect of the samples on phenylephrine- and high K^+-induced contraction	17
Data analysis	17
Results and Discussion	17
Chemical characterization and vasoactivity of **LDC** samples	17
Characterization and vasoactivity of **MBS**, **PBS**, **MSS**, **PSS** and their pectin conjugates	21
Antioxidant performances of **LDC3** and **PSS** samples	26
Preparation and anti-inflammatory activity of a Sangiovese seed extract-fortified kefir	26
MEDICINAL CHEMISTRY SECTION	32
General chemical considerations	32
Chapter 2: Free Fatty Acid Receptors: T2DM and diabetic foot ulcer	33
Materials & Methods	33
INS-1 832/13 Cell culture	33
Insulin secretion detection	33
Computational details	33
HaCaT and THP-1 Cells culture	34
HaCaT cell viability and proliferation assay	35
Scratch wound healing assay	35
TGF-β production and MMP-9 release	35
Immunostimulatory activity	36
Preclinical experimental protocol	36
Statistical analysis	36
FFA1/GPR40: design, synthesis and biological evaluation of Quercetin-oleic acid hybrids	37
Results and Discussion	39
Chemistry	39
Experimental part	41
Docking simulations and functional evaluation in INS-1 832/13 cell line	42

Quercetin-3-oleate as a wound healing agent 46

FFA4/GPR120: design, synthesis and biological evaluation of Pinocembrin-fatty acid hybrids 49

Results and Discussion 50

Chemistry 50
Experimental part 50
Docking simulations and functional evaluation in HaCaT cell line 51

Chapter 3: Quercetin and Morin: semi-synthesis of new K_{Ca}1.1 and Ca_V1.2 channel modulators 55

Materials & Methods 55
Chemicals 55
Cell isolation procedure for $I_{Ca(L)}$ recordings 55
Cell isolation procedure for K_{Ca}1.1 current recordings 55
Whole-cell patch-clamp recordings 56
$I_{Ca(L)}$ and $I_{Ba(L)}$ recordings 56
K_{Ca}1.1 current recordings 57
Solutions for $I_{Ca(L)}$ and $I_{Ba(L)}$ recordings 57
Solutions for K_{Ca}1.1 current recordings 58
Solutions for functional experiments 58
Statistical Analysis 58
Molecular docking simulation 59

Quercetin: a multifaceted tool for the development of new suitable anti-hypertensive agents 60

Results and Discussion 62

Design of new hybrids and docking simulations 62
Chemistry 64
Experimental part 66
Functional evaluation in KCl- and phenylephrine-induced contraction, K_{Ca}1.1 and Ca_V1.2 channel currents 68

Morin: a suitable scaffold for the investigation of new anti-hypertensive agents 71

Results and Discussion 72

Chemistry 72
Experimental part 73
Functional evaluation in KCl- and phenylephrine-induced contraction, K_{Ca}1.1 and Ca_V1.2 channel currents 75

Conclusions 77

References 79

APPENDIX I 86

List of Abbreviations

$(NH_4)_2MoO_4$: ammonium molybdate
12-HHT: 12(*S*)-hydroxyheptadeca-5*Z*,8*E*,10*E*-trienoic acid
ABTS: 2,2'-azino-bis(3-ethylbenzothiazoline-6-sulfonic acid)
AH7614: 4-Methyl-N-9H-xanthen-9-yl-benzenesulfonamide
BLT2: leukotriene B4 receptor 2
$CaCl_2 \times 2H_2O$: calcium chloride dihydrate
$Ca_v1.2$: voltage-dependent L-type calcium channel subunit alpha-1D
CH_3CN: acetonitrile
$CHCl_3$: chloroform
CMC: 1- cyclohexyl-3-(2-morpholinoethyl)carbodiimide
CO_2: carbon dioxide
DCC: *N,N'*-dicyclohexylcarbodiimide
DCM: dichloromethane
DHA: docosahexaenoic acid
DMAP: 4-dimethylaminopyridine
DMEM: Dulbecco's modified Eagle's medium
DMF: *N*,*N*-dimethylformammide
DMSO: dimethyl sulfoxide
DPPH: 2,2-diphenyl-1-picrylhydrazyl
EC: European Community
EGTA: ethylene glycol-bis(β-aminoethyl ether)-*N*,*N*,*N*′,*N*′-tetraacetic acid
eNOS: endothelial nitric oxide synthase
Et_2O: diethyl ether
Et_3N: triethylamine
EtOAc: ethyl acetate
FBS: fetal bovine serum
FFA1: free fatty acid receptor 1
FFA4: free fatty acid receptor 4
FFAs: free fatty acids
GABA: γ-amino butyric acid
GIP: gastric inhibitory polipeptide
GLP-1: glucagon-like peptide 1
GPR120: G-protein-coupled receptor 120
GPR35: G-protein-coupled receptor 35
GPR39: G-protein-coupled receptor 39
GPR40: G-protein-coupled receptor 40
H_2O_2: hydrogen peroxide
H_2S: hydrogen sulfide
H_2SO_4: sulphuric acid
HA: hyaluronic acid
HBSS: Hanks' Balanced Salt solution
HCl: hydrochloric acid
HEPES: 4-(2-hydroxyethyl)-1-piperazineethanesulfonic acid
HOBt: *N*-hydroxybenzotriazole
IC_{50}: inhibitory concentration 50
$K_{Ca}1.1$: calcium-activated potassium channel subunit alpha-1
KCl: potassium chloride
KH_2PO_4: potassium dihydrogen phosphate
LAB: kefir lactic acid bacteria
LCTM: LPS-conditioned THP-1 medium
LDL: low density lipoprotein
L-NAME: Nω-nitro-L-arginine methyl ester
LPS: lipopolysaccharide
MAPK: mitogen-activated protein kinase
MeOH: methanol
$MgSO_4$: magnesium sulfate
$MgSO_4 \times 7H_2O$: magnesium sulfate heptahydrate
MMP-9: matrix metalloproteinase 9
MS^2: tandem mass spectrometry
m-TORC2: mammalian rapamycin complex 2
Na-HEPES: 4-(2-hydroxyethyl)-1-piperazineethanesulfonic acid sodium salt
Na_2CO_3: sodium carbonate

Na_2EDTA: disodium ethylenediaminetetraacetate dihydrate, disodium salt
Na_2SO_4: sodium sulphate anydhrous
Na_3PO_4: trisodium phosphate
NaCl: sodium chloride
$NaHCO_3$: sodium hydrogen carbonate
NF-κB: nuclear factor kappa B
NO: nitric oxide
O_2: molecular oxygen
OA: oleic acid
PKA: protein kinase A
PKC: protein kinase C
PKG: protein kinase G
PPL: Pancreatic Porcine Lipase Type II, 100-500 units/mg protein (using olive oil (30 min incubation)), 30-90 units/mg protein (using triacetin)
PUFAs: polyunsaturated fatty acids
Q3G: Quercetin-3-glucoside
RDB: rings and/or double bonds
RPMI: Roswell Park Memorial Institute 1640
rt: room temperature
$SOCl_2$: thionyl chloride
T2DM: type II diabetes mellitus
TEER: trans-epithelial electric resistance
TGF-β1: transforming growth factor beta 1
TNF-α: tumor necrosis factor alpha
TRPV1: transient receptor potential cation channel subfamily V member 1
TRPV4: transient receptor potential cation channel subfamily V member 4
TUG-891: 3-(4-((4-Fluoro-4-methyl-[1,1-biphenyl]-2-yl)methoxy)phenyl)-propanoic acid, 4-[(4-Fluoro-4′-methyl[1,1′-biphenyl]-2-yl)methoxy]-benzenepropanoic acid
UHT: ultra-high temperature
VEGF: vascular endothelial growth factor

"The incredible discoveries of chemistry strongly express the magic of nature"

(Johann Wolfgang Goethe)

Introduction

An overview about metabolic disorders and aim of the PhD thesis

Metabolic syndrome represents the most common contemporary human affliction. It was defined as the presence of insulin resistance and/or T2DM or glucose intolerance or impaired fasting glycemia combined with two or more of the following additional factors: hypertension, dyslipidemia, obesity and microalbuminuria *(Katsimardou et al., 2019)*. Nutrition and screening programs for high-risk individuals have been opened over the world. The prevalence and incidence of these disorders, in particular T2DM and hypertension, have been well defined in large population-based studies *(Golden et al., 2009)*. Hypertension plays a key role, because it is the main risk cause linked with coronary, ischemic, and rheumatic heart diseases, and other cardiovascular complications. T2DM (formerly known as non-insulin dependent) is the most common form of diabetes characterized by hyperglycemia, insulin resistance, and relative insulin deficiency. It results from interaction amongst alimentary, environmental and behavioural risk factors *(Olokoba et al., 2012)*. Hypertension and T2DM are considered alimentary diseases because they appear, in the most cases, as consequence of a not correct lifestyle. In particular, the use of high amounts of salt in the diet is responsible of hypertension, which in turn is able to promote cardiovascular complications, which culminate in atherosclerosis or heart failure. Thereafter, T2DM is caused by junk food, fast-food products but also by a non-correct use of fats in the diet; in fact, people usually prefer animal-derived fats such as butter or lard, limiting the use of sunflower and olive oils. The last one, in particular, at the dose of 10 g/die works as antidiabetic agent, by reducing gastrointestinal levels of glucose similarly to the natural hormones incretins *(Perez-Martinez et al., 2011)*. In this scenario, in addition to the classic anti-diabetic (sodium glucose co-transporter 2 inhibitors, glucokinase activators, fibroblast growth factor 21 receptor agonists, GLP-1 agonists, biguanides and sulphanylureas) and antihypertensive (thiazides, beta-blockers, calcium channel blockers, angiotensin-converting enzyme inhibitors, angiotensin II receptor blockers, and alpha-blockers) therapies *(Wright et al., 2018)*, several plant extracts, natural products or food-derived compounds, emerged as new interesting tools for the discovery of new metabolism-associated diseases modulators *(Cao et al., 2019; Tian et al., 2020)*. As a consequence, this PhD thesis aims to discover new functional food derived from grape waste industry as potential anti-hypertensive tools, able to promote NO release from the endothelium of rat aorta rings (used as experimental

in vitro model), but also a fortified fermented beverage such kefir, able to reduce inflammatory stimuli in colorectal Caco-2 cell line. From the medicinal chemist point of view, polyphenols have been used as template for the development of new bioactive molecules; in particular Quercetin was used as template for:

- the synthesis of new insulin secretion modulators also able to promote wound healing in keratinocytes targeting FFA1/GPR40;
- the development of selective $K_{Ca}1.1$ ligands as new potential anti-hypertensive agents;
- Pinocembrin was hybridized with fatty acids for the optimization of new wound healing agents targeting FFA4/GPR120;
- Morin was used for the synthesis of selective $Ca_v1.2$ channel blockers as new potential anti-hypertensive agents.

Chapter 1

Wine and Grape Pomaces as source for the development of functional foods

Winemaking process and waste production

Winemaking is the process that leads from grapes to the wine by pressing and fermentation. The first phase of winemaking consists of alcoholic fermentation, a process in which the saccharomyces yeasts transform the sugar contained in the must into alcohol, carbon dioxide and secondary elements such as glycerin, methyl alcohol, acetic acid, succinic acid and higher alcohols *(Miller and Block, 2020)*. There are two main winemaking methods:

red winemaking: it is the process that allows the production of red wines. Following the destemming (separation of the wood stalk from the must to avoid the release of tannins which would give the wine a bitter taste) the must is pumped into the fermentation tanks which can be in steel, wood, fiberglass or cement, open or closed and whether or not equipped with moving parts. The skins remain to macerate in the must for times that can vary from 4-6 days up to 20-30 days. During fermentation, the pomace tends to rise to the surface forming the so-called cap which must be frequently broken to prevent an oxidation and acidification process from starting up in contact with the air, which would ruin the must. Following fermentation, the racking phase begins, that is, the separation of the wine from the marc;

white winemaking: made from white or red grapes: the grapes are gently pressed with horizontal presses. The must obtained is fermented by removing skins, stalks and grape seeds; then the clarification, decantation, centrifugation or filtration phases follow one another. Then the actual fermentation begins which is started with the addition of selected yeasts at a temperature of 18-20 °C.

Following alcoholic fermentation, malolactic fermentation is often triggered, which consists in the natural deacidification of the wine: in this phase the bacteria transform malic acid into lactic acid, with a much less strong flavor, thus promoting the lowering of the acidity of the product. In this way, the wine is considerably enriched with aromas and flavors *(Boulton et al., 2013)*.

According to Decree No. 7407 of August 4, 2010 - Amendments to Article 5 of Ministerial Decree November 27, 2008, no. 5396, concerning "Implementing provisions of regulations (EC) no. 479/2008 of the Council and n.

555/2008 of the Commission as regards the application of the distillation measure of the by-products of winemaking ":

1. Producers who, in application of articles 22 and following of EC regulation no. 555/2008 of the Commission, are required to withdraw the by-products of winemaking, fulfill their obligation with the delivery, in whole or in part, to the distillery or through the withdrawal under control for the following alternative uses:

a) Direct agronomic use, by distributing the by-products on agricultural land, within the limit of 3,000 kg per hectare of agricultural area resulting in the farm file, on condition of an express commitment to use the by-products for agronomic use.

b) Indirect agronomic use, through the use of by-products for the preparation of fertilizers.

c) Energy use, through the use of by-products such as biomass for the production of biogas or to power plants for the production of energy, also used in conjunction with other energy sources intended for the production of biogas or combustible biomass.

d) Pharmaceutical use, through the use of by-products for the preparation of drugs.

e) Cosmetic use, through the use of by-products for the preparation of cosmetics.

2. The pomace intended for the extraction of enocyanine or for the production of agri-food products referred to in Annex 2 to this decree, are considered to be used for alternative use. The use of pomace for the production of further agri-food products is authorized by the General Directorate of Community and international market policies upon request from the Regions and autonomous Provinces.

3. The by-products obtained from the transformation of wine grapes into products other than must and wine are subject to controlled withdrawal; in this case, art. 4 of this decree.

According to this decree, wine industry harvests millions of tons of residues after fermentation whose storage, transformation, and/or elimination pose pertinent financial and ecological problems *(Beres et al., 2017)*. Grape by-products are generally used for animal feeding, soil improver or biogas production *(Lucarini et al., 2018)*. The presence of bioactive compounds in grape waste, in particular polyphenols *(Fontana et al., 2013)*, which are well-known health promoting agents, mainly for their antioxidant and antimicrobial properties, highlights the possibility of its exploitation as a source of valuable molecules to be used as functional ingredients for the pharmaceutical, cosmetic and food industries *(Yu and Ahmedna, 2013)*. In this field, grape pomaces deserve a careful evaluation because of the presence of polyphenols. In fact, polyphenols modulate cellular and molecular mechanisms that drive anti-inflammatory, antioxidant, and hypotensive responses. In this context, various flavonoids exhibited

direct vasodilating activities in isolated arteries. Quercetin and kaempferol, for example, showed a not yet fully understood, endothelium-dependent vasodilation that does not characterize, however, structurally similar compounds. As a consequence, it is worth to highlight that not only wine isolated components, but also pomace extracts and wine can induce vasorelaxation. Interestingly, synergistic effects characterize these mixtures of biologically active agents also. Therefore, a rationale pomace management could lead to a valuable dietary approach to fight cardiovascular diseases *(Fusi et al., 2003; Jiménez et al., 2012; Lodi et al., 2009; Suri et al., 2010)*. The aim of this section was to:

1) investigate the vasoactive properties of wine, must and pomace (seeds and skins) derived from the Calabrian autochtonous Magliocco Dolce *cv.* (Arvino), not investigated yet;
2) investigate the vasoactive properties of pomace (seeds and skins) derived from the Calabrian autochtonous white berries Mantonico and Pecorello *cv.*, also embedded in a polymeric matrix;
3) evaluate the anti-inflammatory activity of a kefir enriched with Sangiovese seed extract.

Materials & Methods

Chemicals

All reagents used in this study were purchased from Merck (Milan, Italy) and VWR International (Milan, Italy) and, unless specified otherwise, were of analytical grade or higher. Deuterated solvents and standards for NMR analyses were purchased from Sigma-Aldrich (St. Louis, MO, USA). Grape pomaces, wine and must were furnished by Dr. Paolo Chirillo, Le Moire srl, Ctr. Strivillati, 88040 Motta Santa Lucia (Catanzaro, Italy), info@lemoire.it . Phenylephrine, acetylcholine, sodium nitroprusside, pinacidil, L-NAME, capsazepine, and nifedipine were purchased from Sigma Chemical Co. (Milan, Italy). Phenylephrine was solubilized in 0.1 M HCl; L-NAME, acetylcholine, and sodium nitroprusside in distilled water; nifedipine in ethanol; capsazepine and pinacidil in DMSO. Kefir grains were obtained from Burumart Commerce S.L. (Arrasate, Gipuzkoa, Spain).

Preparation of the Arvino grape pomace extracts

The by-products of the winemaking process were obtained after the red grapes had been pressed. Samples were milled and stored in polyethylene film bags packed under vacuum and stored at -20 °C until used. Must derives from the red winemaking after 10 days. Seeds and skins were manually separated until extraction. The extracts were prepared using a mixture of 40% ethanol and 60% distilled water. Extraction was done with a solute/solvent

ratio of 1:50 (m/v). The suspensions were shaken in a rotary shaker for 24 h at 100 rpm and at a temperature of 25 °C. After this period of time the mixture was centrifuged at 3500g for 25 min. Ethanol was eliminated with a rotary evaporator and the aqueous solution was freeze-dried and stored at -20°C until use. Wine and must for the production of red wine were only evaporated to eliminate ethanol, centrifuged, filtered and freeze-dried. The obtained samples were named: **LDC1** (skin extract after rosé winemaking process), **LDC2** (skin extract after red winemaking process), **LDC3** (freeze-dried red wine), **LDC4** (freeze-dried red must), **LDC5** (seed extract after rosé winemaking), **LDC6** (seed extract after red winemaking process) *(Gonçalves et al., 2017)*.

Preparation of Mantonico, Pecorello and Sangiovese grape pomace extracts

Grape pomaces derived from Mantonico, Pecorello and Sangiovese winemaking processes were manually separated and extracted by using hydro-alcoholic mixtures in an ultrasound assisted extraction, performed using the ultrasound-bath Branson model 3800-CPXH (Milan, Italy) at 30°C (10 cycles/sec) for 15 min, at an ultrasonic frequency of 40 kHz following the same procedure for both skins and seeds. Starting from 30 g of raw material, were added 200 mL of ethanol/water (50/50 v/v) (pH=2), the mixture was filtered out and concentrated. The extracts were dried under vacuum and stored at 4°C until analysis. Each extraction was performed in triplicate and data expressed as means (±SD) *(Carrera et al., 2012)*. The obtained samples were named: **MBS** (Mantonico skins), **PBS** (Pecorello skins), **MSS** (Mantonico seeds) **PSS** (Pecorello seeds), **sgnbs** (Sangiovese skins), **sgnss** (Sangiovese seeds).

Disposable phenolic groups by Folin–Ciocalteu procedure

6.0 mL of hydroalcoholic solution (50/50 v/v) of each matrix was placed in a volumetric flask (10 mL) and then Folin-Ciocalteu reagent (1.0 mL) was added and the contents of flask were mixed thoroughly. After 3 min, 3.0 mL of Na_2CO_3 (2%) were added, and then the mixture was allowed to stand for 2 h with intermittent shaking. The absorbance was measured at 760 nm against a control prepared using hydroalcoholic mixture (50/50 v/v) under the same reaction conditions. The amount of total phenolic groups in the extracts was expressed as gallic acid equivalent concentrations by using the equation obtained from the calibration curve of the antioxidant molecule. This one was recorded by employing five different gallic acid standard solutions. 0.5 mL of each solution were added to the Folin-Ciocalteu system to raise the final concentration of 8.0, 16.0, 24.0, 32.0, and 40.0 µM, respectively. After 2 h, the absorbance of the solutions was measured to record the calibration curve and the correlation coefficient (R^2), slope and intercept of the regression equation obtained were calculated by the method

of least square. For conjugates and jam, disposable phenolic groups were expressed as gallic acid equivalent per grams of polymers and food matrix, respectively. Each extraction was performed in triplicate and data expressed as means (±SD). UV-Vis absorption spectra were recorded with a Jasco V-530 UV/Vis spectrometer (Jasco, Tokio, Japan) *(Restuccia et al., 2011)*.

Determination of total antioxidant activity

0.3 mL of hydro-alcoholic solution (50/50 v/v) of each matrix were mixed with 1.2 mL of reagent solution (0.6 M H_2SO_4, 28.0 M Na_3PO_4, and 4.0 M $(NH_4)_2MoO_4$). The reaction mixture was incubated at 95°C for 150 min and after cooling to room temperature, the absorbance of the mixture was measured at 695 nm against a control prepared in the same conditions. Measurement was carried out in triplicate and data expressed as means (±SD). The total antioxidant activity of polymeric materials was expressed as catechin equivalent concentration. By using five different antioxidant standard solutions, a calibration curve was recorded. A volume of 0.3 mL of each solution was mixed with 1.2 mL of phosphomolybdate reagent solution to obtain the final concentrations of 8.0, 16.0, 24.0, 32.0, and 40.0 μM, respectively. After 150 min of incubation at 95°C, the solutions were analysed by using a UV-Vis spectrophotometer, and the correlation coefficient (R^2), slope, and intercept of the regression equation obtained by the method of least-squares were calculated. For conjugates and jam, total antioxidant activities were expressed as catechin equivalent per grams of polymers and food matrix, respectively. Each extraction was performed in triplicate and data expressed as means (±SD) *(Cirillo et al., 2012)*.

Determination of scavenging activity on DPPH radicals

1.0 mL of hydro-alcoholic solution (50/50 v/v) of each conjugates, peel, seed and jam extracts was placed in a volumetric flask (10 mL) and then 4.0 ml of hydro-alcoholic solution (50/50 v/v) and 5.0 mL of ethanol solution of DPPH (200 μM) were added, obtaining a solution of DPPH with a final concentration of 100 μM. The sample was incubated in a water bath at 25°C and, after 24 h, the absorbance of the remaining DPPH was determined colorimetrically at 517 nm. The scavenging activity of the tested matrices was measured as the decrease in absorbance of the DPPH and it was expressed as percent inhibition of DPPH radicals calculated according the following equation (1):

$$inhibition\% = \frac{A_0 - A_1}{A_0} \times 100 \qquad (1)$$

where A_0 is the absorbance of a standard that was prepared in the same conditions, but without any polymers, and A_1 is the absorbance of polymeric samples. Each measurement was carried out in triplicate and data expressed as means (±SD) *(Spizzirri et al., 2011)*.

Determination of scavenging effect on the ABTS radical cation

ABTS was dissolved in water at a 7.0 mM concentration. ABTS radical cation ($ABTS^{\cdot+}$) was produced by reacting ABTS stock solution with 2.45 mM potassium persulfate (final concentration) and allowing the mixture to stand in the dark at room temperature for 12-16 h before use. Because ABTS and potassium persulfate react at a ratio of 1:0.5, this leads to an incomplete oxidation of the ABTS. Oxidation of the ABTS started immediately, but the absorbance was not maximal and stable until more than 6 hours. Finally, the concentration of the resulting $ABTS^{\cdot+}$ solution was adjusted to an absorbance of 0.970±0.020 at 734 nm. The radical was stable in this form for more than two days when stored in the dark at room temperature. In order to evaluate the scavenging effect of extracts, conjugates and jams, 500 µL of hydro-alcoholic solution (50:50 v/v) on each matrix were mixed with 2.0 mL of the ABTS radical solution. The obtained mixture was incubated in a water bath at 37°C and protected from light for 5 min. The decrease of absorbance at 734 nm was measured at the endpoint of 5 min. The antioxidant activity was expressed as a percentage of scavenging activity on the ABTS radical according to equation (1). All samples were assayed in triplicate and data expressed as means (±SD) *(Restuccia et al., 2017)*.

NMR analysis

Aliquots of all the samples were analyzed by NMR spectroscopy in order to establish their chemical composition. Specifically, the assignment of the resonances was achieved by analyzing ^1H characteristics and cross-correlated signals in 2D ^1H-^1H TOCSY spectra and by comparison with literature data. Quantification of the recognized compounds was completed by comparison of the signal integral with the reference one, and quantities were expressed in mg of compound normalized for the aliquot weight expressed in g. Each dry aliquot was dissolved in 0.6 mL of D_2O:CD_3OD (2:1 ratio) containing 3-(trimethylsilyl)-propionic-2,2,3,3-d_4 acid sodium salt 2 mM as chemical shift and concentration reference. All spectra were recorded at 298 K on a Bruker AVANCE III spectrometer operating at the proton frequency of 400.13 MHz and equipped with a Bruker multinuclear z-gradient inverse probehead. ^1H spectra were acquired employing the presat pulse sequence for solvent suppression with 128 transients, a spectral width of 6000 Hz and 64K data points for an acquisition time of 5.5 s. The recycle delay was set to 9.5 s in order to achieve complete resonance relaxation between successive scansions. ^1H-^1H TOCSY

experiments were acquired with spectral width of 6000 Hz in both dimensions, a data matrix of 8K × 256 points, mixing time of 110 ms and relaxation delay of 2s *(Sciubba et al., 2014)*.

Mass spectrometry analysis

The samples were dissolved in methanol and injected (flow rate 5 μL min^{-1}) in the electrospray source of a LCQ DECA ion trap (ThermoFinnigan, Bremen, D) and a Orbitrap Q Exactive Plus (Thermo Fisher) at resolution of 30 000 and 140 000 FWHM@m/z 200, in positive and negative ion mode. MS product ion spectra has been resolved in the ion trap with helium as collision gas, and higher energy collisional dissociation (HCD) MS/MS spectra in the Orbitrap Q Exactive Plus by using nitrogen as collision gas at collision energy 18-30% arbitrary units. Phenol-Explorer 3.5 (French National Institute for Agricultural Research) and ChemSpider (Royal Society of Chemistry) have been used as tools for compounds identification *(Giorgetti et al., 2018)*.

Synthesis of pectin conjugates with **MSS**, **PSS**, **MBS**, **PBS**

In a 50 mL glass flask, 500 mg of esterified pectin (55-70%) from citrus fruit were dissolved in 50 mL of H_2O, then 1.0 mL of H_2O_2 5.0 M (5.0 mmol) and 0.25 g ascorbic acid (1.4 mmol) were added and the mixture was maintained at 25°C under atmospheric air. After 2 h, an amount of extract (**MSS**, **PSS**, **MBS**, **PBS**) corresponding to 0.150 mg of gallic acid equivalent concentrations was added to the solution. After 24 h, the solution was introduced into dialysis tubes and dipped into a glass vessel containing hydroalcoholic solution (50:50 v/v) at 20°C for 48 h with eight changes of water. After the reaction time, the mixture were dialyzed by using dalysis membranes of 6-27/32" Medicell International LTD (MWCO: 12-14000 Da). Purified polymers (named **MSSpec**, **PSSpec**, **MBSpec**, **PBSpec**) were checked to be free of unreacted antioxidant and any other compounds by LC analysis of the washing medium. LC analysis was performed on a Knauer (Asi Advanced Scientific Instruments, Berlin, Germany) system equipped with two pumps Smartiline Pump 1000, a Rheodyne injection valve (20 μL) and a photodiode array detector equipped with a semi-microcell. The purified solution was frozen and dried with a freeze drier to afford a vaporous solid. Freeze drier Micro Modulyo, Edwards was employed.

Preparation of kefir

10 grams of kefir grains (Kefiralia) were added in a glass flask at room temperature, containing 50 mL of UHT skimmed milk. The container was closed non-hermetically to overcome the production of CO_2 and was incubated at 20-25 °C for 24 h with or without extracts addition. The kefir grains obtained (**Kwht**) were weighted and the

pH value measured by using the pH 211 Microprocessor pH Meter (HANNA instruments). The enriched kefir (**Ksgn**) was obtained mixing 10 mg of the **sgnss** with 10 mL of **Kwht** in the same experimental conditions.

Cell culture

Caco-2 cells were used as a stable *in vitro* model for the intestinal epithelium *(Sambuy et al., 2005)*. Cells were cultured in 75 cm^2 cell culture flask (Sarstedt, Italy) in DMEM supplemented with 10% FBS, 1% glutamine and 1% penicillin/streptomycin antibiotic (Sigma-Aldrich, Italy) *(Cocetta et al., 2019)*. THP-1 monocytes from the European Collection of Authenticated Cell Cultures were purchased from Sigma-Aldrich (Italy) and cultured in 75 cm^2 cell culture flask in RPMI supplemented with 10% fetal bovine serum (FBS), 1% glutamine, 1% penicillin/streptomycin antibiotic and 0.05 mM 2-mercaptoethanol (Sigma-Aldrich, Italy). For the inflammatory model, THP-1 cells ($1x10^6$/mL) were seeded in 75 cm^2 cell culture flask in HBSS with 10 mM HEPES and 10 mM D-glucose (pH = 7.4) and incubated with 250 ng/mL LPS from *Salmonella enteridis* (Sigma-Aldrich, Italy) for 24 hours. The culture medium was then collected and centrifuged and the supernatant was used for the experiments. Untreated cells medium was used as control. Cells were maintained under a humidified atmosphere of 5% CO_2, at 37 °C.

Measurement of trans-epithelial electric resistance

The efficiency of the barrier functions was evaluated by measuring TEER using a voltmeter. Caco-2 cells ($8x10^5$) were placed in transparent polyester membrane cell culture inserts with 0.4 µm pore size (Sarstedt) *(Governa et al., 2018)*. Culture medium was replaced every other day. The integrity of the cell monolayers was monitored by measuring the TEER of the monolayer from day 14^{th} to day 21^{st} after seeding. When a stable value was reached, a pre-treatment of 24 hours was done adding **Kwht** and **Ksgn** in the apical chamber at different concentrations (10, 1 and 0.1 µg/mL) in appropriate wells and TEER was measured after 0,4, 8 and 24 hours. TEER measurements were performed in HBSS with 10 mM Hepes and 10 mM D-glucose (pH = 7.4), after an equilibration period at room temperature *(Vidau et al., 2009)*. Only cells with TEER value within 360 - 500 Ω x cm^2 were used for the experiments *(Hubatsch et al., 2007)*. After 24 hours of pre-treatment, the basal chamber medium was replaced with LPS-stimulated THP-1 medium and TEER was measured after 0, 4, 8 and 24 h. Millicell® ERS meter, Millipore Corporation (Bedford, MA) connected to a pair of chopstick electrodes was inserted in the apical and basolateral chambers. TEER was expressed as percentage of resistance, normalized to initial value.

Paracellular Permeability Assay

Phenol red flux across Caco-2 cell monolayers was used as a measure of paracellular permeability. At the end of the TEER experiment, the apical medium was replaced with a 500 mM solution of phenol red (Sigma-Aldrich, Italy) in HBSS and the basolateral medium was replaced with fresh HBSS. After 60 minutes of incubation at 37 °C, 100 µL was collected from the basolateral chamber and added to 10 µL of 1N NaOH in 96 multiwell plates. Phenol red leakage was measured using a SAFAS MP96 spectrophotometer (Safas, Principality of Monaco) by recording the absorbance at 540 nm, and quantified according to a calibration curve obtained with serial dilutions (500 - 0.5 mM) of phenol red solution in HBSS *(Gujral et al., 2015)*.

Animals

All animal care and experimental protocols performed in the present study were in strict compliance with the European Union Guidelines for the Care and the Use of Laboratory Animals (European Union Directive 2010/63/EU) and were also approved by the Animal Care and Ethics Committee of the University of Siena and Italian Department of Health (666/2015-PR).

Preparation of rat aortic rings

Male Wistar rats, weighing 250-400 g, obtained from Charles River Italia (Calco, Italy), were anaesthetized with a gas mixture of 4% isoflurane and O_2 by using Fluovac® (Harvard Apparatus, Holliston, Massachusetts, USA), decapitated and exsanguinated. Thoracic aorta was immediately removed and gently cleaned of adipose and connective tissues. Aorta rings (2.5-3.0-mm width), either endothelium-intact or -deprived, were mounted horizontally between two parallel L-shaped stainless steel hooks, one of which connected to an isometric transducer. Rings were allowed to equilibrate for 60 min in a modified Krebs-Henseleit solution (KHS; composition in mM: NaCl 118; KCl 4.75; KH_2PO_4 1.19; $MgSO_4 \times 7H_2O$ 1.19; $NaHCO_3$ 25; glucose 11.5; $CaCl_2 \times 2H_2O$ 2.5; gassed with a 95% O_2/5% CO_2 gas mixture to create a pH of 7.4) under a passive tension of 1 g. Isometric tension was recorded using a digital PowerLab data acquisition system (PowerLab 8/30; ADInstruments) and analyzed by using LabChart 7.3.7 Pro (PowerLab; ADInstruments). Rings pre-contracted with 0.3 µM phenylephrine were tested for the presence of a functional or dysfunctional endothelium as indicated by a ≥75% or ≤10% acetylcholine-induced relaxation, respectively *(Fusi et al., 2016a; Fusi et al., 2018)*.

Effect of the samples on phenylephrine- and high K^+-induced contraction

Rings were pre-contracted by either 0.3 µM phenylephrine or 20-30 mM KCl. Once the plateau was achieved, sample solutions were added cumulatively. In some experiments, preparations were pre-incubated with either 100 µM L-NAME (eNOS inhibitor) for 30 min, or with 5 µM capsazepine (a TRPV1 channel antagonist) for 20 min. Then, phenylephrine was added to the organ bath to elicit contraction and the effects of the extracts assessed always in the presence of the inhibitor or antagonist. At the end of the experimental protocols, the NO-donor sodium nitroprusside (100 µM) alone (phenylephrine-pre-contracted rings) or the $Ca_V1.2$ channel blocker nifedipine (1 µM) followed by sodium nitroprusside (KCl-pre-contracted rings) were added to test the functional integrity of smooth muscle. The induced relaxation was calculated as a percentage of the contraction induced by either 0.3 µM phenylephrine or 20-30 mM KCl (taken as 100%) *(Fusi et al., 2016b)*.

Data analysis

Graghpad Prism version 5.04 (GraphPad Software Inc., San Diego, CA, USA) was used to analyze the vasoactivity data. Data are reported as mean ± SEM; n, indicated in parentheses, is the number of rings isolated from at least three independent animals. Statistical analysis performed were either one-way ANOVA followed by Dunnett's post-hoc test, or unpaired Student's t-test (two tailed) using Graghpad Prism software: $P<0.05$ was considered significant. Where possible, nonlinear regression analysis was performed to calculate the IC_{50} value.

Results and Discussion

Chemical characterization and vasoactivity of **LDC** *samples*

The different **LDC** samples contained flexible amounts of amino acids, organic acids, carbohydrates, and flavonoids. **LDC1**, in particular, contained amino acids such as alanine and GABA, organic acids (i.e., quinic and malic acids), glucose and traces of glycosylated flavonoids. **LDC2** precisely presented a wide spectrum of amino and organic acids with low traces of catechins and flavonoids. To the point, **LDC3** comprised a huge amount of GABA, gallic acid, and flavonoids. **LDC4** looked like rich in amino acids and glucose, whereas entirely lacking of glycosylated flavonoids and catechin. **LDC5** and **LDC6** showed a higher content of polyphenols such as catechin and gallic acid. The relative amounts of substances contained appeared in Table 1 (the corresponding assignments and NMR spectra are reported in Supplementary Material).

Considering the vasoactivity, in rings with an intact endothelium, all **LDC** samples excluding the must **LDC4** triggered a concentration-dependent relaxation of phenylephrine-induced contraction. E_{max} values were

58.1±12.1% (1 mg/mL **LDC1**, n=5), 65.8±5.8% (0.3 mg/mL **LDC2**, n=7), 80.6±5.3% (0.1 mg/mL **LDC3**, n=6), 79.8±3.6% (10 µg/mL **LDC5**, n=6), and 76.6±5.1% (10 µg/mL **LDC6**, n=7), (Figure 1 A-F).

Table 1. Quantitative analysis of **LDC** samples by NMR spectroscopy

	Molecule	Amount (µmol/g)					
		LDC1	LDC2	LDC3	LDC4	LDC5	LDC6
Aminoacids	Isoleucine	-	1.28 ± 0.04	-	3.56 ± 0.11	-	7.85 ± 0.24
	Valine	-	1.92 ± 0.06	-	5.63 ± 0.17	-	11.40 ± 0.34
	Alanine	22.92 ± 0.69	11.60 ± 0.35	30.90 ± 0.93	26.37 ± 0.79	30.11 ± 0.90	23.62 ± 0.71
	GABA	59.77 ± 1.79	3.84 ± 0.12	134.24 ± 4.03	21.33 ± 0.64	-	-
	Glutamate	-	15.12 ± 0.45	-	-	-	-
	Glutamine	-	17.04 ± 0.51	-	-	-	-
	Tyrosine	-	-	-	1.67 ± 0.05	-	-
	Phenylalanine	-	1.68 ± 0.05	-	2.67 ± 0.08	-	10.53 ± 0.32
	Triptophan	-	1.92 ± 0.06	-	5.78 ± 0.17	-	9.51 ± 0.29
Organic acids	Lactic acid	-	14.08 ± 0.42	42.51 ± 1.28	14.37 ± 0.43	-	-
	Quinic acid	104.92 ± 3.15	66.00 ± 1.98	869.41 ± 26.08	285.33 ± 8.56	-	-
	Malic acid	369.92 ± 11.10	93.60 ± 2.81	896.94 ± 26.91	430.00 ± 12.90	309.38 ± 9.28	202.64 ± 6.08
	Citric acid	-	16.68 ± 0.50	603.18 ± 18.10	103.33 ± 3.10	-	-
	Succinic acid	-	59.76 ± 1.79	857.24 ± 25.72	18.28 ± 0.55	-	51.11 ± 1.53
	Fumaric acid	8.54 ± 0.26	2.76 ± 0.08	-	-	-	-
	Formic acid	1.38 ± 0.04	1.20 ± 0.04	3.76 ± 0.11	3.11 ± 0.09	5.45 ± 0.16	1.36 ± 0.04
Phenols	Gallic acid	5.19 ± 0.16	3.72 ± 0.11	67.53 ± 2.03	2.56 ± 0.08	51.05 ± 1.53	91.81 ± 2.75
	p-Coumaric acid	-	5.16 ± 0.15	-	-	-	-
	Caffeic acid	-	7.20 ± 0.22	-	-	-	-
	Catechin	-	3.72 ± 0.11	18.12 ± 0.54	-	283.64 ± 8.51	171.40 ± 5.14
	Glycosidated flavonoids (eq Q3G)	20.69 ± 0.62	9.84 ± 0.30	90.51 ± 2.72	-	-	-
Carbohydrates	Sucrose	18.23 ± 0.55	-	-	-	-	190.42 ± 5.71
	Glucose	3497 ± 104	123.36 ± 3.70	613.65 ± 18.41	11081 ± 332	1468.15 ± 44.04	309.74 ± 9.29
	Fructose	-	36.00 ± 1.08	597.65 ± 17.93	-	242.84 ± 7.29	234.34 ± 7.03
Miscellaneous	2,3 Butanediol	-	2.72 ± 0.08	205.41 ± 6.16	-	-	17.74 ± 0.53
	Nicotinamide	0.46 ± 0.01	0.72 ± 0.02	7.29 ± 0.22	3.33 ± 0.10	5.24 ± 0.16	1.13 ± 0.03

Skin extracts **LDC1** and **LDC2** exhibited a biphasic relaxing behavior, an initial primary activity plateauing, and a secondary effect starting at concentrations of 300 µg/mL and 100 µg/mL, respectively (Figure 1 A,B). Seed extracts **LDC5** and **LDC6** were the most potent of the series (IC_{50} values of 1.7±0.3 µg/mL, n=6, and 1.3±0.3 µg/mL, n=7, respectively;) but, at concentrations >10 µg/mL they showed an hermetic behavior giving rise to vessel contraction. Finally, also the wine **LDC3** noticeably relaxed aortic rings with an IC_{50} value of 39.1±13.9 µg/mL (n=6). In endothelium-deprived preparations, **LDC** samples did not cause vasorelaxation; only **LDC5** and

LDC6, at the maximum concentration assessed (1 mg/mL), significantly reverted phenylephrine-induced active tone (E_{max} of 83.1±4.1% and 83.5±5.3%, respectively n=5; Figure 1 E,F). Additionally, pre-exposure of endothelium-intact rings to L-NAME antagonised the vasorelaxant activity of **LDC1**, **LDC2**, and **LDC3** (Figure 1 A-D). As a final point, capsazepine did not affect **LDC3**-induced spasmolysis in endothelium-intact preparations. Seed extracts **LDC5** and **LDC6**, when cumulatively added, evoked a light decrease of the active tension, in endothelium-denuded rings depolarized with 20-30 mM KCl (E_{max} values of 42.1±18.2% and 47.3±15.5%, respectively; n=6; Figure 2). The other extracts were not able to induce relaxation also at high concentration (Figure 2), contrary to the control (pinacidil 100 µM), which completely reverted the tone to the basal level. To sum up, **LDC1-LDC3** and **LDC5-LDC6** evoked an endothelium-dependent vasorelaxation. In particular, the spasmolysis operated by **LDC1-LDC3** induced the activation of eNOS, because pre-exposure of the rings to L-NAME (an eNOS inhibitor) completely abolished this phenomenon. eNOS is constitutively expressed in the endothelial cells but also strongly regulated at transcriptional and post-translational level. In line with this, the influx of extracellular Ca^{2+} activates, binding to calmodulin, TRPV1 channels: this complex in turn, is able to release caveolin-1 from eNOS, enhancing the production of NO *(Vanhoutte et al., 2016)*. However, TRPV1 channels were not involved in the activation of eNOS operated by **LDC3**, as capsazepine, a specific blocker of this channel, did not affect **LDC3**-induced spasmolysis. This implies the involvement of other mechanisms, e.g., phosphorylation at Ser^{1177} by several kinases such as Akt, PKA, and AMPK, among others *(Heiss et al, 2018)*. Considering the presence of gallic acid, succinic acid, and flavonoids (such as Quercetin) in **LDC3** sample, a suitable vasorelaxation mechanism should be the activation of eNOS through phosphorylation of Ser^{1177}. This hypothesis is supported from the observation that **LDC4**, lacking many of these constituents, was lacking of any relaxing activity. Furthermore, **LDC1**-**LDC4** failed to relax rings pre-contracted with 20-30 mM KCl indicates that these extracts may not harbor any agent capable to open K^+ channels (the consequent flux of K^+ towards the extracellular environment, hyperpolarize the vascular smooth muscle cell membrane, thus closing voltage-dependent Ca^{2+} channels and causing vasorelaxation), or may harbor it but not in sufficient concentration. This assumption is additionally supported by the fact that pinacidil, an ATP-dependent K^+ channel opener, contrary to **LDC1-LDC4** extracts, was able to revert KCl-induced active tone under the same experimental conditions. Only **LDC5** and **LDC6** showed a moderate relaxation, though only at high concentration, due to the presence of gallic acid and catechins, which were able to open K^+ channels *(Carullo et al., 2020a)*.

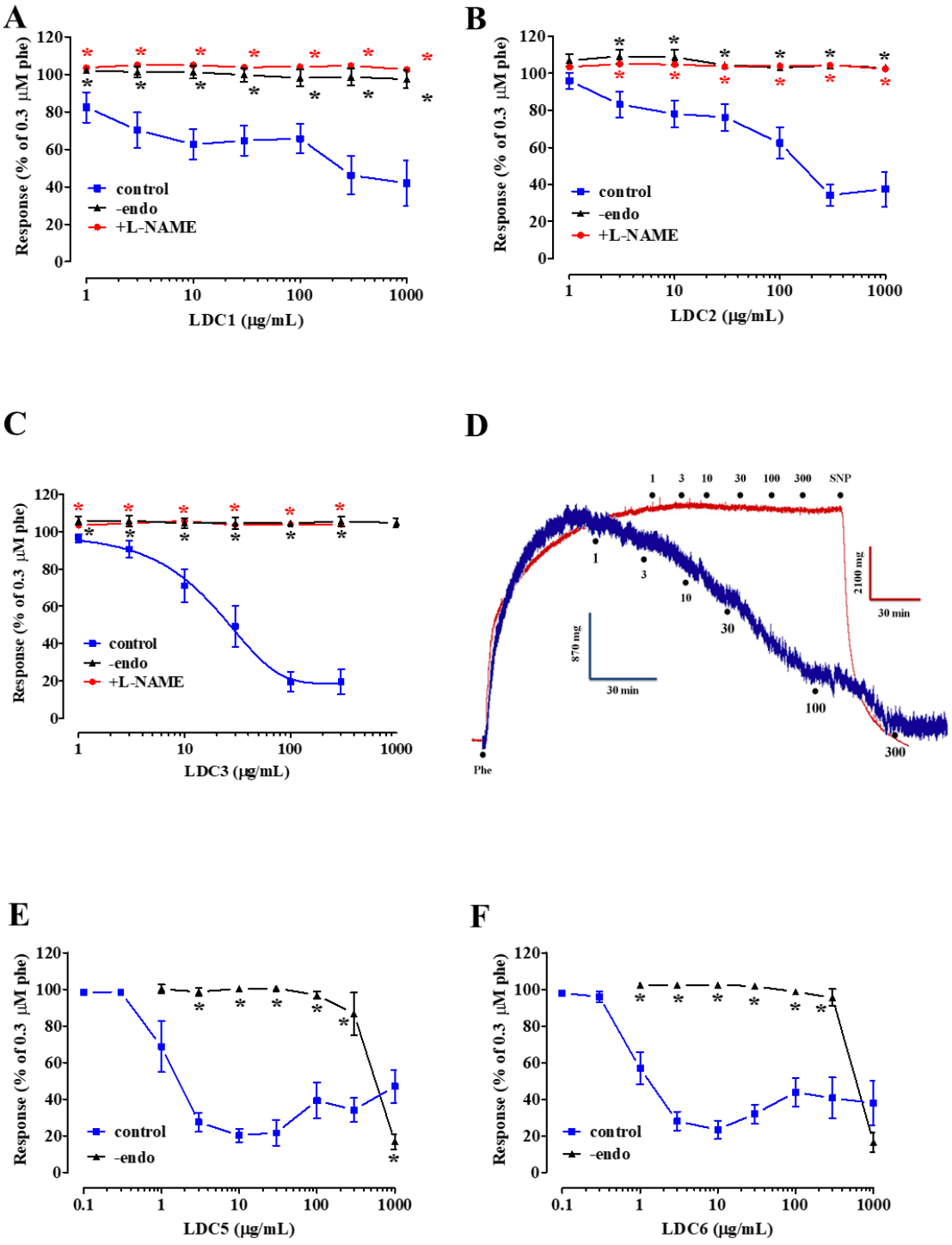

Figure 1. Effects of **LDC** samples on phenylephrine-induced contraction in either endothelium-intact or deprived rat aorta rings.

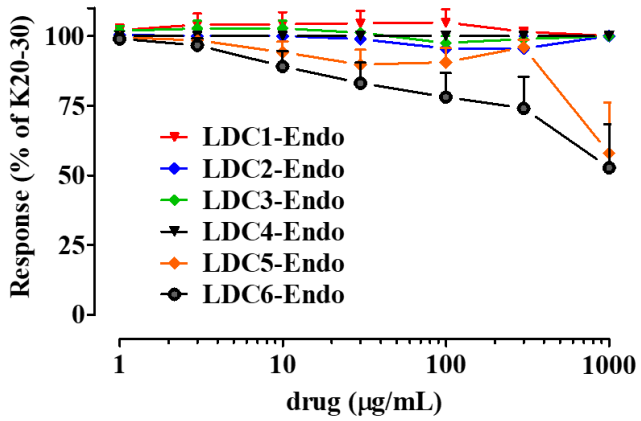

Figure 2. Effect of **LDC** extracts on high KCl-induced contraction of rat aorta rings

Characterization and vasoactivity of **MBS**, **PBS**, **MSS**, **PSS** *and their pectin conjugates*

White grape pomaces were analyzed for the first time in order to investigate the chemical composition of the samples. It was found that **MSS** showed a little aminoacidic component, while there were interesting amounts of ascorbic acid and catechin. The corresponding **MBS** extract showed an excessive amount of glucose and interestingly the presence of hydroxymethylfurfural. **PBS** extract showed an abundant acidic component, with high levels of glucose. On the other hand, **PSS** showed the most interesting chemical composition due to an exciting amino-acidic component, including GABA and tryptophan and considerable amounts of catechin and organic acids, in particular p-coumaric and gallic acids. Regarding the vasoactivity, in endothelium-intact rings (pre-contracted with phenylephrine), **MSS** and **PSS** demonstrated a concentration dependent relaxation that, at higher concentrations, was followed by a return to basal values (Figure 3A). **PSS** gave the impression to be more efficacious than Mantonico as a vasorelaxant extract. The removal of the endothelium abolished only vasoconstriction and significantly shifted the vasorelaxant activity to the right, in the case of **MSS**. Conversely, **PSS** showed a biphasic vasorelaxant effect, which was more pronounced at concentrations>300 µg/mL (Figure 3A).

Table 2. Quantitative analysis of **MBS**, **PBS**, **MSS**, **PSS** samples by NMR spectroscopy

	Substance	PSS (µmol/g)	PBS (µmol/g)	MSS (µmol/g)	MBS (µmol/g)
Aminoacids	Valine	6.32	12.55	7.26	5.21
	Isoleucine	4.50	2.82	4.50	2.52
	Leucine	2.59	2.82	9.76	3.51
	Threonine	15.28	4.87	11.25	2.52
	Alanine	11.34	5.72	12.91	5.61
	Proline	50.20	53.33	-	54.81
	GABA	26.86	-	-	-
	Tyrosine	2.93	-	-	-
	Phenylalanine	3.21	2.42	-	2.42
	Tryptophan	3.38	-	-	-
Organic acids	Lactic acid	27.31	5.77	8.33	7.77
	Butyric acid	-	8.06	-	-
	Acetic acid	9.49	5.16	-	4.83
	Quinic acid	46.05	64.21	-	69.94
	Tartaric acid	25.78	33.11	-	46.57
	Sorbic acid	-	21.40	22.30	21.14
	Succinic acid	26.84	6.35	17.36	7.88
	Ascorbic acid	-	45.50	418.10	-
	Malic acid	96.28	21.40	274.67	315.61
	p-coumaric acid	18.90	6.34	-	3.05
	Gallic acid	17.46	1.41	-	1.41
	Shikimic acid	-	2.87	-	4.54
	Formic acid	1.09	0.87	3.04	3.26
Carbohydrates	Glucose	1413.30	3422.90	2721.30	2721.30
	Rhamnose	21.08	50.19	49.40	49.40
	Saccharose	25.33	16.65	12.53	12.53
	Raffinose	15.66	10.84	7.97	7.97
Miscellaneous	2,3-Butanediol	1.11	4.44	5.22	1.33
	Glycosylated flavonoids (Q3G eq.)	36.50	4.78	51.07	12.02
	Ethanol	-	996.74	-	54.05
	Acetamide	4.91	5.59	-	-
	Choline	6.05	-	-	-
	Catechin	6.10	4.41	191.97	3.14

In endothelium-denuded rings, myorelaxant activity occurred at higher concentrations as matched to endothelium-intact specimens. This support the hypothesis that both extracts are capable to directly target the smooth muscle cells and activate vasorelaxant mechanisms thus ensuring a persistent decrease of active muscle tone. Taking into account the chemical composition of the extracts, **MSS** vasoactivity is likely due to the presence of the vasodilating agents catechin and ascorbic acid *(Ghayur et al., 2007)*. On the other hand, **PSS** vasodilation could be ascribed to

GABA, which inhibits noradrenaline release from sympathetic nerves thus exerting an antihypertensive effect *(Hayakawa et al., 2002)*, L-proline, which improves NO bioavailability *(Leal et al., 2019)* and gallic acid, which is a well-known, endothelium-dependent and -independent vasodilator agent *(de Oliveira et al., 2016)*. At concentrations ≤30 μg/mL both endothelium-dependent and –independent vasorelaxant mechanisms concur to the relaxation observed with **MSS** and **PSS**, which resulted more efficacious. When vascular preparations were challenged with **MBS** and **PBS** (Figure 3B), an endothelium-dependent relaxation occurred, but potency resulted one order of magnitude lower while efficacy higher than those observed with **MSS** and **PSS**. In endothelium-denuded arteries, **MBS** and **PBS** caused a concentration-dependent vasodilation with similar efficacy but a significant lower potency as compared to endothelium-intact rings. Contrary to **PSS** and **MSS**, **PBS** and **MBS** appeared to stimulate the release from the endothelium of only vasorelaxant factors. In rings depolarized with high extracellular K^+ concentrations, **MSS**, **PSS**, **MBS** and **PBS** were partially effective on this contraction, the relaxant effect starting at quite high concentrations and maximal effect never exceeding 50% of the active muscle tone (Figure 3C andD). These results suggest that the extracts are scarcely efficacious as $Ca_V1.2$ channel blockers. Considering the more pronounced vasoactivity in endothelium-intact rings, it can be speculated that they affect either the IP_3-induced Ca^{2+} release from the intracellular stores *(Fransen et al., 2015)*. Taken together, these data do not indicate any marked difference in the vasoactivity of the two extracts except for the seed extracts, and in particular **PSS**, that contains the larger chemical variety of aminoacids, like GABA, tyrosin and tryptophan, capable to release contracting factors, such as prostanoids and/or endothelin-1, from the endothelium *(Detremmerie et al., 2016)*. The most interesting extract resulted **PSS**, of which the suitable mechanism of action was investigated. Specifically, endothelium-denuded rings were contracted with low extracellular K^+ concentrations (20-30 mM). Cumulative concentrations of **PSS** (up to 300 μg/mL) did not affect muscle active tone (Figure 3E). Conversely, the subsequent addition of 100 μM pinacidil, completely reverted K^+-induced contraction to 6.5 ± 1.8% of control (n=6), thus demonstrating that **PSS** is not capable to open K^+ channels.

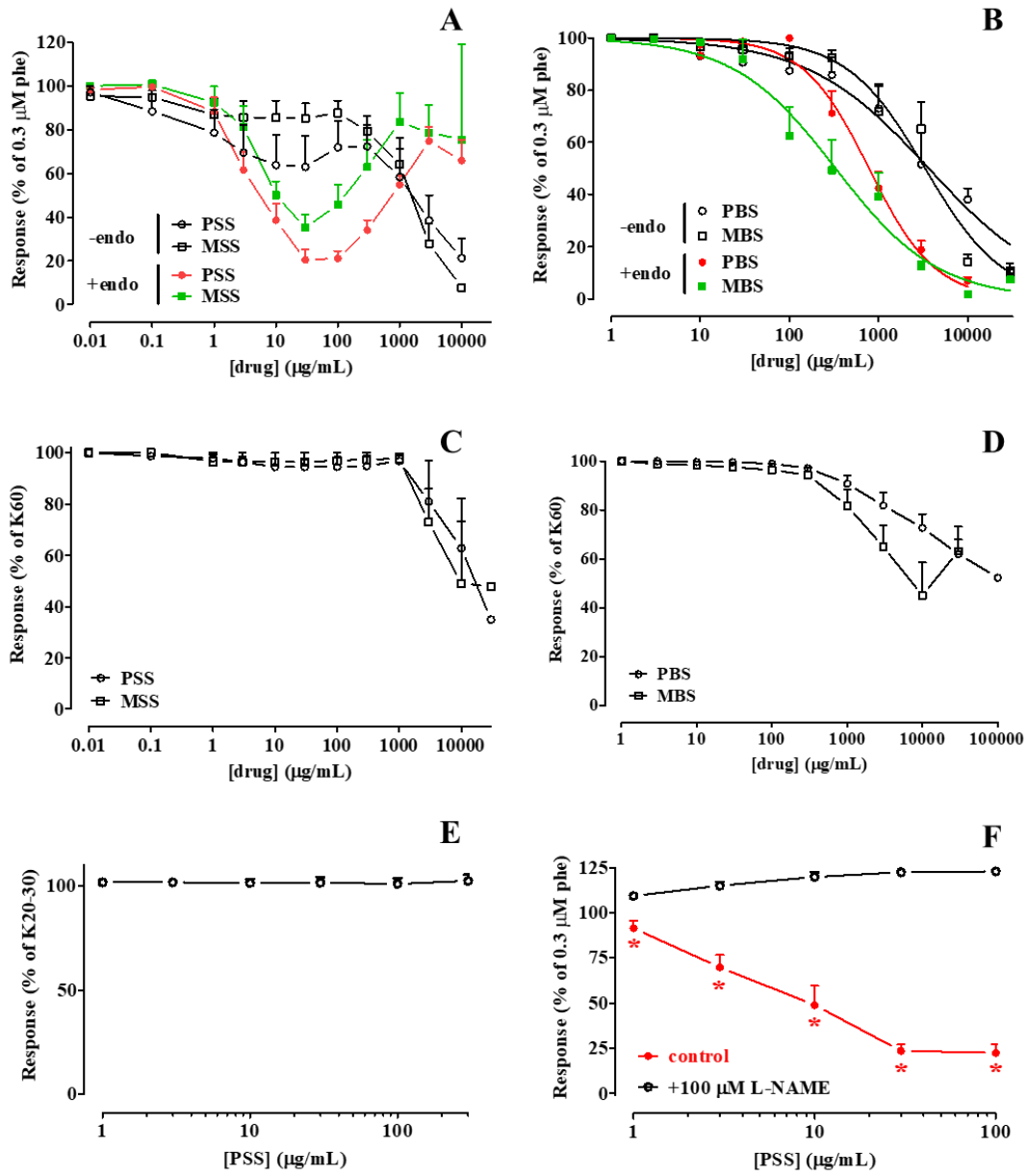

Figure 3. Effects of **MBS, PBS, MSS, PSS** samples on phenylephrine-induced contraction and on high KCl-induced contraction in either endothelium-intact or deprived rat aorta rings.

As already shown in Figure 3A, the cumulative addition of **PSS** relaxed intact aorta rings pre-contracted with phenylephrine (Figure 3F). This effect was suppressed by pre-incubation of tissues with 100 µM L-NAME. The subsequent addition of sodium nitroprusside, a well-known NO-donor, completely reverted phenylephrine-induced contraction, thus confirming that **PSS** was able to induce an endothelium-dependent relaxation mediated by eNOS.

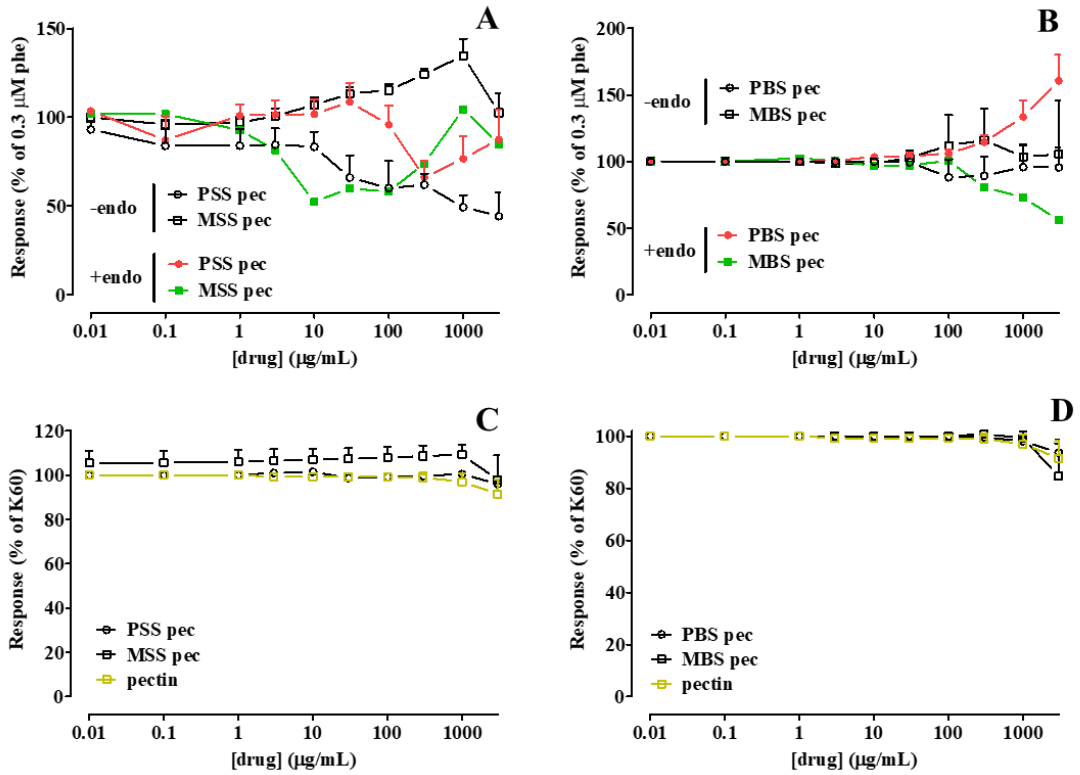

Figure 4. Effect of pectin-embedded polymers on phenylephrine-induced contraction and on high KCl-induced contraction of rat aorta rings

The extracts conjugated to pectin, as well as pectin alone, were investigated for their vasoactivity either on endothelium-intact or -denuded aorta rings. Only at the highest concentration (3 mg/mL) tested, either a modest increase (about 18% of control) or a modest decrease (about 22% of control) of active muscle tone was observed in the presence or absence of the endothelium, respectively. In endothelium-intact rings, the vasoactivity of **MSS pec** was partly reduced by conjugation while that of **PSS pec** was markedly reduced and shifted to the right. Their main features (i.e. vasorelaxation followed by the return to basal values), however, were similar to those observed in the absence of the polymer (Figure 4A; compare to Figure 3A). Pectin conjugation did not modify **PSS** activity in rings deprived of endothelium. Under the same experimental conditions, **MSS pec** lost its vasorelaxant activity, rather showing a constricting effect. In endothelium-intact rings, **MBS pec** was at least one order of magnitude less active (Figure 4B). **PBS pec** lost its vasorelaxant activity and rather potentiated the constricting effect of pectin. In the absence of a functional endothelium, both **MBS** and **PBS** vasoactivity disappeared. Similar results were obtained in rings deprived of endothelium and depolarised with 60 mM K^+. Pectin conjugates lack of activity, confirming the already weak efficacy of the extracts (Figure 4C, D). Taken together, these results indicate a general

loss of vasoactivity when pectin polymer was used as a delivery system for Mantonico and Pecorello extracts *(Carullo et al., 2019a)*.

Antioxidant performances of **LDC3** *and* **PSS** *samples*

LDC3 and **PSS** were evaluated in colorimetric assays in order to investigate their antioxidant properties, considering that, in most cases, a good antioxidant power could be associated with a translational use in human conditions. As reported in Table 3, the two samples demonstrated an interesting antioxidant profile, with similar results in all the conducted assays, demonstrating how the presence of polyphenols and amino acids, contributed to the antioxidant activity.

Table 3. Antioxidant profile of **LDC3** and **PSS** samples

	Disposable phenolic equivalent (meq GA/g extract)	**Total antioxidant activity** (meq CT/g extract)	IC_{50} (mg mL^{-1})	
			DPPH radical	**ABTS Radical**
PSS	0.243±0.011	0.403±0.009	0.312±0.015	0.0041±0.0001
LDC3	0.306±0.0012	0.512±0.008	0.033±0.017	0.020±0.0011

Preparation and anti-inflammatory activity of a Sangiovese seed extract-fortified kefir

Kefir is a fermented milk beverage originating from the Balkans and Caucasus with acidic-alcoholic taste and natural carbonation. Its microflora is primarily composed by lactic acid bacteria (*Lactobacillus*, *Leuconostoc*, *Lactococcus*, and *Streptococcus spp.*), acetic acid bacteria (*Acetobacter spp.*) and yeasts (*Saccharomyces* and *Kluyveromyces spp.*), even if many modifications can be found depending on the processing and origin of the product *(Gao et al., 2016)*. Kefir bacterial and fungal species live in symbiosis in the grains, which are closed matrices composed by microbial-derived proteins and polysaccharides (mainly kefiran). Kefir is generally accepted as a powerful probiotic font to improve gut health, with positive nutritional attributes related to its content of carbohydrates, proteins, vitamins, antioxidants and minerals *(Bourrie et al., 2016)*. Kefir exerts interesting effects on immune system, anti-inflammatory activity, hypocholesterolemic funtion, β-galactosidase activity, gastrointestinal proliferation, bacterial colonization, anti-diabetic features, anti-allergic and anti-oxidative properties, effect on blood pressure and lipid level and protection against apoptosis *(Ahmed et al., 2013)*. Little information is available on the influence of polyphenol-containing extracts on the kefir beverage. So, the aim of this part of the thesis, was to evaluate the effect of extract addition on kefir anti-inflammatory properties (in Caco-2 cell line). The obtained extracts were assayed for their antioxidant activity. Lower amounts of phenolic compounds were detected in **sgnbs** compared to the **sgnss** (Table 7). ESI-MS analyses displayed the presence of

a great variety of molecules bearing phenolic rings, to which the radical scavenging activity may be attributed. As reported in Tables 4 and 5, the substances that should be responsible of the antioxidant profile are peonidin glucoside, malvidin-3-O- glucoside, malvidin cumaroyl glucoside, but also methyl glucuronic acid, ethyl glucuronic acid, hydroxymethyl monoglycosylpyranosonic acid and ferulic acid. Considering the antioxidant data reported in Table 7, **sgnss** was selected to perform kefir preparation.

Table 5. ESI(+) mass spectrum of **sgnss**

m/z	Formula $[M+H]^+$	RDB	Error (ppm)	MS^2	Tentative identification
130.0863	$C_6H_{12}NO_2$	1.5	0.1		Pipecolic acid
130.0498	$C_5H_8NO_3$	2.5	-0.5		Oxoproline
189.0758	$C_8H_{13}O_5$	2.5	0.1		
280.2636	$C_{18}H_{34}NO$	2.5	0.4		Too many possible compounds. Octadecadienamide
284.2952	$C_{18}H_{38}NO$	0.5	1.5		Stearamide
302.3054	$C_{18}H_{40}NO_2$	-0.5	0.1	**MS^2**: 284.2948, 266.2819, 254.2834, 240.2679, 109.1007 $C_8H_{13}^+$ 97.0993 $C_7H_{13}^+$ 95.0841$C_7H_{11}^+$ 83.0859 $C_6H_{11}^+$ 81.0689 $C_6H_9^+$ 69.0683 $C_5H_9^+$ 67.0538 $C_5H_7^+$ 60.0435 $C_2H_6ON^+$	Dihydrosphingosine or isomer
318.3006	$C_{18}H_{40}NO_3$	-0.5	1.0		Phytosphingosine
331.2340	$C_{15}H_{31}N_4O_4$	2.5	0.1		Too many possible compounds
439.1387	$C_{24}H_{23}O_8$	13.5	-0.1	**MS^2**: 277.0891 (-162)	Flavonoid glycoside
463.1240	$C_{22}H_{23}O_{11}$	11.5	1.1		Peonidin glucoside
493.1335	$[C_{23}H_{25}O_{12}]^+$	11.5	-1-1	**MS^2**: 331, 315, 287,137	Malvidin-3-O- glucoside
639.1714	$C_{32}H_{31}O_{14}$	17.5	0.9		Malvidin cumaroyl glucoside

Table 6. ESI (-) mass spectrum of **sgnss**

m/z	Formula [M-H]-	RDB	Error (ppm)	MS^2	Tentative identification
133.0145	$C_4H_5O_5$	2.5	1.9		Malic acid
149.0094	$C_4H_5O_6$	2.5	1.6		Tartaric acid
163.0249	$C_5H_7O_6$	2.5	0.5		2-Dehydro-D-xylonate
191.0198	$C_6H_7O_7$	3.5	0.3		Citric acid
191.0561	$C_7H_{11}O_6$	2.5	-0.2	**MS^2 191:** 173 (-18); 147 (-44 CO2); 136 (-58); 111 (-80) ; 85 (-106) **MS^3 191->173:** 155 (-18), 129 (-44), 111 (-62)	Quinic acid
193.0352	$C_6H_9O_7$	2.5	-0.9		Glucuronic acid
193.0564	$C_{10}H_9O_4$	6.5	0.1		Ferulic acid
205.0352	$C_7H_9O_7$	3.5	-0.8		Acid methyl citric / Acid homocitric
207.0509	$C_7H_{11}O_7$	2.5	-0.4		Methyl glucuronic acid
221.0666	$C_8H_{13}O_7$	2.5	-0.3		Ethyl glucuronic acid
223.0460	$C_7H_{11}O_8$	2.5	0.5	**MS^2 223:** 205 (-18); 191 (-32 CH_3OH); 163 (-60); 131 (-92 (60+32)); 113 (131-18); 103 (131-28); 87 (-136: 131+44)) **MS^3: 223->131:** 103 (-28); 87 (-44); 59(-44+28)) **MS^3: 223->113:** 85 (-28)	Hydroxymethyl monoglycosylpyranosonic acid
311.0622	$C_{10}H_{15}O_{11}$	3.5	0.7		Glycosyl tartrate
359.0757	$C_{12}H_{20}O_{10}Cl$	2.5	3.1		anhydrodisaccharide

Kefir was prepared by adding **sgnss** extract to milk before the fermentation. The growth was maintained for 12 and 24 h. pH levels and weight of grains have been evaluated. pH levels were similar at t=0, while after 12 h they

were lower (pH=2.95) in **Ksgn** compared to **Kwht**. Nevertheless, after 24h, which is the usual fermentation time for kefir growth, pH levels were much higher, but still in the medium acidic range.

Table 7. Antioxidant profile of **sgnbs** and **sgnss** samples

	Disposable phenolic equivalent (meq GA/g extract)	**Total antioxidant activity** (meq CT/g extract)	IC_{50} (mg mL^{-1})	
			DPPH radical	**ABTS Radical**
sgnbs	0.549±0.019	0.859±0.018	0.160±0.005	0.085±0.001
sgnss	1.620±0.054	0.520±0.014	0.012±0.001	0.004±0.001

The weight of grains increased considerably after 12 h in **Ksgn**, with a decrease after 24 h. No significant increase has been observed in **Kwht** (Figure 5).

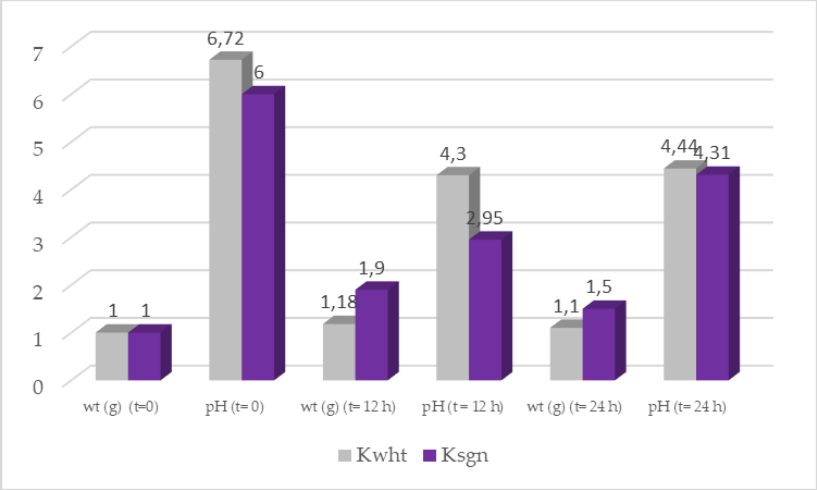

Figure 5. Kefir growth during fermentation

The metabolites in the samples were analyzed in order to attribute the biological activity: the same aminoacids, carbohydrates and organic acids composition was found in both **Ksgn** and **Kwht,** suggesting that, the extract did not affect the end products of the microbiota metabolic pathways. Though, different concentrations have been found for some molecules (mainly carbohydrates, alanine, phenylalanine, succinic and citric acid) meaning that the presence of the extract influenced the rate and/or the route of formation/accumulation of some metabolites from a quantitative point of view. As shown, most of the compounds found in **sgnss** were not detected in kefir samples, indicating their conversion into other chemical species by microbial metabolism. In particular, the chosen level of supplementation allowed to reach the proper kefir functionalization avoiding, at the same time, possible

negative effects. A limitation in the use of polyphenols-rich extracts for dairy fortification, is related to the antimicrobial effect of such extracts on LAB, as well as their negative impact on sensory and rheological features of the functional product, but the concentration used limited this behavior *(Tabasco et al., 2011)*. Ethanol was never found in the samples, indicating that only homo-fermentation took place during the kefir preparation. In control kefir, lactose was totally degraded to galactose and glucose by kefir microbiota. On the contrary, the fortified sample still contained lactose (2.26 g L^{-1}), although glucose and galactose concentrations were higher (8.31 g L^{-1} and 10.72 g L^{-1}, respectively) compared to the non-fortified counterpart (4.22 g L^{-1} and 3.65 g L^{-1}, respectively)

Table 8. Quantitative analysis of kefir samples

Molecule	Kwht	Ksgn
	Amminoacids (mg L^{-1})	
Valine	28.12	28.82
Isoleucine	17.84	20.59
Alanine	33.50	4.28
Tyrosine	9.78	9.24
Phenylalanine	22.80	40.20
	Carbohydrates (g L^{-1})	
Galactose	4.22	10.72
Glucose	3.65	8.31
Lactose	-	2.26
	Organic Acids (mg L^{-1})	
Lactic acid	1480	2610
2-hydroxy-isobutyrric acid	13.45	6.41
Acetic acid	7.21	10.09
Pyruvic acid	31.00	16.82
Succinic acid	21.72	2.83
Citric acid	278.96	1006
Fumaric acid	4.87	11.72
Formic acid	3.31	3.31

The last aspect could be related to the production of kefiran by homo-fermentative LAB. This extracellular exopolysaccharide, is a hetero-polysaccharide made of glucose and galactose in equal amounts and forming the major portion of the gelatinous matrix containing the kefir microflora.

Organic acids were found in both samples (1.48 g L^{-1} and 2.61 g L^{-1}, **Kwht** and **Ksgn**, respectively). For the first time, 2-idroxy-isobutyric acid was detected. Some organic acids can be further converted in volatile flavor

compounds. The presence of many organic acids in **sgnss**, could have influenced metabolite profiles and distributions in fortified sample. As far as aminoacids are concerned, only alanine, valine, isoleucine, tyrosine and phenylalanine were detected in kefir samples *(Coda et al., 2012)*.

Phenolic compounds present in **sgnss** are able to interact with milk proteins; these may further affect the sensory and functional properties, as well as microbiological quality and oxidative stability, of the dairy products. The results of antioxidant activity (TAC and DPPH free radical scavenging assays) showed that **Ksgn** had higher antioxidant activity compared to **Kwht**.

Specifically, the addition of the extract displayed an increase of TAC value by 40.7%, while IC_{50} value against DPPH radical highlighted a decrease by 16.0%, compared to control kefir, clearly showing that enriched kefir possess higher antioxidant performances compared to the unfortified sample. This finding is consistent with those reported in the literature, highlighting a positive correlation between vegetables-enriched fermented products and antioxidant activity (Table 9).

Table 9. Antioxidant profile of **Kwht** and **Ksgn** samples

	Disposable phenolic equivalent (meq GA/g extract)	**Total antioxidant activity** (meq CT/g extract)	**IC_{50}** (mg mL^{-1})
			DPPH radical
Kwht	1.6159±0.005	0.558±0.004	0.107±0.001
Ksgn	1.975±0.004	0.785±0.003	0.090±0.001

The reproduced inflammatory-impaired intestinal barrier was simulated in Caco-2 cells treated with LCTM. LPS caused a marked release of pro-inflammatory cytokines from THP-1 cells, which significantly reduced LCTM-stimulated Caco-2 monolayer TEER values by approximately 25%, compared to the untreated control, after 24 hours (Figure 6 A,B). Consistently, phenol red permeability was approximately two-fold higher in inflamed Caco-2, compared to the untreated control (Figure 6C). **Kwht** and **Ksgn** did not alter Caco-2 TEER in basal condition (Figure 6D). On the contrary, **Kwht** totally counteracted the cytokines-impaired TEER and phenol red permeability at each of the tested concentrations. Comparable results were obtained with **Ksgn**, even if no statistical significance was obtained on TEER with the lowest concentration of 0.1 µg/mL (Figure 6 E, F) *(Carullo et al., 2020b)*.

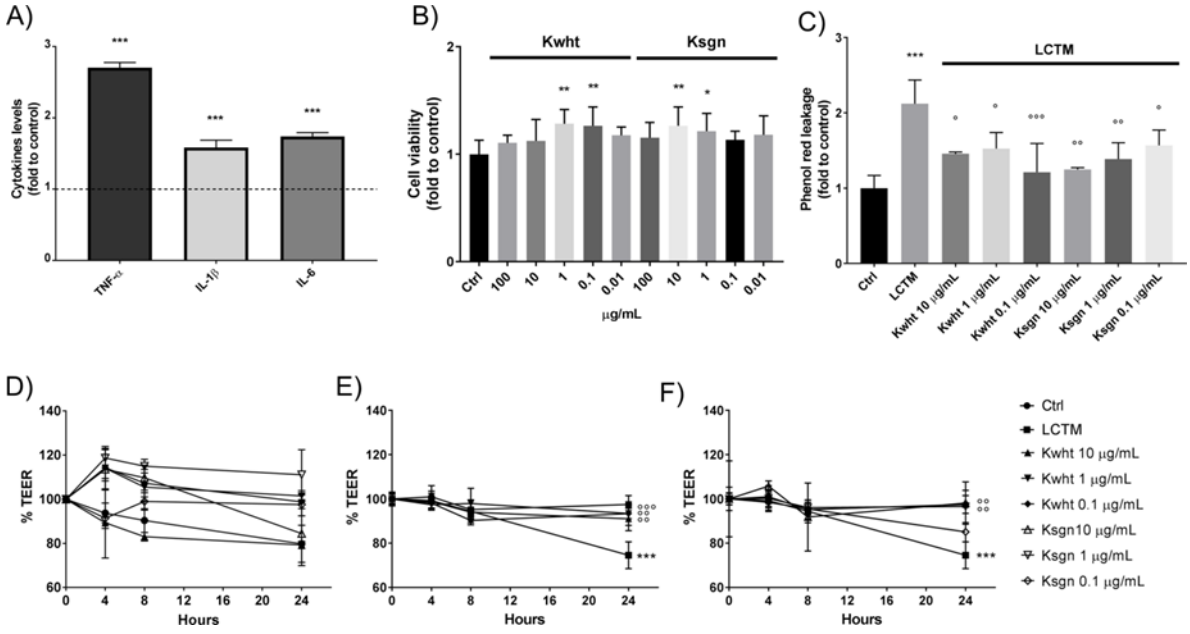

Figure 6. Effects of **Kwht** and **Ksgn** in the *in vitro* model of inflamed intestinal epithelium.

**p<0.05 vs Ctrl; **p<0.01 vs Ctrl; ***p<0.001 vs Ctrl; °p<0.05 vs stimulus; °°p<0.01 vs stimulus; °°°p<0.001 vs stimulus.*

General chemical considerations

Commercially available reagents (Merck products) were used without further purification, and all solvents were of HPLC quality. Reactions under nitrogen atmosphere were performed in oven- or flame-dried glassware and anhydrous solvents. All reactions were monitored by thin-layer chromatography (TLC) Merck 60 F254 silica plates. Analytical TLC was conducted on Merck aluminum sheets covered with silica (C60). The plates were either visualized under UV-light or stained by dipping in a developing agent followed by heating [$KMnO_4$ (3 g in water (300 mL) along with K_2CO_3 (20 g) and 5% aqueous NaOH (5 mL)]. Flash column chromatography was performed using silica gel 60 (0.040-0.063 mm). All new compounds were characterized ^{1}H-NMR, ^{13}C-NMR and melting point (m.p.) when applicable. For recording of ^{1}H-NMR and ^{13}C-NMR, a Bruker Advance (operating at 300 MHz) was used. Unless otherwise stated, all NMR spectra were recorded at 25 °C. The chemical shifts (δ) are reported in parts per million (ppm) and the coupling constants (*J*) in Hz. For spectra recorded in $CDCl_3$, signal positions were measured relative to the signal for $CHCl_3$ (7.26 ppm for ^{1}H-NMR and 77.16 ppm for ^{13}C-NMR). For spectra recorded in DMSO-d_6, signal positions were measured relative to the signal for DMSO (δ 2.50 ppm for ^{1}H-NMR and 39.52 ppm for ^{13}C-NMR). For spectra recorded in Acetone d_6, signal positions were measured relative to the signal for Acetone (δ 2.60 ppm for ^{1}H-NMR and 30.0 and 206 ppm for ^{13}C-NMR). For spectra recorded in CD_3OD signal positions were measured relative to the signal for methanol (δ 3.48 ppm for ^{1}H-NMR and 50.0 ppm for ^{13}C-NMR). Quercetin used was anhydrous 99% (HPLC) powder, oleic acid ≥99% (GC), DCC, DMAP, PPL, trans-ferulic acid, α-lipoic acid, acetic anhydride, $SOCl_2$, 3-nitrobenzoic acid, linoleic acid ≥99% (GC) and linolenic acid ≥99% (GC) were purchased from Merck (Italy).

Materials & Methods

INS-1 832/13 Cell culture

The pancreatic insulin-secreting INS-1 832/13 β-cells (kindly donated by Prof. C. Newgard, Duke University, Durham, NC), a cell line stably transfected with a plasmid coding for human proinsulin, were maintained in RPMI-1640 medium supplemented with 10% fetal bovine serum (FBS), 10 mM HEPES, 2 mM L-glutamine, 1 mM sodium pyruvate, 50 mM β-mercaptoethanol, 100 IU/mL penicillin, and 100 IU/mL streptomycin. Cells were incubated under 95% O_2 and 5% CO_2 at 37 °C in 100-mm Petri dishes as described (*Kane et al., 2010*). Media were refreshed every 2–3 days and cells were trypsinized and passaged weekly. Cells were subcultured when they approached ≥70% confluence.

Insulin secretion detection

A total of $5 \cdot 10^5$ INS-1 832/13 β cells were plated in 24-well plates with RPMI 1640, 11 mM glucose, and 10% FBS. The media were switched to 5 mM glucose and after 16 h incubation, β-cells were washed and secretion medium HBSS containing 3 mM glucose was added to the cultures. After 2 h, secretion medium was replaced with fresh secretion medium containing 23 mM glucose to initiate the GSIS (at 0; 5; 15; 30; 60 and 120 min) with or without **AV1** and **AV2** at different concentrations ranging from 2.5 to 40 μM. 8 μM **DC260126** (*Hu et al.,* 2009) was added 30 min before starting GSIS to the culture media 2 h before GSIS. The samples were then collected and spun for 5 min at 2500 r.p.m. and at 4 °C in order to pellet down cellular debris. The supernatant was stored at -80 °C until assayed. Levels of insulin were detected by commercial ELISA kit (Calbiotech, Inc., CA) according to manufacturer's instructions. Each sample was run in triplicate. The insulin secretion data are presented only at 5 min.

Computational details

The structure of ligands was submitted to the LigPrep routine (implemented inMaestro 9.2 within the Schrödinger Suite 2011), using OPLS 2005 as the force field and Epik 2.2 to generate possible tautomers at pH 7 ± 2. The structure of GPR40 (resolution 2.33 Å, protein data bank entry 4phu) was refined by means of the Protein

Preparation Wizard to add hydrogens, assign bond orders and sample water molecule orientation. SiteMap 2.5, with default settings, was then applied to identify potential ligand binding sites on GPR40. Next, Glide 5.7 wasused to perform docking calculations on GPR40 ligands. A distinct receptor grid was generated for each potential binding site identified in the previous step. Grid size was adjusted manually to best fit shape and size of each site. Rotation of all receptor hydroxyl groups contained within the gridbox was allowed during grid generation. Root mean square deviation was calculated for the crystallographic structure of both TAK-875 and the oleoyl glycerol in comparison to the best docked pose and was found less than 1 Å in both cases, thus suggesting the ability of Glide in handling such structural systems and the reliability of docking calculations. The computational protocol applied to dock the ligand to the structure of GPR120 was previously described. Briefly, ligands were built with Maestro 9.2 (Schrödinger Suite 2011) and submitted to LigPrep. OPLS 2005 force field and Epik 2.2 were used to generate possible tautomers at pH 7 ± 2. The homology modeling server CPHmodels 3.2 was applied to build the three-dimensional structure of GPR120. In detail, the UniProt sequence Q5NUL3 (377 amino acids) of the Free Fatty Acid Receptor 4 (also known as GPR120) was used as the query sequence. The search for a template structure done by the remote homology modeling server led to identify bovine rhodopsin (pbd entry 2i36) as the best template. Although a low identity, a Z-score = 65.7 is indicative of a high reliability homology model. The structure of GPR120 was refined by means of the Protein Preparation Wizard. Next, SiteMap 2.5, was used to find ligand binding pocket on GPR120. Finally, Glide 5.7 was applied to dock the ligands on GPR120. Receptor grid size was adjusted manually to best fit shape and size of each putative binding site. Receptor hydroxyl groups within the gridbox were allowed to rotate during grid generation.

HaCaT and THP-1 cells culture

Human keratinocytes from adult skin (HaCaT) were cultured in 75 cm^2 flasks (Sarstedt, Milan, Italy) in complete DMEM, which was composed of DMEM (Sigma-Aldrich, Milan, Italy) medium with 10% FBS and 1% L-glutamine (Sigma-Aldrich). EDTA-trypsin (Sigma-Aldrich) solution was used for detaching cells from flasks, and cell counting was performed using a hemocytometer by Trypan Blue staining. THP-1 cells were culturedin 75 cm^2 flasks (Sarstedt) in complete RPMI medium, which was composed of RPMI (Sigma-Aldrich) medium with 10% heat-inactivated FBS (Sigma-Aldrich), 1% L-glutamine (Sigma-Aldrich) and 0.05 mM 2-mercaptoethanol. Cell counting was performed using a hemocytometer by Trypan Blue staining. Samples were solubilized in DMSO and diluted in complete medium in order to reach the final concentration. DMSO concentration in each final treatment

was maintained below 0.1% and the untreated control was represented by the same amount of DMSO present in the treatments.

HaCaT cell viability and proliferation assay

Cell viability and proliferation were assessed by means of sulforhodamine B (SRB, Sigma-Aldrich) assay (Vichai eta al. 2006) Briefly, HaCaT cells (1×10^4) were seeded into 96-well plates and allowed to grow for 24 h. Cells were then treated with increasing concentrations of samples (0.01 – 50 µM) and incubated for 72 h. Medium were then replaced, and cells were fixed by adding trichloroacetic acid to a final concentration of 10% (v/v) for one h at 4 °C. Cells were washed, and 0.4% SRB solution was added to each well and incubated for 30 min at rt. Cells were then washed with 1% (v/v) acetic acid, and SRB was solubilized with 10 mM of Tris (Sigma-Aldrich, pH = 10.5). Absorbance was recorded at 540 nm using a MP96 spectrophotometer (Safas, Montecarlo). Treatments were performed in sextuplicate in three independent experiments, and cell proliferation was calculated by normalizing the absorbance of the test wells to the untreated control.

Scratch wound healing assay

HaCaT cells (5×10^4) were seeded into six-well cell culture plates and allowed to grow to 70–80% confluence as a monolayer. The monolayer was gently scratched across the center of the well with a sterile one-mL pipette tip. A second scratch was performed in a perpendicular way to the first, creating a cross in each well. After scratching, the medium was removed, and the wells were washed twice in PBS (Sigma-Aldrich) solution. Fresh medium containing 5% v/v of heat-inactivated FBS and treatments was added to each well, and cells were grown for 24 h. Images were obtained from the same fields immediately after scratching (t0) and after six and 24 h using a Leica DMIL microscope and were analyzed using ImageJ software by manually selecting the wound region and recording the total area. The experiments were conducted in duplicate, in three independent experiments (n = 6). Untreated scratched cells represented the control. The percentage of wound closure was calculated using the following formula:

% Wound closure = $[(\text{Wound area } t_0 - \text{Wound area } t)/\text{Wound area } t_0] \times 100$

TGF-β production and MMP-9 release

After the scratch wound-healing assay, supernatants were collected, centrifuged (4 °C, 15000 g, 15min) and frozen at -80 °C for MMP-9 dosage. Adherent cells were washed twice in PBS and lysed for TGF-β dosage. Protein

content of sample lysate was determined by Bradford protein assay. TGF-β production and MMP-9 release were assessed by non-competitive "sandwich" ELISA kit (Biolegend e-Bioscience DX Diagnostic, Monza, Italy), according to the provider datasheet. Absorbance was recorded at 450 nm using a SAFAS MP96 spectrophotometer.

Immunostimulatory activity

THP-1 cells (1 x 10^6) were seeded into 24-well cell culture plates in FBS free medium and incubated with samples for 24 h. Then, supernatants were collected, centrifuged (4 °C, 15000 g, 15 min) and frozen at -80 °C for cytokines dosages. IL-1β, IL-6 and TNF-α release was assessed by noncompetitive "sandwich" ELISA kit (Biolegend e-Bioscience DX Diagnostic), according to theprovider datasheet. Absorbance was recorded at 450 nm using a SAFAS MP96 spectrophotometer.

Preclinical experimental protocol

24 weeks old, albino wistar rats (450-500 g) were purchased from Charles River Laboratories s.r.l. (Calco, Lecco, Italia). Rats were kept in clean cage with food and water ad libitum according to EU Directive 2010/63/EU and Basel declaration. The experimental protocols and the procedures reported here were approved by the Animal Care Committee of the University of Catanzaro, Italy. All efforts were made to minimize animal suffering and to reduce the number of animals used. Before performing experimental wound, rats were anesthetized with isoflurane using soft bonds. After shaving the skin on the back, lesion was done (2.5*2.5 cm, and 3 mm thickness) using straight stainless steel scissor. Each rat was then kept in clean cage with food and water ad libitum. Wound area was measured every 3 days for 27 days. The rats were then euthanized. The wound area (mm2) was measured using Image Pro Plus program (Milan, Italy).

Statistical analysis

Data were expressed as mean ± standard deviation from three independent experiments in triplicate. Statistical differences were determined by one-way analysis of variance (ANOVA) followed by Tukey's Multiple Comparison Test. Differences were considered statistically significant for $p<0.05$ (*****), $p<0.01$ (******), $p<0.001$ (*******).

FFA1/GPR40: design, synthesis and biological evaluation of Quercetin-oleic acid hybrids

Targets to treat T2DM, together with obesity and other comorbidities, still are unmet medical needs. In the 90's, the deorphanization of several G-protein coupled receptors led to the discovery of FFA1/GPR40 *(Li et al., 2018)*. Its signal transduction is complex and involves the activation of Gq and Gs proteins in different cells, i.e. in the entero-endocrine cells, stimulating the release of the incretins GLP-1 and GIP, while its activation in pancreatic β-cells favors insulin release through the Ca^{2+}-mobilizing G-protein $G_{\alpha q}$ *(Shapiro et al., 2005)*. Moreover, GPR40 is also functionally linked to biased agonism (ligand-specific responses) by the β-arrestin 2-mediated insulinotropic signaling axis. Islets from diabetic mice models have a lower GPR40 expression with decreased insulin secretion, hence GPR40 knockout leads to reductions of both glucose- and arginine- stimulated insulin secretion *in vivo* without changes in insulin sensitivity *(Fang et al., 2012)*. The GPR40 gene is located on human chromosome 19q13.1, and shares approximately 30-40% identity with GPR41 and GPR43. A conserved sequence, named HR2, is a potent β-cell-specific enhancer that binds transcription factors PDX1 and BETA2, and also regulates the transcriptional levels of the gene in β-cells *(Ridner et al., 2008)*. The deletion of GPR40 decreases glucose-stimulated insulin secretion (GSIS) *in vivo* without affecting islets' metabolism. Islets from GPR40 knockout mice have a reduced capacity to release insulin in response to fatty acids, suggesting a central role of GPR40 in regulating insulin secretion *(Alquier et al., 2009)*. The activation of GPR40 inhibits the voltage-gated K^+ channels, resulting in a higher Ca^{2+} efflux via L-type channels and an enhanced depolarization of the plasma membrane thus augmenting GSIS. The endogenous GPR40 ligands such as palmitic, oleic, linoleic and linolenic acids are very lipophilic substances which prefer the orthosteric binding site. Various academic groups and pharmaceutical companies designed new and interesting hydrophobic compounds bearing a typical structural triad constituted by a heteroaryl chain, a spacer (bearing a heteroatom such as -O- or –NH) and an acid head *(Briscoe et al., 2003)*. In 2010, the discovery of TAK-875 by Takeda Pharmaceutical Company Limited, was a success in terms of activity and selectivity (human EC_{50}=0.014 μM – human Ki=0.038 μM) *(Negoro et al., 2010)*. This compound was indicated as an ago-allosteric modulator of GPR40 by exerting its effect cooperatively with endogenous plasma FFAs in human patients as well as in diabetic animals. However, it was not able to activate GLP-1 and clinical data demonstrated a high toxicity due to an increase of cytosolic reactive oxygen species (ROS) generation in hepatocytes. In addition, AMG 837 was also validated as a selective GPR40 agonist with no GLP-1 activity. The results from phase I clinical trials in healthy volunteers were encouraging and showed that AMG 837 did not lower glucose or increase insulin levels, as expected under normo-glycemic conditions *(Yabuki et al., 2013)*. Under this

scheme, several structure-activity relationships were established to develop additional agonists, such as GW9508, which led to the identification of amino acid residues with crucial roles for its recognition (His137, Arg183, Asn244 and Arg258) and GPR40 activation (Tyr12, His86, Tyr91, His137, Arg183, Leu186, Asn244 and Arg258) *(Houze et al., 2012)*. Another class of interesting TAK-based compounds was the TUG family, particularly TUG-770, which preserved the typical feature of its precursor. Nevertheless, the most interesting compounds were the GPR40 agonists which can activate also GLP-1. In this field, several compounds were validated also for favourable pharmacokinetic profiles, namely AS2575959, LY3104607, BMS-986118, Yhhy4488, and compound 12 *(Rodrigues et al., 2018; Christiansen et al., 2013; Hamdouchi et al., 2018; Guo et al., 2015; Meegalla et al., 2018)*. Additional derivatives were designed based on amide linkers *(Krasavin et al., 2016; Chen et al., 2018)*. Also natural products demonstrated good agonist activity against GPR40. Among them, very interesting tools were represented by berberine *(Rayasan et al., 2010)* and epicatechin *(Yang et al., 2018)*. In the family of flavonoids, Quercetin presents various biological activities *(D'Andrea, 2015)*, including antidiabetic one. In fact Quercetin was able to reduce oxidative damage in β cells via the ERK1/2 pathway; Quercetin also increases the activity of glycogen synthase, ameliorates hyperglycemia, and prevents β-cell death *via* the mitochondrial pathway and NF-κB signaling; it is also able to directly increase insulin secretion by activating MAPK transactivated from G_q *(Vinayagam and Xu, 2015)*. Quercetin is commonly present in daily diet since it is contained in various vegetables, such as red onion, red and white grapes, peppers, capers, cranberries, blueberries, lettuce, pears, spinach and red wine, though it has a poor bioavailability that limits its biological effect *(Wach et al., 2007; Mukhopadhayay and Prajapati, 2015)*. In this context, the research would investigate the suitable GPR40 interaction of Quercetin-OA hybrids, considering that OA is the endogenous GPR40 ligand, but able to induce insulin secretion at high, lipotoxic, doses. Furthermore, Quercetin was able to up-regulate VEGF and TGF-β1 expressions, rendering him a suitable wound healing agent, with a typical GPCR signal transduction. GPCRs appeared as intriguing wound-healing targets, *via* various signalling pathways *(Weiß et al., 2017)*. Among these, GPR39 resulted spatial temporally expressed during skin wound repair, leading to a faster healing during the intermediate stage *(Zhao et al., 2015)*. Of note, GPR35 signalling promotes mucosal repair by inducing fibronectin and integrin α5 expression, coupling to Gi protein, and activating ERK1/2 in colonic epithelial cells *(Tsukahara et al., 2017)*. Fatty acids are versatile GPCR ligands, promoting wound healing through various signalling pathways. In particular, 12-HHT is a BLT2 receptor ligand, involved in a 12HHT/BLT2 axis, responsible of an accelerated wound closure through the production of TNF-α, which in turns upregulated MMP-9 activity *(Liu et al., 2014)*. GPR40 agonists demonstrated suitable wound healing properties; effectively, arachidonic acid, through GPR40, enhanced skin

wound healing by targeting mTORC2 *(Oh et al., 2015)*. On the other hand, all the endogenous GPR40 ligands, , linoleic acid, DHA and myristic acid, were able to reduce the production of cytokines (CCL-5 and CCL-17), suppressing allergic inflammation in skin, promoting wound closure *(Fujita et al., 2011; Cardoso et al., 2011)*. So, insulin secretion and wound healing were described for Quercetin-oleoyl derivatives.

Results and Discussion

Chemistry

The chemical synthesis used to obtain the acyl derivatives of Quercetin was simple and original, as reported in Scheme 1. As first step, the catechol group was protected as diphenylmethylketal heating Qu with α,α-dichlorodiphenylmethane. Next, the final oleoyl derivatives were obtained by a conventional Steglich coupling reaction, using 1 equivalent amount of **AV** and OA as acyl donor, DCC and DMAP as activator of the carboxyl group and as catalyst, respectively, in dry DCM under inert atmosphere at rt in the dark. The reaction with an equivalent of OA selectively provided the acyl derivative on **C3** (**AV1**); conversely, 2 equivalents of OA afforded a double functionalization on **C3–7** (**AV4**). Since the hydroxyl group on **C5** is involved in a hydrogen bond interaction with the **C4** chromene carbonyl, the **C5**-substituted derivative has never been isolated. Therefore, **C3** selectivity in comparison to **C7** position can be achieved just by controlling the amount of acylating agent. OA was chosen as acyl donor, because it can direct the flavonol in a pocket of the GPR40 receptor deep, different from those occupied by TAK-875.

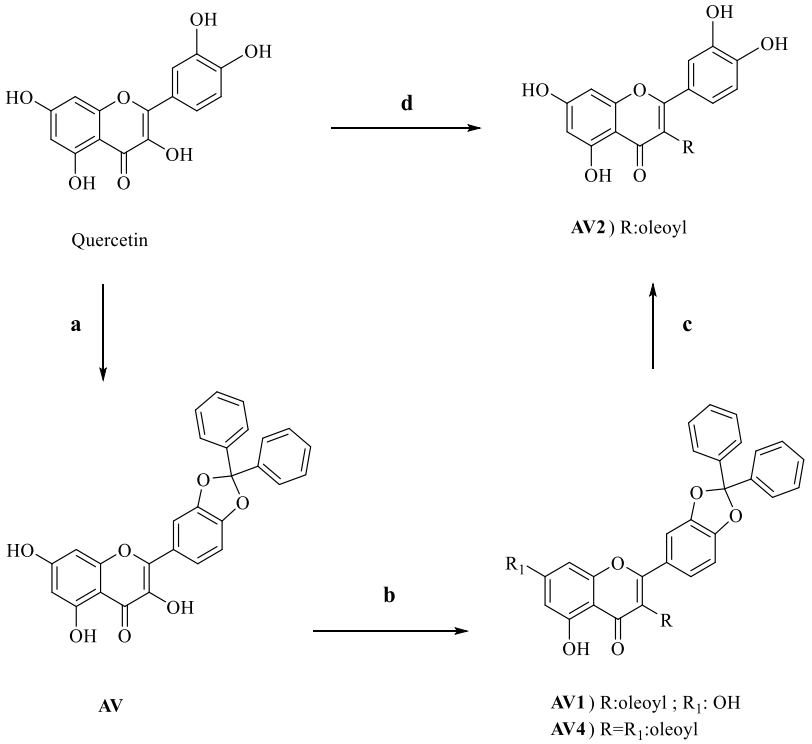

Scheme 1. Semi-synthesis of oleoyl derivatives of Quercetin as GPR40 ligands

Reagents and conditions: a) α,α-dichlorodiphenylmethane, 175 °C (neat conditions), 15 min. b) 1) OA (1 equiv. for **AV1**; 2 equiv. for **AV4**), DCC (1.2 equiv.), DMAP (10 % mol), dry DCM (2 mL), 0 °C, 30 min. 2) **AV** (1 equivalent) in dry DCM dropwise. c) **AV1** (1 equiv.), acetic acid (10 equiv.), distilled water (3 equiv.). d) OA (1 equiv.), PPL (260 mg), pH = 7.8, 37 °C at 130 rpm, incubation time of 48 h.

AV2 could be synthesized starting from **AV1** through cleavage of ketal backbone or, interestingly avoiding the preventive catechol protection and considering several literature observations *(Natoli et al., 1992)*. In particular, biotechnological approaches emerged as new interesting methods for the acylation of flavonoids. *Candida antartica Lipase* B® (the most used acylating enzyme) was not able to produce esters of Quercetin *(Vaisali et al., 2017)*. In this study, PPL was used because of its low cost and also because it is the endogenous enzyme with the task of degrading fats (triglycerides) in the body, but also favouring transesterification reactions. The exact acylation site was determined by comparing the chemical shifts between pure Quercetin and its acylated analogues **AV1** and **AV4**. The chemicals shifts were found to be slightly shifted to downfield or upfield values. For examples, substitutions at 3 and 7 hydroxyls to form **AV4** moved the chemical shifts of the neighbouring protons (6 and 8) to higher field. The presence of diphenyl methyl ketal backbone moved the chemical shifts of the 20 and 50 protons to lower and higher field, respectively *(Saik et al., 2017)*. The mono-substitution of Quercetin-3-oleate did not move the chemical shifts of 6,8 protons in a significant manner, confirming the 7-OH free and at the same time, 20 and 50 protons of catechol did not move. To confirm the 3-acylated position, the obtained **AV2** was also

compared with the compound obtained by cleavage of the diphenylmethylketal (they are the same). The resulted compound showed an ^{1}H-NMR spectrum that matches perfectly with the spectrum of final compound obtained by lipase catalysis.

Experimental part

Procedure a): synthesis of 2-(2,2-diphenylbenzo[d][1,3]dioxol-5-yl)-3,5,7-trihydroxy-4H-chromen-4-one **AV**: **AV** was prepared according to a described procedure *(Li et al., 2009)* by adding to Quercetin (1 equiv.) α,α-dichlorodiphenylmethane (1 equiv.) without any solvent. The reaction mixture was heated at 175°C under argon atmosphere for 10 min. The reaction was diluted with water and extracted with EtOAc. The organic layer was washed with brine and dried over Na_2SO_4. Filtration and evaporation of solvent furnished a residue that was purified by crystallization with *n*-hexane. Yellow crystals, 45% yield. Mp: 218–219 °C. Spectroscopic data are in agreement with those reported.

Procedure b): synthesis of 2-(2,2-diphenylbenzo[d][1,3]dioxol-5-yl)-5,7-dihydroxy-4-oxo-4H-chromen-3-yl oleate **AV1**: A well-stirred solution of OA (1 equiv.), DCC (1.2 equiv.) and DMAP (10 % mol) in dry DCM (2 mL) at 0°C, was stirred for 30 min; then a solution of compound **AV** in dry DCM was added dropwise. The reaction mixture was stirred at 25°C, in the dark under argon atmosphere, overnight. The reaction mixture was filtered on Celite®, and washed with DCM several times. The solvent was removed under reduced pressure, giving a residue that was purified by flash chromatography using a mixture of *n*-hexane:EtOAc (70:30) as eluent. Amorphous yellow solid, 58.4% yield. ^{1}H-NMR (300 MHz, Acetone d_6) δ 7.80-7.40 (m, 10H), 7.20-7.10 (m, 1H), 6.57 (d, 1H, *J* = 2.0 Hz), 6.32 (d, 1H, *J* = 2.0 Hz), 5.50-5.20 (m, 2H), 2.63 (t, 2H, *J* = 7.3 Hz), 2.20-2.10 (m, 4H), 1.80-1.70 (m, 2H), 1.50-1.20 (m, 20H), 0.90 (s, 3H). ^{13}C-NMR (75 MHz, Acetone d_6) δ 178.0, 176.0, 170.0, 163.0, 161.0, 156.0, 150.0, 148.0, 140.0 (x2C), 130.0 (x2C), 129.5, 129.0 (x4C), 126.4 (x2C), 126.2 (x4C), 122.0, 121.0, 119.0, 110.0, 109.0, 105.0, 99.0, 94.0, 33.0 (x2C), 31.9, 29.6, 29.5, 29.3, 29.1, 28.6, 28.3, 28.1, 26.0, 24.0, 22.0, 14.1.

Synthesis of 2-(2,2-diphenylbenzo[d][1,3]dioxol-5-yl)-5-hydroxy-4-oxo-4H-chromene-3,7-diyl dioleate **AV4**: the same procedure described to obtain monoester derivative was followed, but using 2 equiv. of acyl donor (OA). The residue was purified by column chromatography with *n*-hexane:EtOAc (60:40) as eluent. Yellow solid, 52.5% yield. Mp:72.4 °C. ^{1}H-NMR (300 MHz, $CDCl_3$) δ 12.22 (bs, 1H, OH-C5), 7.66–7.55 (m, 6H), 7.47–7.37 (m, 6H), 7.06-6.97 (m, 2H), 6.56 (dd, 1H, *J* = 2.0, 5.0 Hz), 6.32 (dd, 1H, *J* = 1.8, 8.5 Hz), 5.43-5.20 (m, 4H, 2xCH=CH),

2.70-2.50 (m, 4H), 2.10-1.90 (m, 8H), 1.70-1.50 (m, 4H), 1.45-1.10 (m, 39H), 0.90-0.80 (m, 6H, 2xCH_3). ^{13}C-NMR (75 MHz, $CDCl_3$) δ 175.0, 163.8, 160.9, 157.2, 156.3, 148.7, 147.5, 145.0, 139.8, 135.6, 130.0 (x4C), 129.7, 129.3, 128.9, 128.7, 128.4, 128.3, 127.4, 126.2 (x2C), 125.3, 124.7, 122.8, 108.6 (x2C), 107.8, 103.3, 99.1, 94.1, 49.4, 33.8 (x4C), 33.1, 32.9, 31.9, 29.7 (x4C), 29.6 (x6C), 29.5, 29.3, 29.1 (x2C), 29.0, 27.2, 27.1, 25.6, 24.8, 24.3, 23.9, 22.6, 14.1 (x2C). *(Badolato et al., 2017)*

Procedure c) Semi-synthesis of [2-(3,4-dihydroxyphenyl)-5,7-dihydroxy-4-oxo-4H-chromen-3-yl-octadec-9-enoate] **AV2**: **AV1** (1 equiv.) was added of acetic acid (1 equiv.) and distilled water (3 equiv.). The reaction was refluxed at 120 °C for 6 h and the solvent was evaporated in vacuum. The crude residue was purified by flash chromatography with *n*-hexane/EtOAc (50:50) as eluent. Yellow resin, 29.8% yield. ^{1}H-NMR (300 MHz, DMSO d_6) δ 7.78 (d, 1H, *J* = 1.9 Hz), 7.64 (dd, 1H dd, *J* = 1.7 Hz, 8.5 Hz), 6.98 (d, 1H, *J* = 8.5 Hz), 6.50 (d, 1H, *J* = 1.3 Hz), 6.28 (d, 1H, *J* = 1.4 Hz), 5.42-5.38 (m, 2H), 2.29 (t, 2H, *J* = 7.3 Hz), 2.05 (m, 4H), 1.57 (m, 2H), 1.34-1.24 (m, 20H), 0.94 (m, 3H). ^{13}C-NMR (75 MHz, DMSO d_6) δ 176.2, 174.8, 164.3, 161.1, 156.5, 148.1, 147.2, 145.4, 136.1, 130.0, 129.9, 122.4, 120.3, 115.9, 115.4, 103.4, 98.5, 93.7, 34.0, 31.7, 29.5, 29.4, 29.2, 29.1, 29.0, 28.9, 28.9, 26.9, 24.9, 22.5, 14.4, 14.2. *(Carullo et al., 2019b)*

Procedure d) Bio-catalytic approach for the semi-synthesis of **AV2**: In a round-bottom flask, to a solution of Quercetin (1 equiv.) and OA (1 equiv.) in 30 mL of acetone, PPL was added (260 mg). The temperature was maintained at 37 °C, with an agitation rate of 130 rpm. After 48 h, the mixture was filtered, washed with a cold solution of $NaHCO_3$ and extracted with Et_2O, to afford the corresponding oleate. 88% yield. *(Carullo and Aiello, 2018).*

Docking simulations and functional evaluation in INS-1 832/13 cell line

AV1 and **AV4** have been subjected to molecular docking experiments (as reported in computational details section), to evaluate the interaction with the GPR40. TAK-875 was used as a model. In the receptor structure it is possible to identify multiple sites of interaction: site 3 (green) accommodates the agonist TAK-875, while the oleoyl-glycerol derivative present in the crystallographic structure of the active site is linked to site 2 (gray). In addition there are two small globular sites (site 4, red, and site 5, yellow) located near the extracellular portion. Finally, site 2 (magenta) is arranged in such a way as to make the receptor "face" with the cytoplasm (Figure 7A). Of the two derivatives only **AV1** showed affinity for the receptor; in particular, it does not interact with site 3 like

TAK-875, but occupies a pocket at the interface between the red (4) and yellow (5) sites (Figure 7B). The alkyl portion of **AV1** is located on site 4 while the portion of Quercetin is accommodated in site 5 with the projecting diphenylmethylketalic portion (Figure 7C). It should be noted, however, that site 5 is adjacent to site 3 (which accommodates TAK-875), separated from Arg183, a well-known amino acid residue that permits the receptor transactivation performed by carboxylic group of allosteric agonists (Figure 7D). While in TAK-875 only carboxylic group is able to interact, in **AV1** there is a double interaction, coupled by carboxylic function of oleic ester and by the hydroxyl group in C5 of Quercetin (Figure 7D). The oleic portion of **AV1**, on the other hand, is arranged similarly to the oleoyl-glycerol derivative present in the active site. From this experiment it is possible to affirm that **AV1** behaves as a potential allosteric positive modulator of the GPR40 receptor, having its own binding site, different from that of the known agonists. Considering that **AV1**, effectively occupies the orthosteric binding site of the GPR40 groove, DC260126 was chosen as selective orthosteric antagonist in order to perform docking simulations and functional assays. Molecular docking data show that DC260126 occupies a portion close to the ICL2 intracellular loop of the receptor (Figure 7 E,F); the sulphonyl oxygen forms a bifurcated hydrogen bond with the basic chains of Arg37, as well as the 5-OH of Quercetin in **AV1**. The second sulfonyl interacts with –NH of Ala116. DC260126 fluorophenyl is interposed between the TM3 domain in a region delimited by Arg104, Arg218 and Arg221 (Figure 7G). The central phenyl ring of DC260126 perfectly overlaps with the ester grouping of **AV2** (Figure 7 E-F) while the butyl chain occupies the part of the pocket where the oleic chain of **AV2** is also located, demonstrating how the power of partial agonist of **AV2** is given by specific bonds that it forms when it interacts with the receptor. In particular, it can be noted that the portion of GPR40 occupied by **AV2** is the same that occupies DC260126 in the lower part (linked to ICL2) while the oleoyl-derivative occupies the upper part of the transmembrane domain (Figure 7F).

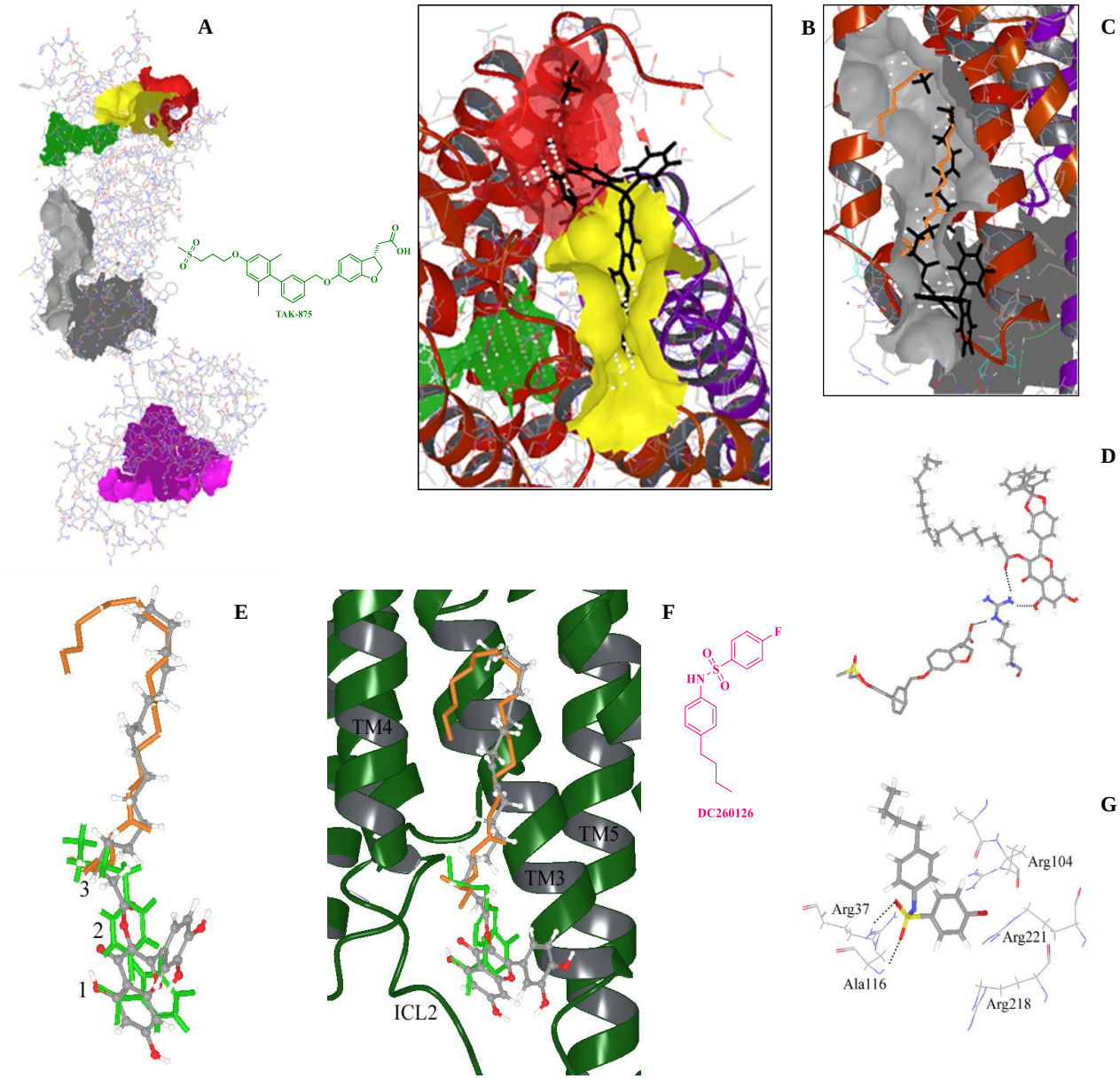

Figure 7. Docking simulations of **AV1** and **AV2** on GPR40 structure

INS-1 832/13 cell line was used to evaluate the insulin secretory power of **AV1** and **AV2**. The dose-response curve was constructed to evaluate the EC_{50} of the compound. As shown in Figure 8A the EC_{50} for **AV1** is ~ 5.1 µM. The typical sigmoid pattern makes **AV1** a full agonist. Since the site occupied by **AV1** is different from that of the positive allosteric modulator TAK-875, the antagonist DC260126 was chosen because it occupies the

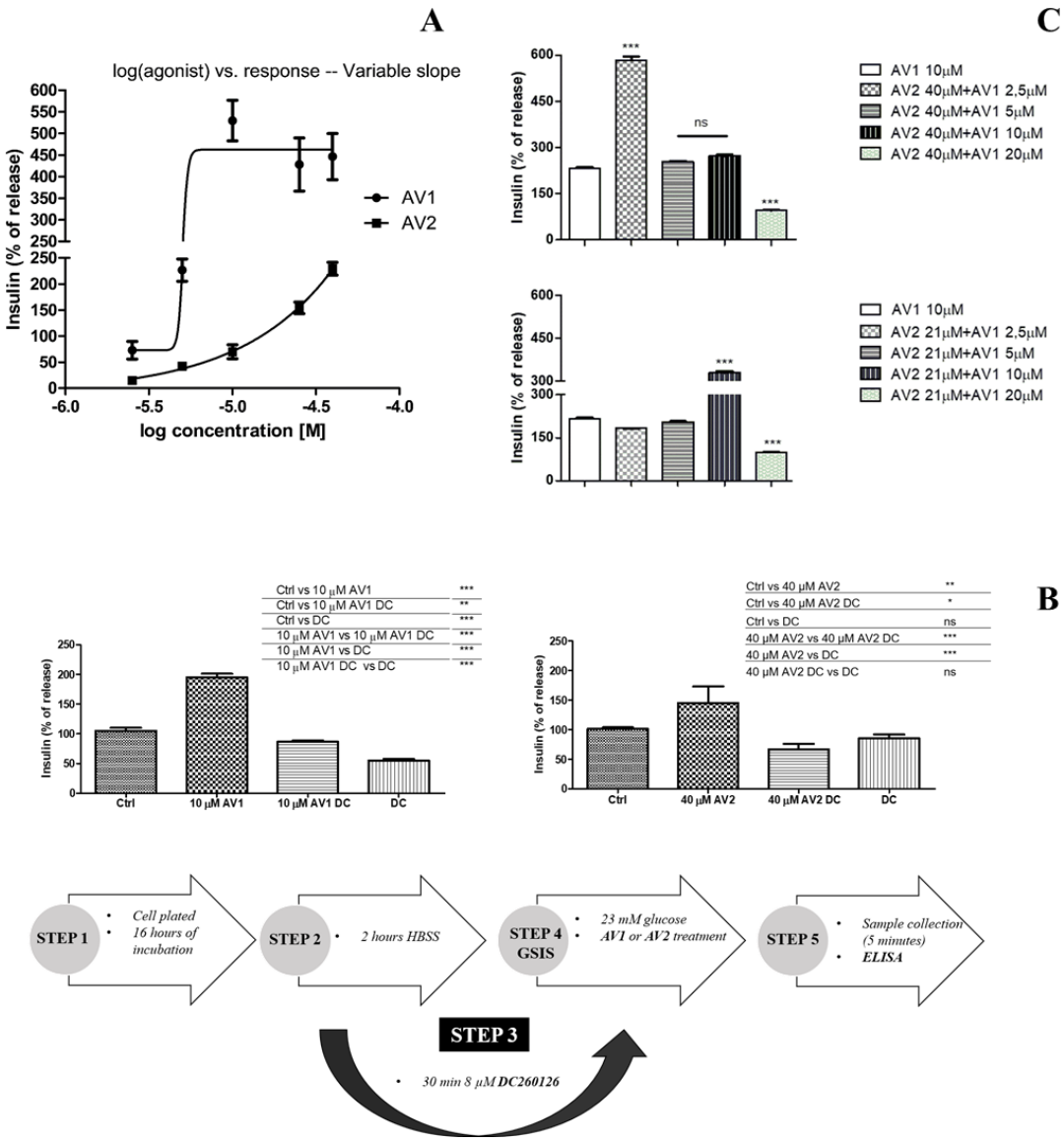

Figure 8. Functional profile of **AV1** and **AV2** in INS-1 832/13 cell line

same site occupied by the synthesized ligands. Pretreatment (30 min) with DC260126 (8 μM) significantly reduces **AV1**-induced GSIS (Figure 8B) demonstrating its receptor full agonist character. In fact, **AV1** interacts with GPR40 in a way that is not entirely identical to DC260126. Surprisingly, **AV2** did not favor GSIS at a dose of 10 μM, but it was necessary to reach the concentration of 40 μM to have a maximum secretion, but not saturated, with a curve not typically as a full agonist and an EC_{50} = 21 μM (Figure 8A-B). The same experiment conducted with DC260126 did not block **AV2**-induced insulin secretion showing different characteristics compared to **AV1**. This abnormal behaviour could be explained by a **AV2** partial agonism profile, whereby the cells were treated with doses 21 and 40 μM and pre-treated with increasing doses of **AV1** (2.5, 5, 10, 20, and 40 μM). Figure 8C shows how, at the lowest dose of **AV1** there is an accentuated increase in insulin secretion, greater than just treatment

with **AV1**, which demonstrates an additive effect of **AV2**. At higher doses of **AV1**, **AV2** exhibits antagonistic behavior by drastically reducing GSIS. When using 40 μM **AV2**, there is an additive effect up to the maximum secretion dose of **AV1** or 10 μM and subsequent reduction in insulin secretion, confirming that **AV2** is a GPR40 partial agonist *(Carullo et al., 2019b)*.

Quercetin-3-oleate as a wound healing agent

In order to assess the effect of **AV2** on wound healing and to verify the involvement of GPR40, the assays were performed by using Quercetin, OA and their physical mixture (QUE + OLE) at two different time points: 6 and 24 h. The reliability of the model was assessed by evaluating the spontaneous migration of untreated cells and by treating cells with 4 ng/mL TGF-β. Compared to the untreated control, TGF-β increased the wound healing rate by 49%, after 24 h. After 6 h we observed no increase in wound healing rate (data not shown); nevertheless, after 24 h of treatment, significant improvement of wound healing was obtained with Quercetin at the highest concentration tested (+25%, compared to the untreated control), while OA did not influence wound healing. Cotreatment with QUE + OLE improved the potency of the treatment, with the active concentration being 0.1 μM (+24% compared to the untreated control). The molecular hybrid **AV2**, instead, stimulated HaCaT wound healing by 47%, 35% and 51% compared to the untreated control, at the concentration of 0.01 μM, 0.1 μM and 1 μM, respectively (Figure 9 A-D). The activity of **AV2** was comparable to that of the positive control TGF-β, which is a well-known wound healing agent. **AV2** wound healing activity is related to the increase of keratinocytes growth factors, so the intracellular levels of TGF-β were dosed (Figure 9E). TGF-β levels are slightly, yet significantly, upregulated by 0.01 μM **AV2** (+ 6%, compared to the untreated control). MMP-9 release by skin keratinocytes and fibroblasts can be induced by stress-related physical and chemical factors but also by physiological stimuli such as growth factors, and is known to modulate the wound healing process. Consistently with the data obtained on TGF-β, MMP-9 was not released by HaCaT cells after **AV2** treatment (Figure 9F), suggesting that its wound healing effect may be mediated by different intracellular pathways. Cytokine production within the wound site participates in the recruitment of immune cells, which are necessary for the removal of cell debris and for fighting pathogens, and stimulates cell migration and wound closure. **AV2** was able to increase IL-6 release by 17%, compared to the untreated control, at the concentration of 0.01 μM (Figure 9G). Nevertheless, IL-1β and TNF-α releases were not affected by the treatment, thus excluding the possibility of an exaggerated inflammatory reaction (Figure 9 H-I). In the presence of DC260126 (pre-treatment 8 μM), **AV2** completely lost its activity, suggesting that **AV2** may act as a GPR40 agonist, leading to wound healing *(Carullo et al., 2019c)*.

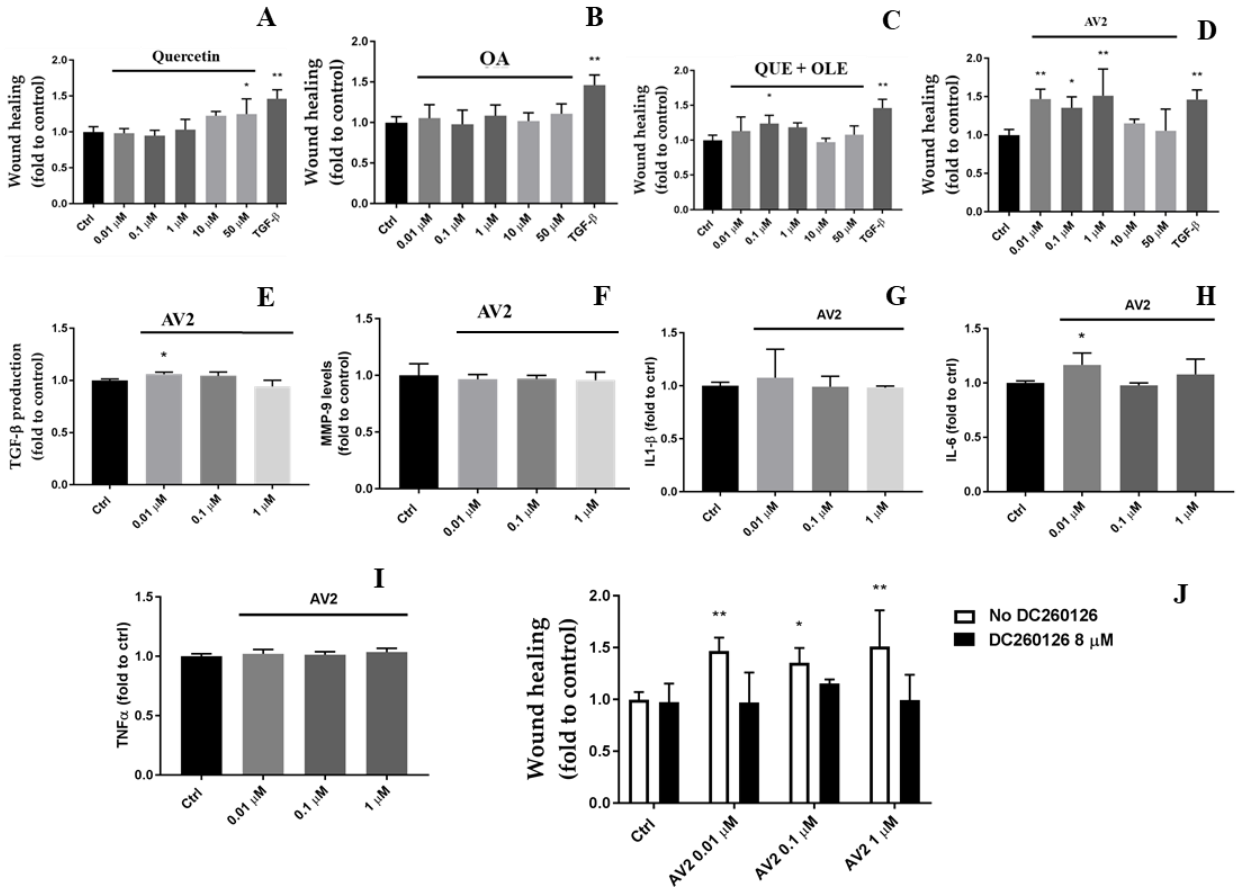

Figure 9. Wound healing activity of **AV2** in HaCaT cell line

Preliminary *in vivo* studies were realized in rats. After 24 h of surgery, rats were divided in three groups as follows: Group 1: Control-group: (n=9) receiving a daily topical treatment of iodopovidone; Group 2: Vehicle-group: (n=9) receiving a daily topical treatment of HA 0.2%; Group 3: (n=9) receiving a daily topical treatment with a fixed combination of HA + **AV2** 0.1%.

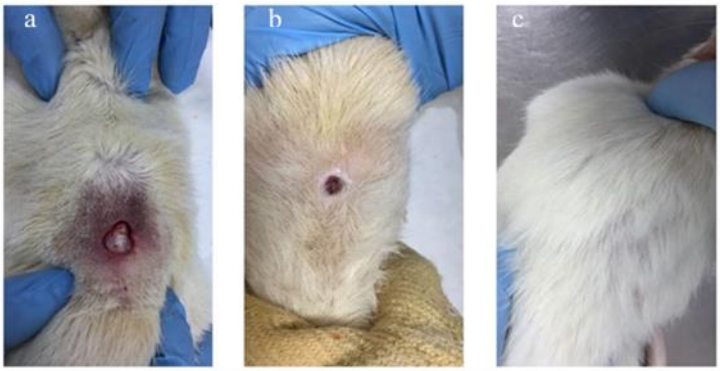

Figure 10. Representative imagine of experimental skin wound of group 3. Lesion before treatment, day 0 (a); at 9 days (b) and 27 days (c) after the beginning of the treatment with **AV2** 0.1% in hyaluronic acid 0.2%.

Time dependent wound healing is improved in HA + **AV2** 0.1% group 3 compared to others (Table 10). Data are expressed as mean ±standard deviation. * p<0.01 vs Group 1; #p<0.01 vs Group 2 (Figure 10). The recorded results are not thorough to establish the wound healing property of **AV2**, but suggest its favourable translation to patients, thanks to the low active doses and to the simple and cost-efficient synthetic method used.

Table 10. Time dependent wound healing in animal groups with experimental wound. Group 1: control group; Group 2: vehicle 0.2% HA. Group 3: HA + **AV2** 0.1%. Data are expressed as mean ± standard deviation. * P<0.01 vs Group 1; #P<0.01 vs Group 2.

Wound surgery and temporal treatment	**Group 1**	**Group 2**	**Group 3**	**P values**
Day 0				
Height (cm)	2±0.04	2.1±0.05	2.1±0.03	P>0.05
Length (cm)	2±0.03	2.1±0.04	2.08±0.02	P>0.05
Thickness (mm)	2.5±0.05	2.5±0.04	2.55±0.05	P>0.05
Day 6th				
Height (cm)	2±0.04	1.9±0.03	0.9±0.03*#	P<0.01
Length (cm)	2±0.03	1.9±0.03	1±0.04*#	P<0.01
Thickness (mm)	2.5±0.05	2.2±0.04	1.5±0.04*#	P<0.01
Day 9th				
Height (cm)	2±0.04	1.7±0.03*	0.5±0.03*#	P<0.01
Length (cm)	2±0.03	1.7±0.03*	0.5±0.03*#	P<0.01
Thickness (mm)	2.3±0.04	1.8±0.03*	0.5±0.03*#	P<0.01
Day 15th				
Height (cm)	1.5±0.03	0.8±0.02*	0.3±0.03*#	P<0.01
Length (cm)	1.3±0.02	0.8±0.02*	0.3±0.02*#	P<0.01
Thickness (mm)	1.8±0.03	0.6±0.02*	0.1±0.02*#	P<0.01
Day 27th				
Height (cm)	1±0.02	0.5±0.01*	0.1±0.01*#	P<0.01
Length (cm)	0.9±0.02	0.5±0.01*	0.05±0.01*#	P<0.01
Thickness (mm)	1.1±0.02	0.4±0.01*	0.03±0.01*#	P<0.01

FFA4/GPR120: design, synthesis and biological evaluation of Pinocembrin-fatty acid hybrids

GPR40 was the first member of the FFARs family to be deorphanized, demonstrating an involvement in metabolic disorders, including T2DM. Overall, chiefly GPR120 is activated by PUFAs with a signal transduction pathway that comprises $G_{q/11}$ proteins, with a consequentially increase in intracellular [Ca^{2+}] levels. However, experimental evidence reflects an activation of $G_{i/0}$ family and β-arrestin *(Watson et al., 2012)*. A growing number of molecules deriving from a similar core structure, decorated with a carboxylic head, a long aromatic chain, widely substituted, *(Milligan et al., 2017)* often interconnected by heteroatoms *(Adams et al., 2017)* are ligands of GPR120 which is a validated drug target in diabetes management. In line with this, chemically diverse new molecules were synthesized as selective GPR120 agonists *(Liu et al., 2015; Song et al., 2017)*. Another pharmacological interest is based on its potential role in inhibiting proliferation of DU145 prostate cancer cells. Also, it is an anti-obesity mark due to the involvement in the regulation of adipogenesis and inflammation *(Olmo et al., 2019)*. FFAs are eligible targets for diabetes management, albeit the distribution pattern of GPR120 suggests that it could be useful in other conditions, ranging from cancer to lung function *(Sebastiani et al., 2018)*. An additional scenario, that see GPCRs as key players, including GPR120, is the skin wound healing process. Skin wound healing represents a clinical problem, and nowadays a lot of natural products are counted as possible remedies *(Tsioutsiou et al., 2016)*. In fact the proton-sensing GPR4, GPR65 (TDAG8), GPR68 (OGR1) and GPR132 (G2A) are activated *via* a decrease in pH (as it happens in the wound) and transduce this signal to molecular intracellular pathways that converge in tissue repair *(Weiß et al., 2017)*. PUFAs, the endogenous FFA ligands, demonstrated to be fruitful wound healing agents, *(Komprda et al., 2018)* with particular emphasis on DHA, which is able to promote wound healing targeting GPR120 *in vitro* and *in vivo (Chao et al., 2014; Arantes et al., 2016)*. Several GPR120 ligands have been synthesized over the years, but only fatty acids resulted from a natural source. A recent study proposed a virtual screening in order to identify new and effective GPR120 ligands of natural origin. Based on this model, the flavanone Pinocembrin (**HW0**) was found to be a good hit for the development of new GPR120 ligands *(Chintakunta et al., 2018)*. **HW0** is a remarkable flavanone, found in bee products and licorice leaves, *(Aiello et al., 2017)* with well-known anti-inflammatory *(Frattaruolo et al., 2019)* and wound healing properties *(Governa et al., 2019)*. In this field, in order to highlight the bioavailability of the **HW0**, its acylation with fatty acids was proposed. Three hybrid molecules were synthesized with the same biocatalytic approach used for **AV2** and assayed in scratch wound healing assay as suitable GPR120 ligands in HaCaT cell line.

Results and Discussion

Chemistry

The representative oleoyl (ω-9), linoleoyl (ω-6) and linolenoyl (ω-3) ester derivatives of **HW0** were synthesized by using a bio-catalytic approach. Employing the 1:1 ratio between acyl donor and **HW0**, by using acetone as solvent and PPL, three new compounds were synthesized: (*S*)-5-hydroxy-4-oxo-2-phenylchroman-7-yl oleate (**HW1**), (*S*)-5-hydroxy-4-oxo-2-phenylchroman-7-yl (9Z,12Z)-octadeca-9,12-dienoate (**HW2**) and (*S*)-5-hydroxy-4-oxo-2-phenylchroman-7-yl (9*Z*,12*Z*,15*Z*)-octadeca-9,12,15-trienoate (**HW3**). The hybrid compounds were obtained in good yields after a simple filtration as unique product of the reaction, with the possibility of re-use the enzyme, which is a sustainable alternative. This procedure demonstrated for the first time that, PPL was able to catalyze the acylation of 7-OH position in polyphenol core, in absence of an alcoholic position in the ring, that resulted preferred when present.

Experimental part

Procedure e) General procedure for the preparation of semisynthetic pinocembrin derivatives

In a round-bottom flask, to a solution of Pinocembrin (1 equiv.) and fatty acid (1 equiv.) in acetone (30 mL) PPL (260 mg) was added. Temperature was maintained at 37 °C, with an agitation rate of 130 rpm. After 24 h, the crude mixture was filtered, washed with a cold solution of $NaHCO_3$ and extracted with Et_2O, to afford the corresponding product (Scheme 1).

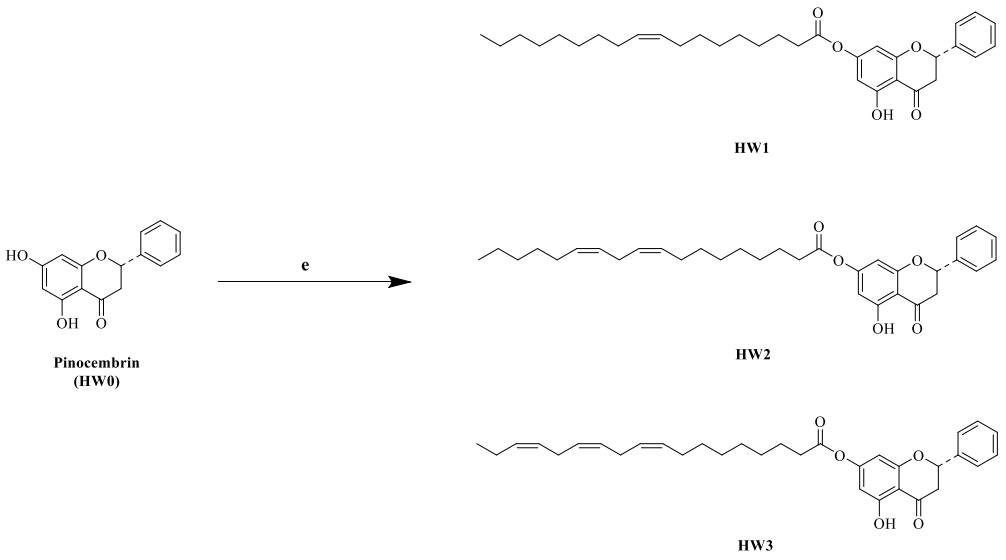

Scheme 2. Synthesis of Pinocembrin derivatives

Reagents and conditions: e) fatty acid (1 equiv.) [OA for **HW1**, linoleic acid for **HW2**, linolenic acid for **HW3**], PPL (260 mg), pH = 7.8, 37 °C at 130 rpm, incubation time of 48 h.

5-Hydroxy-4-oxo-2-phenylchroman-7-yl oleate **HW1**: White resin, 84% yield. ^{1}H-NMR (300 MHz, $CDCl_3$) δ 12.1 (bs, 1H), 7.6-7.3 (m, 5H), 6.0-5.9 (m, 2H), 5.6-5.5 (m, 3H), 3.2-3.1 (m, 2H), 2.8-2.7 (m, 2H), 2.1-1.9 (m, 4H), 1.6-1.4 (m, 2H), 1.4-1.2 (m, 20H), 0.89 (t, 3H, J= 3.6 Hz.). ^{13}C-NMR (75 MHz, $CDCl_3$) δ 195.5, 175.9, 163.1 (x2C), 157.0, 129.9 (x2C), 129.6 (x2C), 128.8 (x2C), 126.0, 98.0, 97.0, 96.7, 79.1, 43.2, 31.8, 29.7, 29.6 (x2C), 29.4 (x3C), 29.3, 29.2, 29.1, 29.0 (x2C), 24.8, 22.6, 14.0.

5-hydroxy-4-oxo-2-phenylchroman-7-yl-octadeca-9,12-dienoate **HW2**: Light brown amorphous solid, 82% yield. ^{1}H-NMR (300 MHz, Acetone d_6) δ 12.1 (bs, 1H), 7.6-7.3 (m, 5H), 6.0 (dd, 2H, J= 2.12, 9.30 Hz.), 5.6-5.2 (m, 5H), 3.2-3.1 (m, 2H), 2.8-2.7 (m, 2H), 2.27 (t, 2H, J = 3.1 Hz.), 2.1-2.0 (m, 4H), 1.6-1.5 (m, 2H), 1.4-1.2 (m, 14H), 0.89 (t, 3H, J = 2.47 Hz.). ^{13}C-NMR (75 MHz, Acetone d_6) δ 195.7, 176.3, 166.7, 164.3, 163.2, 139.1, 129.8 (x2C), 129.7 (x2C), 128.5 (x2C), 128.4, 127.8 (x2C), 127.8, 102.2, 96.1, 78.9, 42.7, 33.5, 31.7, 31.3, 29.7, 29.4, 29.3, 29.1, 28.9 (x2C), 25.3, 24.8, 22.2, 13.4.

5-Hydroxy-4-oxo-2-phenylchroman-7-yl-octadeca-9,12,15-trienoate **HW3**: Dirty white resin, 93% yield. ^{1}H-NMR (300 MHz, CD_3OD) δ 12.1 (bs, 1H), 7.6-7.3 (m, 5H), 6.1-6.0 (m, 2H), 5.5-5.0 (m, 7H), 3.5-3.0 (m, 2H), 2.9-2.7 (m, 4H), 2.4-2.0 (m, 6H), 1.8-1.6 (m, 2H), 1.5-1.2 (m, 8H), 1.1-0.9 (t, 3H, J= 8.08 Hz.). ^{13}C-NMR (75 MHz, CD_3OD) δ 195.7, 176.3, 166.9 (x2C), 163.1, 138.8, 131.3, 129.7, 128.3 (x2C), 128.2 (x2C), 127.8, 127.4, 126.8, 125.8 (x2C), 98.6, 98.5, 95.9, 78.9, 42.8, 33.6, 29.4, 29.3, 28.9, 28.8, 26.8, 25.2 (x2C), 25.1, 20.1, 13.4. *(Mazzotta et al., 2020)*.

Docking simulations and functional evaluation in HaCaT cell line

HW0 was able to stimulate HaCaT wound healing after 6 and 24 h (about +30% compared to the untreated control). **HW1** and **HW2** were less active (about +10% compared to the untreated control) only after a 24 h of treatment. **HW3** stimulated HaCaT wound closure (about +40% compared to the untreated control) after 6 and 24 h (Figure 11). Thus, the remaining experiments were focused on **HW0** and **HW3**. In the attempt to confirm the involvement of GPR120 in the wound healing mechanism of action of **HW0** and **HW3**, docking simulations were performed and the scratch wound healing assay in the presence of a GPR120 antagonist (AH7614 10 µM).

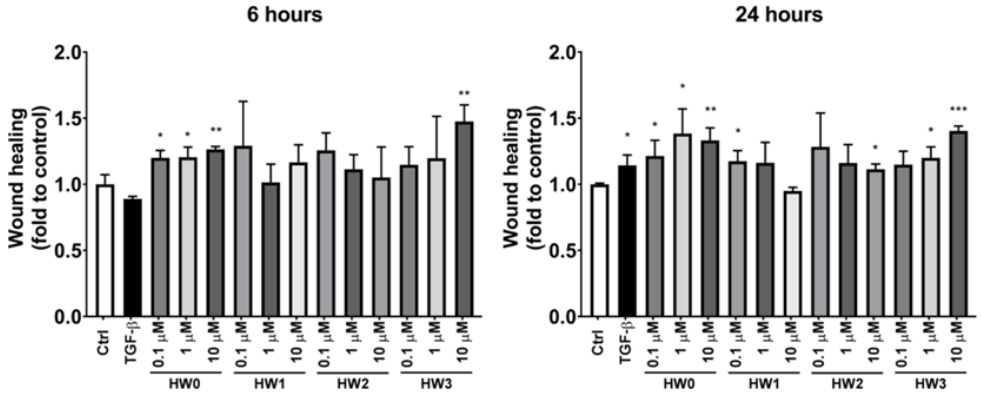

Figure 11. Scratch wound healing assay of **HW** compounds

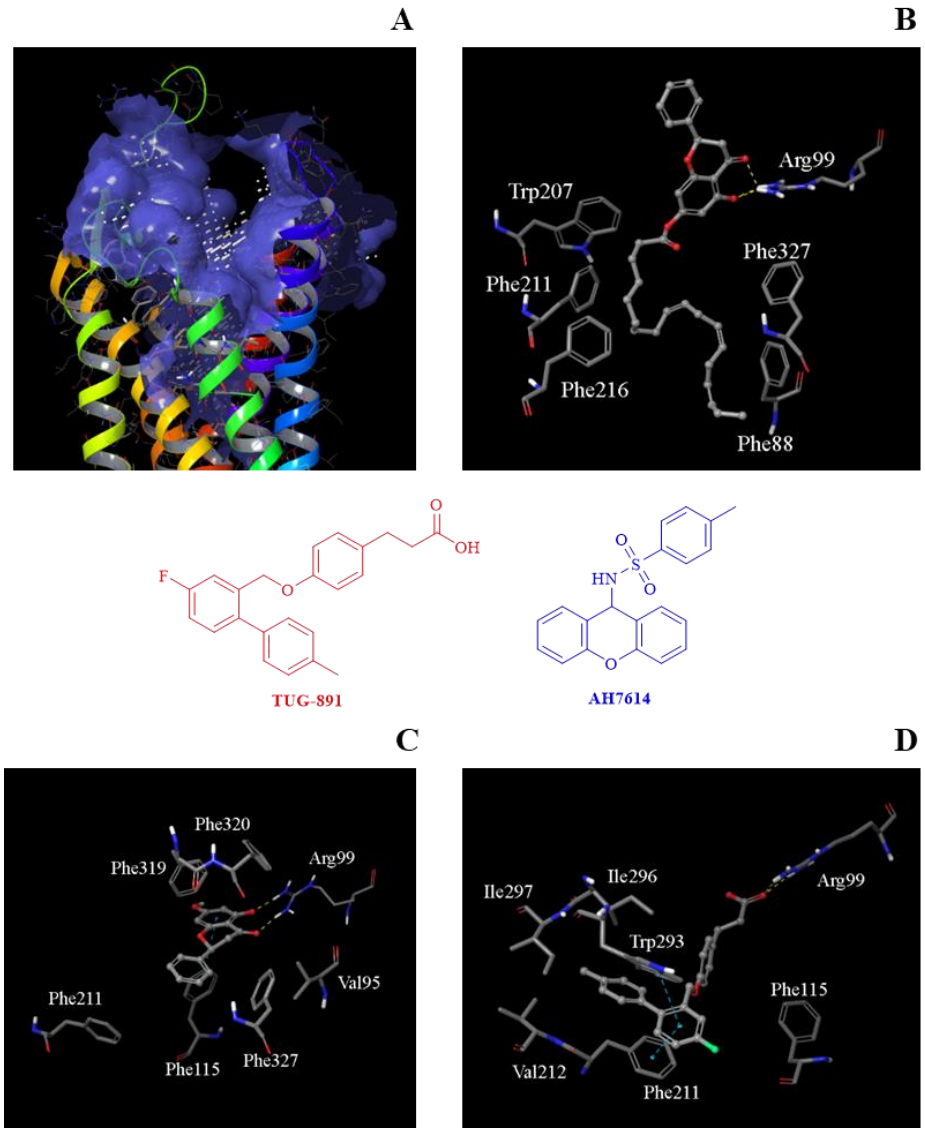

Figure 12. Docking simulations of **HW0** and **HW3** on GPR120 structure

The homology model was used because the crystal structure of the receptor is not available yet (Figure 12A). Results from docking calculations (realized as reported in computational detaiòs section) show that the best docked

pose of **HW3** is characterized by its Pinocembrin scaffold located at the extracellular entrance of the binding pocket, while the long alkyl chain is penetrating within a tunnel between protein helices. The most important anchor points for the ligand are represented by multiple hydrogen bonds between the C4 carbonyl and the C5 hydroxyl oxygen atoms with the guanidino moiety of Arg99. A significant number of additional hydrophobic interactions are found between the long alkyl chain and aromatic residues, such as Phe88, Trp207, Phe211, Phe216, and Phe327 (Figure 12B). On the other hand, when the simple structure of Pinocembrin was docked, the best result shows the pendant phenyl ring embedded within an aromatic cage defined by Phe88, Phe211, Phe319, Phe320, and Phe327. A π-π interaction is found between the condensed aromatic ring of the ligand and the side chain of Phe115. Additional hydrophobic contacts with Val95 and Val323 are profit-able for binding (Figure 12C). Moreover, the C4 carbonyl oxygen and the C5 hydroxyl group are involved in multiple hydrogen bonds with the terminal guanidino moiety of Arg99. An additional hydrogen bond is found between the C7 hydroxyl group of **HW0** and the backbone carbonyl oxygen of Cys194. Finally, considering that a hypothesis for the competition of **HW** compounds and the GPR120 agonist TUG-891 emerged from experimental results, docking simulations have been also performed on such a compound following the same computational protocol. As a result, the terminal carboxyl group of TUG-891 makes two hydrogen bond with the guanidino group of Arg99. The complex is further stabilized by π-π interactions between the central phenyl ring and both Phe211 and Trp293. The terminal tolyl moiety is accommodated within a hydrophobic cavity defined by Val212, Ile297, Ile300, Ile296, and Phe211 (Figure 12D). These computational results suggest that HW compounds could be able to bind the human GPR120 by occupying a long binding site located between the extracellular region and the inter-helical space. Moreover, the same binding site seems to be shared with the GPR120 agonist TUG-891 that shows a competitive activity toward HW compounds. As shown in Figure 13A, both **HW0** and **HW3** completely lose their activity when the GPR120 antagonist was added, thus, confirming the results obtained by molecular docking simulation. Moreover, **HW0** and **HW3** reversibly reduced the wound healing activity of a known GPR120 agonist (TUG-891), which could be due to a competition for the same binding pocket (Figure 13B), hypothesized by molecular docking simulations. Consistently with Arantes and colleagues,[23] the activation of GPR120 by **HW0** and **HW3** led to the increase of TGF-β levels (Figure 14A), which contributes to wound healing. Moreover, **HW0** did not altered MMP-9 levels, which is consistent with the observation of Fukushima and co-workers.[35] Nevertheless, a slight increase on MMP-9 levels was observed with **HW3** at high concentrations. The modulation of the immune response is also strictly involved in the wound healing process.[36] **HW3** was able to stimulate the release of IL-1β

(+10%) and TNF-α (+10%), but not IL-6, in THP-1 monocytes, compared to the untreated control (Figure 14C, D, E).

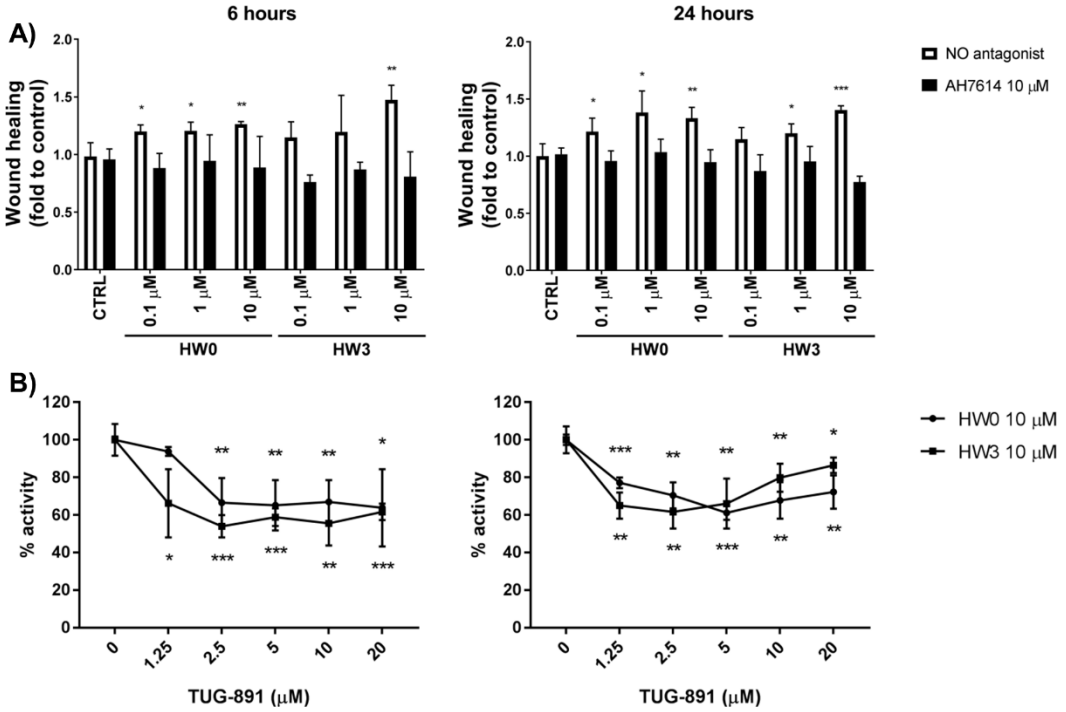

Figure 13. HW0 and **HW3** accelerate HaCaT cells wound healing through GPR120/FFA4

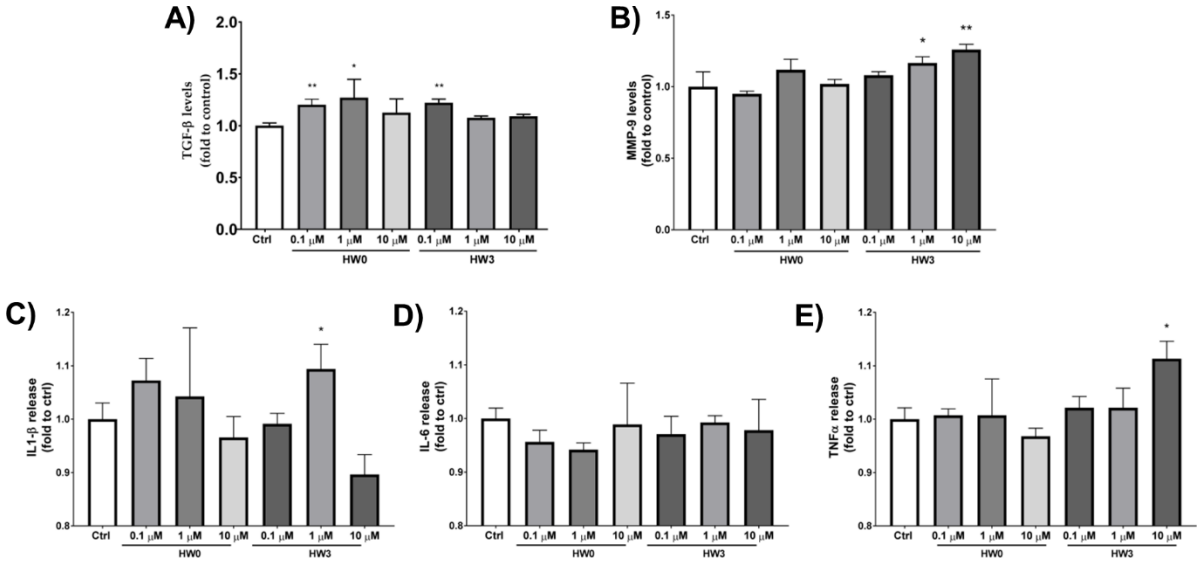

Figure 14. Effect of **HW0** and **HW3** on TGF-β (A) and MMP-9 (B) levels in HaCaT cells and on IL-1β (C), IL-6 (D) and TNF-α (E) release by THP-1 cells.

Chapter 3

Quercetin and Morin: semi-synthesis of new $K_{Ca}1.1$ and $Ca_v1.2$ channel modulators

Materials & Methods

Chemicals

The chemicals included collagenase (type XI), trypsin inhibitor, BSA, tetraethylammonium chloride, papain, DL-dithiothreitol, EGTA, BAPTA, taurine, nicardipine, carbachol, phenylephrine. Nicardipine dissolved directly in ethanol, while substances, dissolved in DMSO were diluted at least 1000 times before use. The resulting concentrations of DMSO and ethanol (below 0.1%, v/v) failed to alter the response of the preparations (data not shown).Phenylephrine was dissolved in bidistilled water.

Cell isolation procedure for $I_{Ca(L)}$ recordings

Smooth muscle cells were freshly isolated from the tail main artery incubated at 37°C in 2 ml of 0.1 mM Ca^{2+} external solution (see below for composition) containing 1 mg/mL collagenase (type XI), 1 mg/mL soybean trypsin inhibitor, and 1 mg/mL BSA, gently bubbled with a 95% O_2, 5% CO_2 gas mixture. Cells exhibited an ellipsoid form (10-15 µm in width, 35-55 µm in length) and were continuously superfused with external solution containing 0.1 mM Ca^{2+} and 30 mM tetraethylammonium using a peristaltic pump (LKB 2132; Bromma, Sweden) at a flow rate of 400 µL/min. Cell membrane capacitance averaged 40.53 ± 1.46 pF (n= 49) and was not affected by the application of the substances. The τ of the voltage-clamp averaged 0.52 ±0.05 ms (n= 49).

Cell Isolation Procedure for $K_{Ca}1.1$ Current Recordings

Smooth muscle cells were isolated from the tail main artery stored overnight at 4°C in 1 mL of solution for enzymatic cell isolation containing 1.5 mg papain, 0.4 mg of DL-dithiothreitol, and 1.6 mg of BSA and incubated, the day after, for 5 to 15 min at 37°C in the abovementioned solution, gently bubbled with a 95% O_2, 5% CO_2 gas mixture. Cells, characterized by an elongated shape (8–-12 µm in width, 40-50 µm in length), were continuously superfused with the recording solution at a flow rate of 400 µL/min using a peristaltic pump (LKB 2132; Bromma, Sweden). Cell membrane capacitance averaged 22.72 ± 1.56 pF (n= 34) and was not affected by the application of substances. The τ of the voltage-clamp averaged 0.32 ± 0.03 ms (n= 34).

Whole-Cell Patch-Clamp Recordings

The conventional whole cell patch-clamp method was employed to voltage-clamp smooth muscle cells. Recording electrodes were pulled from borosilicate glass capillaries (WPI, Berlin, Germany) and fire polished to obtain a pipette resistance of 2 to 5 MΩ when filled with internal solution. A low-noise, high-performance Axopatch 200B patch-clamp amplifier (Molecular Devices Corporation, Sunnyvale, CA) driven by a personal computer in conjunction with an A/D,D/A board (DigiData 1200 A/B series interface; Molecular Devices Corporation) was used to generate and apply voltage pulses to the clamped cells and record the corresponding membrane currents. At the beginning of each experiment, the junction potential between the pipette and bath solutions was electronically adjusted to zero. Cell break-in was accomplished by gentle suction at a holding potential (V_h) of either -40 or -50 mV for $K_{Ca}1.1$ current recordings and for $I_{Ca(L)}$ and $I_{Ba(L)}$ recordings, respectively. V_h then was set to -80 mV [$I_{Ca(L)}$ and $I_{Ba(L)}$ recordings]. Micropipette seals had to be GΩ in nature with leak currents less than 0.25 pA/mV. Current signals, after compensation for whole-cell capacitance and series resistance (between 70 and 80%), were low-pass filtered at 1 kHz and digitized at 3 kHz before being stored on the computer hard disk. Electrophysiological responses were tested at t = 20-22°C) only in those cells that were phase-dense. The findings presented here, obtained with the traditional whole-cell patch-clamp technique, may not necessarily reflect normal cellular physiology because of cytoplasmic disruption, non-physiological ionic concentrations, artificial Ca^{2+} buffering, and loss of soluble signaling molecules during dialysis.

$I_{Ca(L)}$ and $I_{Ba(L)}$ Recordings

$I_{Ca(L)}$ or $I_{Ba(L)}$ was always recorded in 30 mM tetraethylammonium- and 5 mM Ca^{2+}-containing external solution or 5 mM Ba^{2+}-containing external solution, respectively. Current was elicited with 250-ms clamp pulses (0.067 Hz), eitherto 0 mV or to 10 mV, from a V_h of -80 mV until a stable current response was achieved (usually 7-10 min after the whole-cell configuration had been obtained). At this point, the various protocols were performed as detailed below. Both $I_{Ba(L)}$ and $I_{Ca(L)}$ did not run down over the next 20 to 30 min under these conditions. Current-voltage relationships were fitted with the equation $I_{Ba} = G_{Ba}\ (1/1 + \exp((E_{50} - E_m)/k))\ (E_m - E_{rev})$, where G_{Ba} is the maximal available conductance, E_{50} is the membrane potential at half-maximal current activation, E_m is the membrane potential, k is the slope factor, and E_{rev} is the reversal potential. Steady-state inactivation curves, recorded twice from the same cell (in absence and presence of the substance, respectively), were obtained using a double-pulse protocol. Once various levels of the conditioning potential had been applied for 5 s, followed by a

short (5 ms) return to the V_h, a test pulse (250 ms) to 0 mV was delivered to evoke the current. Under control conditions, the 50% inactivation potential evaluated by fitting a Boltzmann distribution to the first curve was not significantly different from that of the second curve recorded after 10 min. Activation curves were derived from the current-voltage relationships Conductance (G) was calculated from the equation $G = I_{Ba}/(E_m - E_{rev})$, where I_{Ba} is the peak current elicited by depolarizing test pulses in the range of -50 to 10 mV from V_h of -80mV, E_m is the membrane potential, and E_{rev} is the reversal bi-ionicpotential (166 mV, as estimated with the bi-ionic equation assuming a permeability ratio P_{Ba}/P_{Ca} for $Ca_{v1.2}$ channels of 0.4; G_{max} is the maximal Ba^{2+} conductance (calculated at potentials -10 mV). The ratio G/G_{max} was plotted against the membrane potential and fitted with the Boltzmann equation. The window current was calculated by multiplying the activation conductance curve by the inactivation curve. Permeability (PS) was derived from the Goldman-Hodgkin-Katz current equation. A two-pulse protocol was applied to measure the time course of recovery from inactivation: 2-s clamp pulses to 0 mV from a V_h of -80 mV were followed by a return to the V_h of variable duration to allow some channels to recover from inactivation. A second pulse (250 ms) to 0 mV was delivered to determine how much recovery had occurred during the time interval. K^+ currents were blocked with 30 mM tetraethylammonium in the external solution and Cs^+ in the internal solution. Current values were corrected for leakage using 300 µM Cd^{2+}, which was proven to block completely $I_{Ba(L)}$ and $I_{Ca(L)}$. Following control measurements, each cell was exposed to the substances by flushing through the experimental chamber solution containing the substance.

K_{Ca}1.1 Current Recordings

K_{Ca}1.1 recordings were performed in the presence of nicardipine, a Ca_v1.2 channel blocker, as well as at low external Ca^{2+} concentration (i.e., 0.1 mM) to minimize the contribution of extracellular Ca^{2+} influx to the current recorded. K_{Ca}1.1 current was measured over a range of test potentials (500 ms) from -20 to 100 mV from a V_h of -40 mV. Data were collected once the current amplitude had been stabilized usually 8 to 10 min after the whole-cell configuration had been obtained. K_{Ca}1.1 current did not run down over the next 20 to 30 min under these conditions.

Solutions for $I_{Ca(L)}$ and $I_{Ba(L)}$ Recordings

The external solution contained 130 mM NaCl, 5.6 mM KCl, 10 mM HEPES, 20 mM glucose, 1.2 mM $MgCl_2 \times 6$ H_2O, and 5 mM sodium pyruvate (pH 7.4). For cell isolation, external solution containing 20 mM taurine was prepared by replacing NaCl with equimolar taurine. $CaCl_2$ or $BaCl_2$ (both 5 mM, final concentration) and

tetraethylammonium (30 mM) were added to the external solution for $I_{Ca(L)}$ and $I_{Ba(L)}$ recordings. The internal solution (pCa 8.4) consisted of 100 mM CsCl, 10 mM HEPES, 11 mM EGTA, 2 mM $MgCl_2$, 1 mM $CaCl_2$, 5 mM sodium pyruvate, 5 mM succinic acid, 5 mM oxalacetic acid, 3 mM Na_2-ATP, and 5 mM phosphocreatine; pH was adjusted to 7.4 with CsOH. The osmolarity of the 30 mM tetraethylammonium- and 5 mM Ca^{2+}- or Ba^{2+}-containing external solution was adjusted to 320 mOsmol and that of the internal solution to 290 mOsmol by means of an osmometer (Osmostat OM 6020; Menarini Diagnostics, Florence, Italy).

Solutions for $K_{Ca}1.1$ current recordings

Solution for enzymatic cell isolation contained 110 mM NaCl, 5 mM KCl, 2 mM MgCl × 6 H_2O, 0.16 mM $CaCl_2$, 10 mM NaHEPES, 10 mM $NaHCO_3$, 0.5 mM KH_2PO_4, 0.5 mM NaH_2PO_4, 10 mM glucose, 0.49 mM Na_2EDTA, and 10 mM taurine (pH 7). Recording solution contained 145 mM NaCl, 6 mM KCl, 10 mM glucose, 10 mM HEPES, 5 mM sodium pyruvate, 1.2 mM $MgCl_2$ × 6 H_2O, 0.1 mM $CaCl_2$, and 0.003 mM nicardipine (pH 7.4). Internal solution contained 90 mM KCl, 10 mM NaCl, 10 mM HEPES, 10 mM EGTA, 1 mM MgCl2×6 H_2O, and 6.41 mM $CaCl_2$ (pCa 7.0), pH 7.4.

Solutions for functional experiments

The physiological salt solution contained 125 mM NaCl, 5 mM KCl, 2.7 mM $CaCl_2$, 1 mM $MgSO_4$, 1.2 mM KH_2PO_4, 25 mM $NaHCO_3$, and 11 mM glucose (pH 7.35).

Statistical Analysis

Acquisition and analysis of data were accomplished by using pClamp 9.2.1.8 software (Molecular Devices Corporation) and Prism version 5.02 (GraphPad Software, Inc., La Jolla, CA). Data are reported as the mean ± S.E.M.; *n* is the number of cells or rings analyzed (indicated in parentheses) isolated from at least three animals. Statistical analyses and significance as measured by either analysis of variance (ordinary or repeated measures followed by Dunnett's post-test), one sample *t* test, or Student's *t* test for unpaired and paired samples (two-tailed) were obtained using InStat version 3.06 (GraphPad Software, Inc.). In all comparisons, $p < 0.05$ was considered significant.

Molecular docking simulations

The best template for *Rattus norvegicus* K^+ channel homology models was identified with the query sequence (in FASTA format) of target proteins and was uploaded in the designated entry. Parameters were selected as follows: Protein Data Bank (PDB) proteins as template search database and BLOSUM45 as substitution matrix, to gain a more restrictive score for aligning any possible pair of residues. Remaining parameters were selected by default. The choice of the template represents a compromise between "identity sequence" (89 %) and "query cover" (99 %). Template crystal structure, chosen for the genetic relationship through the BLASTP web tool, was downloaded from PDB (https://www.rcsb.org/). The PDB code for Homo sapiens $K_{Ca}1.1$ transmembrane domain (5TJ6) was Q62976 (RMSD value 0.345). Channel homology modelling was performed by Pymod 2.0; mutagenesis experiments were performed on binding pockets, only on residues critical to channel modulation. To establish molecule behaviour towards the phospholipid double layer and their metabolic fate, the relationship between TPSA and Consensus Log $P_{o/w}$ was evaluated by SWISSADME web tool. AutoDock/VinaXB was used to perform all ligand-protein docking simulations; parameters used were selected by default. The grid boxes were set to 20 Å×20 Å×25 Å, with a grid space value of 1 Å. By default, a maximum of 10 poses per ligand were collected. Docking simulation results were analysed using PyMOL v. 2.0. PLIP and LigPlot+ tools, used in default configuration, predicted all relevant K^+ channel-molecule interactions, and detected key residues necessary for biological activity *(Fusi et al., 2020)*. The rat $Ca_v1.2$ channel α1C subunit sequence (NP_036649.2) was retrieved from the NCBI ProteinDatabase (http://www.ncbi.nlm.nih.gov/protein/). This hasfour repeats, each containing six transmembrane helices (S1–S6) and a P-loop between S5 and S6. The quality of the homology model is given by the accuracy of the sequence alignment and the resolution of the template structures used. A PSI-BLAST search for rat α1C subunit sequences was firstly performed in order to obtain the best template of the unit and the tetrameric portion of the model. The disposition of both P-loops and inner helices was derived from earlier structure templates. When viewed from the extracellular side, the repeats I–IV were arranged clockwise around the central pore. This channel model was built using the Swiss Pdb Viewer-Deep View version 4.1, which allowed us also to define the consistency of bond distances, bond angles and torsion angles with the values of standard proteins. Docking of ligands was simulated by using flexible side chains protocol with AutoDock/Vina version 1.1. This program used an iterated local search global optimizer algorithm based on a succession of steps, which consisted of mutation and local optimization. The generation and affinity grid maps, view of docking poses and analysis of virtual screening results were carried out by using AutoDock plug-in of PyMOL. The dimensions of the box for docking calculation (60Å×60Å×60Å) were sufficiently great to include not only the active docking site, but also significant

portions of the surrounding surface. The corresponding ΔG values were computed by comparing them with the wild type protein, thus allowing the evaluation of individual residue contribution towards ligand interaction *(Saponara et al., 2016)*.

Quercetin: a multifaceted tool for the development of new suitable anti-hypertensive agents

Quercetin is natural compound that captured scientific attention, since it has numerous beneficial properties, and especially because it is easily detachable from a variety of food sources, such as cherries, apple, red wine, cappers and red onion *(Gharras, 2009)*. Both Quercetin and its derivatives are involved in several physiological functions, exerting anti-inflammatory, anti-infectious, anticancer/chemopreventive, neuroprotective, blood glucose lowering and antihypertensive properties have been reported. Focusing on cardiovascular disease, results from clinical studies demonstrated how Corvitin (Quercetin for intravenous administration) had beneficial effects on clinical forms of ischemic heart disease, including myocardial infarction. The antiarrhythmic action of Corvitin may be the result of its membrane-stabilizing action, as well as of the improvement of intracardiac hemodynamics due to reduction of myocardial stress. Quercetin action results in faster stabilization of the necrotic zone and the decreased mass of the necrotized myocardium *(Shebeko et al., 2018)*. In isolated heart (*ex vivo* models) of ischemia/reperfusion injury, an acute administration of Quercetin (15 mmol/L infusion for 15 min before the onset of ischemia or during whole reperfusion, respectively) improved recovery of cardiac function after global ischemia/reperfusion (25 min/2 h) in Langendorff-perfused rat hearts *(Barteková et al., 2010)*. Quercetin pre-treatment (50 mg/kg) of rats with isoproterenol-induced myocardial infarction induced cardio-protective effects manifested by significantly attenuated oxidative stress, inflammation, as well as protected heart architecture, with a downregulation of the expression of calpain *(Kumar et al., 2017)*. Lewis rats treated with Quercetin (10 mg/kg) obtained a protection against progression of myocarditis by suppression of oxidative and endoplasmic reticulum stress via endothelin-1/MAPK signalling *(Arumugam et al., 2012)*. Furthermore, in patients with stable coronary heart disease, Quercetin (120 mg/day for 2 months, p.o.) significantly improved the left ventricular systolic function in terms of ejection fraction and improved left ventricular diastolic function in terms of the ratio of the phases of the transmitral flow *(Malishevskaia et al., 2013)*. From the medicinal chemistry point of view, the cardiovascular properties of Quercetin could be attributed to various targets. In particular, Quercetin was able to activate various cation channels. Among the Ca^{2+}- channels, Ca_v channels constitute the dominant Ca^{2+} influx route. Ca_v channels possess several functions in the cardiovascular system: action potential generation and

pacemaking activity, generation of systolic Ca^{2+} influx in cardiomyocytes (cardiac inotropism and atrial excitability), generation of Ca^{2+} influx in vascular smooth muscle and endothelial cells (arterial myogenic tone and vascular resistance). Ca^{2+} channels form hetero-oligomeric complexes that are composed of a pore-forming α1 subunit. The ten cloned α1 subunits can be grouped into three families: the high-voltage activated dihydropyridine-sensitive (L-type, CaV1.x; $Ca_v1.2$ in cardiacand vascular myocytes) channels; the high-voltage activated dihydropyridine-insensitive (CaV2.x) channels and the low-voltage-activated (T-type, CaV3.x) channels. The α1 subunit has four homologous repeats (I–IV) bearing six transmembrane domains and a pore-forming region between transmembrane domains S5 and S6. The pore loop contains a unique structural feature, i.e. a pair of glutamate residues that confers Ca^{2+} selectivity to the channel. Quercetin is a stimulator of $Ca_v1.2$ current in clonal rat pituitary GH4C1 cells, *via* cAMP-induced activation of PKA *(Huang et al., 2009)*. In vascular smooth muscle cells, stimulation of $Ca_v1.2$ channels is rather specific, since Quercetin does not affect the co-expressed $Ca_v3.1$ channels (*Saponara et al., 2002*). Also, $Ca_v1.2$ channel stimulation by Quercetin determines an influx of extracellular Ca^{2+} that is not sufficient to overcome its myorelaxing activity. This hypothesis is corroborated by the observation that maximal activation of $Ca_v1.2$ channels by Bay K 8644 (i.e. larger influx of extracellular Ca^{2+} as compared to that measured with Quercetin alone) indeed prevails over Quercetin-induced myorelaxation, thus causing smooth muscle contraction *(Fusi et al., 2003)*.

Quercetin was also able to activate $K_{Ca}1.1$ channel currents. K^+ channels are widely expressed in cardiovascular system, divided in: voltage-gated (K_V), K_{Ca}, two-pore domain (K_{2P}), and inwardly rectifying (K_{ir}) K^+ channels. Specifically, K_{Ca} channels are divided into three different classes: the big-conductance ($K_{Ca}1.1$), the small-conductance ($K_{Ca}2.1$, 2.2, and 2.3), and the intermediate-conductance K^+ ($K_{Ca}3.1$) channels *(Eichhorn et al., 2007)*. K_{Ca} channels possess a pore-forming, voltage sensitive α-subunit and a regulatory β-subunit; α-subunit contains an additional seventh transmembrane region (S0). Ca^{2+}-sensitivity is conferred by four intracellular domains (S7-S10) and by the interaction of S0 with an auxiliary β1 subunit (the predominant isoform in vascular smooth muscle). $K_{Ca}1.1$ channels are stimulated by membrane depolarization and/or changes in the sub-plasmalemmal Ca^{2+} concentration, and controlled by numerous intracellular chemical ligands such as Mg^{2+}, protons, carbon monoxide, ethanol, heme, and lipid molecules as well as by signalling molecules such as PKA, PKC and H_2S. The role of $K_{Ca}1.1$ channels in cardiomyocytes is limited by their low expression. Decreased $K_{Ca}1.1$ channel function, which may lead to vasoconstriction, has been linked to a number of pathological conditions, including hypertension, diabetes, ischemia/reperfusion, haemorrhagic shock, atherosclerosis, and brain injury *(Zhang et al., 2010)*. Thus, $K_{Ca}1.1$ channels may be important targets for therapeutic intervention in a variety of cardiovascular

disorders. Quercetin causes coronary vasodilation that has been ascribed, at least in part, to a H_2O_2-mediated increase of the iberiotoxin-sensitive $K_{Ca}1.1$ currents (EC_{50} value between 1 and 10 μM). This activity is related to the free-radical scavenger activity of Quercetin. Specifically, Quercetin increases the frequency of spontaneous transient $K_{Ca}1.1$ currents, which are triggered by Ca^{2+} sparks, and hyperpolarizes the cell membrane, thus potentiating a fundamental feedback mechanism in vascular function that contrasts membrane depolarization and vasoconstriction. Noticeably, this effect on $K_{Ca}1.1$ currents was already significant at low concentrations, similar to those observed in human plasma after the ingestion of quercetin-rich foods (0.1−7 μM). Quercetin stimulated vascular $K_{Ca}1.1$ current with a mechanism that looked to be tissue-specific, decreasing rat tail main artery partly via a PKG-mediated, catalase-independent stimulation of smooth muscle $K_{Ca}1.1$ channels *(Iozzi et al., 2013)*. Additionally, Quercetin decreased both the frequency and the amplitude of spontaneous transient $K_{Ca}1.1$ currents by reducing the amount of Ca^{2+} releasable from the sarcoplasmic reticulum and likely Ca^{2+} sparks triggering these transient currents *(Fusi et al., 2020)*. So, the aim of this section was to design new Quercetin derivatives as potential $K_{Ca}1.1$ and $Ca_v1.2$ modulators in order to evaluate if they are suitable anti-hypertensive agents.

Results and Discussion

Design of new hybrids and docking simulations

In order to investigate the functional properties of Quercetin derivatives realized in this project, typical carboxylic acids contained in food matrices, able to prevent cardiovascular diseases *(Fuentes and Palomo, 2014)*, were chosen as suitable acyl donors to design new hybrids. In this field, hydroxycinnamic acids were used. Twenty four molecules were designed by changing the substitution of acyl moiety in Quercetin core, positions C4', C3, C7 (Figure 15). The designed compounds were subjected to docking simulations on $K_{Ca}1.1$ model, demonstrating how four molecules resulted the best interesting. In particular the derivatives **1C**, **1E**, **1F** and **3F** demonstrate to be the suitable ligands to evaluate the functional profile. As reported in Figure 16, in cyan surface/cartoon is reported $K_{Ca}1.1$ 3D structure. The bilayer is shown as a light grey box. Binding residues are shown in orange and blue (involved in hydrophobic interactions and hydrogen bonds respectively). Hydrogen bonds are indicated as yellow dot lines.

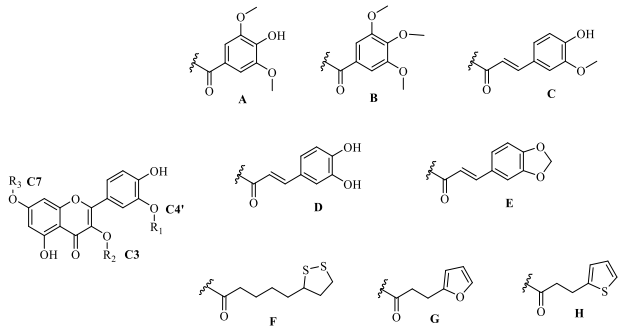

	C4’	C3	C7
1A	**residue A**	H	H
2A	H	**residue A**	H
3A	H	H	**residue A**
1B	**residue B**	H	H
2B	H	**residue B**	H
3B	H	H	**residue B**
1C	**residue C**	H	H
2C	H	**residue C**	H
3C	H	H	**residue C**
1D	**residue D**	H	H
2D	H	**residue D**	H
3D	H	H	**residue D**
1E	**residue E**	H	H
2E	H	**residue E**	H
3E	H	H	**residue E**
1F	**residue F**	H	H
2F	H	**residue F**	H
3F	H	H	**residue F**
1G	**residue G**	H	H
2G	H	**residue G**	H
3G	H	H	**residue G**
1H	**residue H**	H	H
2H	H	**residue H**	H
3H	H	H	**residue H**

Figure 15. Designed Quercetin derivatives

Specifically, **3F** interacts with the active site by hydrophobic interactions among the lipoyl moiety and Val344 and Leu368, while the flavonoid moiety (ring B) hydrophobically interacts with Trp329 and Trp341; C5-OH and the C=O moiety interact by hydrogen bonds with Arg367, while oxygen interacts with Thr364 but C3’-OH interacts with Thr339. On the other hand, the isomer **1F** showed a little interaction with the active site; in fact, only two H-bonds with Thr339 and Thr364 were mediated by oxygen and C=O, respectively, while the lipoyl moiety interacts with Trp341, Val344 and Cys343 with hydrophobic interactions. Furthermore, **1C** and **1E** demonstrated similar hydrogen interactions; in detail, C5-OH, C7-OH, C3-OH and oxygen interact with Glu330, Asn334, Glu342 and Thr364, respectively. Several hydrophobic interactions were reported among the cinnamoyl moieties and Leu368 or Tyr345. Regarding the $Ca_v1.2$ channel, only compound **1F** demonstrated a suitable interaction with the active site. In particular, in figure 18 in teal surface/cartoon is reported $Ca_v1.2$ transmembrane domain 3D structure.

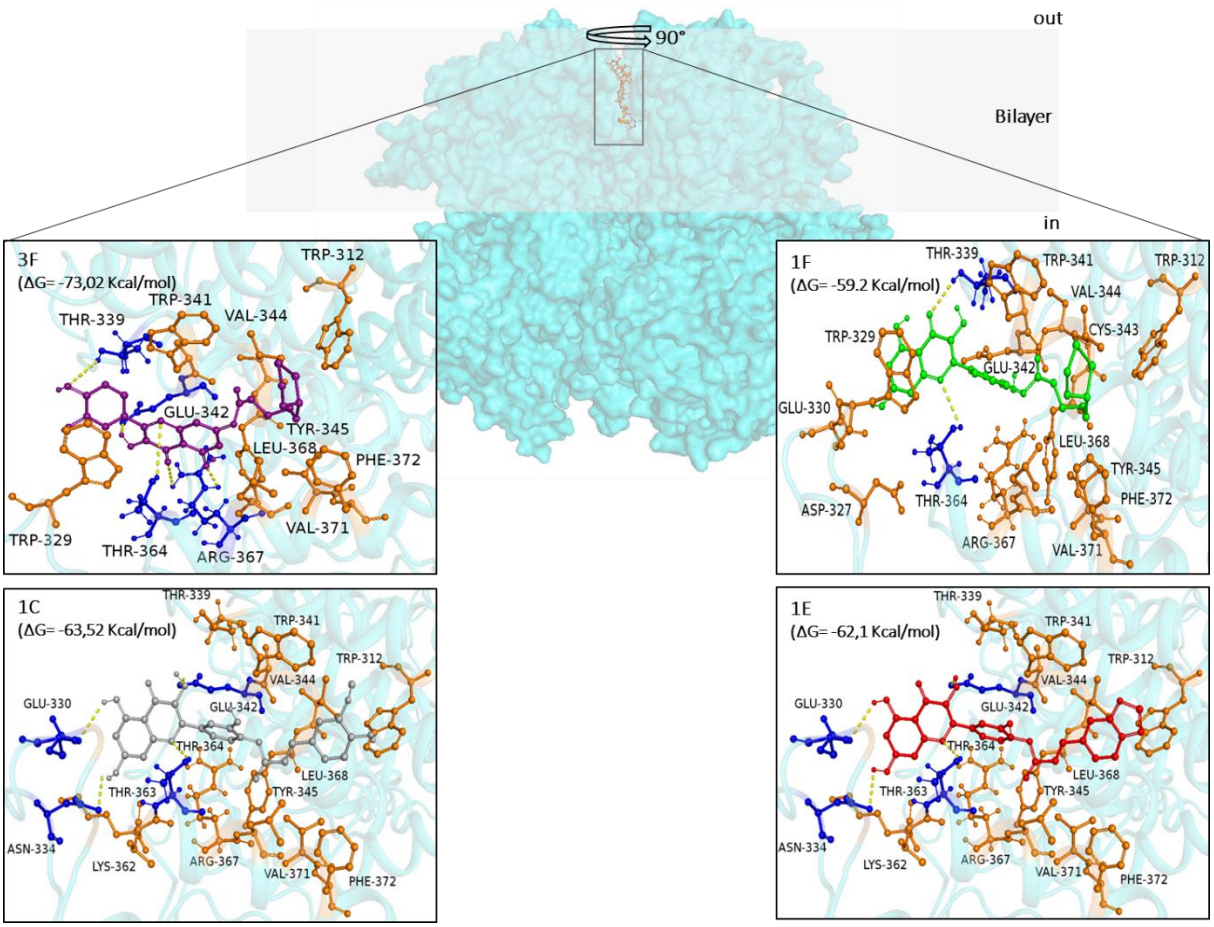

Figure 16. Docking of selected compounds on $K_{Ca}1.1$

Binding residues of **1F** are shown in orange, blue and red (involved in hydrophobic interactions, hydrogen bonds and π-stacking respectively). In particular, a selective π-stacking interaction was observed between C4' and Phe1143, responsible of the inhibition of the channel, while C3-OH, C=O, C5-OH and C7-OH formed hydrogen bonds with Asn771, Gly735, Glu736 and Glu1144 respectively.

Chemistry

The compounds have been synthesized by simple chemical procedures. In particular, the derivative **1C** was synthesized starting from ferulic acid converted to the corresponding acyl chloride in $SOCl_2$ and successively under Schotten-Baumann conditions, in a mixture acetone/DCM, to ester. Nevertheless, this procedure could not be used in the case of compounds **1E** and **1F** because of the less solubility of the acyl chlorides obtained in the mixture acetone/DCM; in fact, in order to maximize the selective synthesis of the C4'-substituted compound, the acyl chloride should be dropped in the solution of Quercetin in acetone.

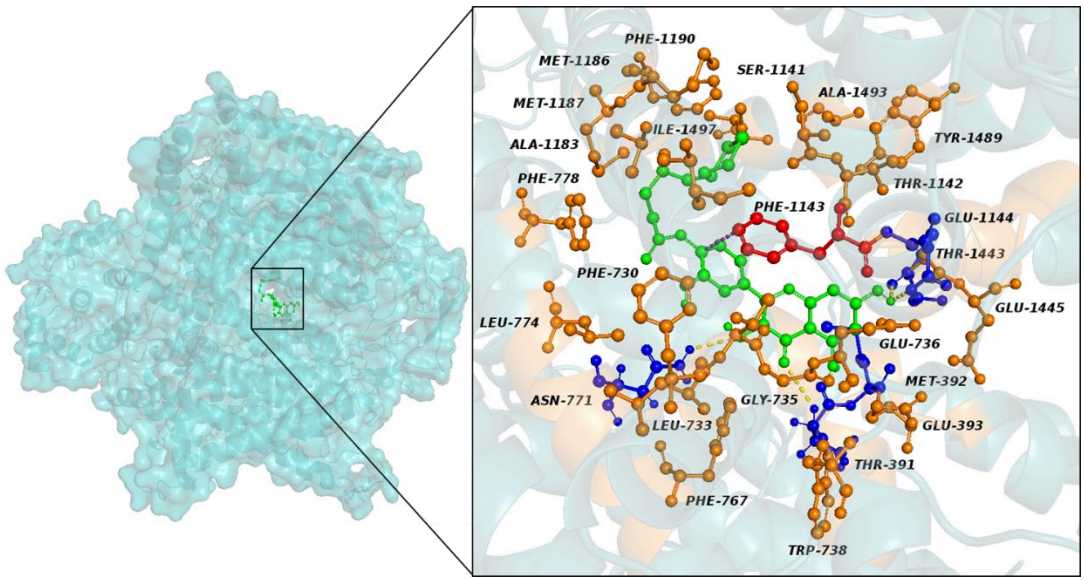

Figure 17. Docking of compound **1F** on $Ca_v1.2$ channel

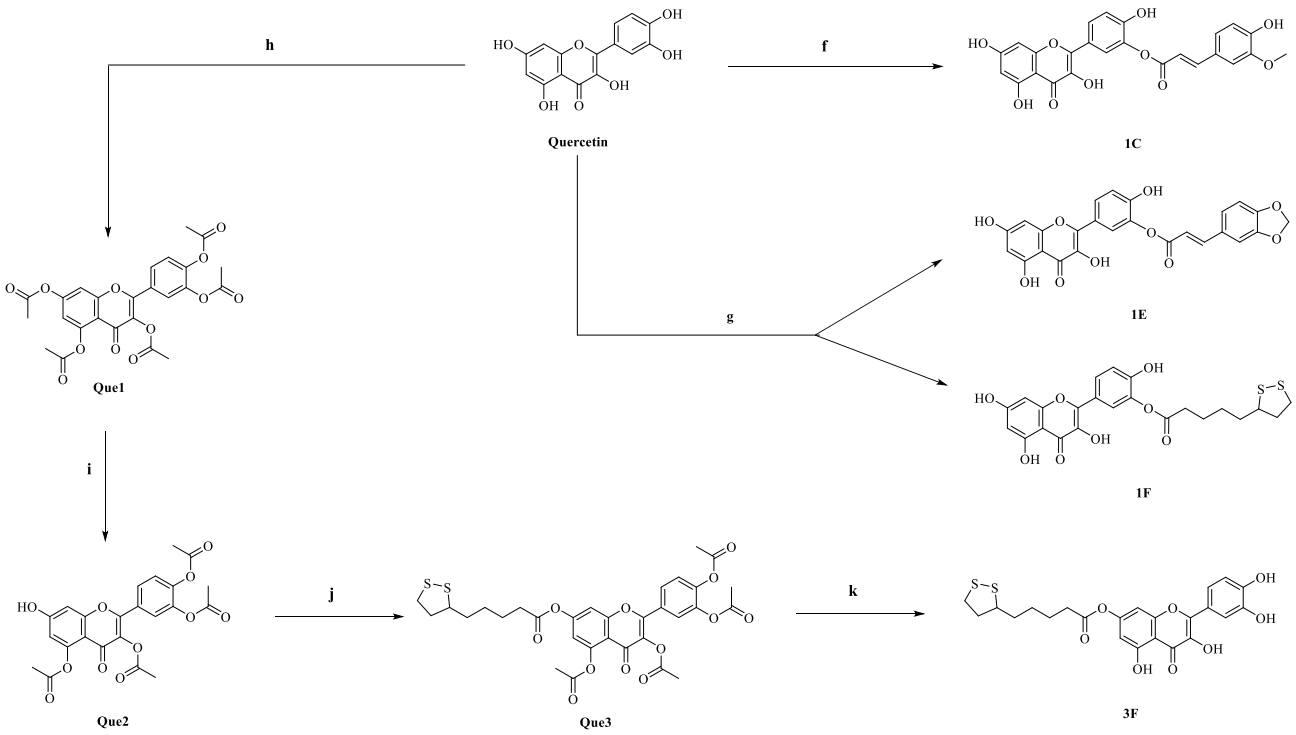

Scheme 3. Synthesis of the selected Quercetin derivatives as $K_{Ca}1.1$ channel modulators

Reagents and conditions: f) 1) trans-ferulic acid, $SOCl_2$, DMF, dry DCM, rt, 1h, 2) Et_3N, acetone, rt, 3 h; g) 3,4-(methylenedioxy)cinnamic acid (for **1E**), α-lipoic acid (for **1F**), HOBt, CMC, DCM, DMF, 0°C, 15 min, then rt, 24 h; h) acetic anhydride, pyridine, reflux, 5 h; i) imidazole, DCM, -15°C, then rt, 2 h; j) α-lipoic acid, HOBt, CMCs, DCM, DMF, 0°C, 15 min, then rt, 24 h; k) 6N HCl, CH_3CN.

So, a simple Steglich reaction was applied to synthesize **1E** and **1F**, by using CMC and HOBt, selectively obtained in good yield. The synthesis of **3F** opened the way to a different approach, because the C7-OH position is the third in order of reactivity of Quercetin core. Firstly, Quercetin was converted to its penta-acetylated derivative **Que1**, which was selectively deacetylated in C7 position with imidazole. The obtained **Que2** was subjected to Steglich conditions in order to obtain the ester compound **Que3**, which in acidic conditions was converted to the final compound **3F**.

Experimental part

Procedure f): synthesis of 2-hydroxy-5-(3,5,7-trihydroxy-4-oxo-4H-chromen-2-yl) phenyl (E)-3-(4-hydroxy-3-methoxyphenyl) acrylate **1C**: According with published procedures *(Dias et al., 2017; Zhang et al., 2012)*, to a mixture of trans-ferulic acid (1 equiv.) in dry DCM (5 mL), $SOCl_2$ (10 equiv.) and DMF (25 mL) were added, and the resulting solution was stirred under argon atmosphere for 1 h. After evaporation of the solvent, a solution of Quercetin (1 equiv.) in acetone (10 mL) and Et_3N (1 equiv.) were added; the reaction was stirred at rt for 3 h. After this time, the solvent was removed under reduced pressure and the resulting residue was purified through crystallization in DCM. Yellow resin, 37% yield. ^{1}H-NMR (DMSO d_6): δ 12.60 (OH-(C5), bs, 1H), 12.00 (OH fer, s, 1H), 10.71 (OH-(C7), bs, 1H), 9.50 (OH-(C3), bs, 1H), 9.25 (OH-(C3'), bs, 1H), 7.50 (dd, 1H, *J* = 3.0, 15.0 Hz), 7.30-7.10 (m, 2H), 7.09-6.90 (m, 3H), 6.85-6.60 (m, 2H), 6.30 (dd, 1H, *J* = 3.0, 15.0 Hz), 6.15 (s, 1H), 3.80 (s, 3H). ^{13}C-NMR (DMSO d_6): δ 176.2, 168.3, 164.3, 161.1, 156.5, 149.5, 148.3, 148.1, 147.0, 146.5, 145.4, 144.9, 143.0, 141.1, 140.0, 136.1, 126.2, 123.2, 122.4, 121.0, 120.0, 116.0, 115.9, 111.6, 56.1.

Procedure g): synthesis of compounds **1E** *and* **1F***:* According with a published procedure (*Aiello et al., 2016*), a solution of carboxylic acid (1 equiv.), Quercetin (1 equiv.), and HOBt (1.2 equiv.) in DCM/DMF (65:35) (5 mL) was cooled at 0 °C and stirred under argon atmosphere for 15 min. Thereafter, a solution of CMC (1.5 equiv.) in DCM (3.5 mL) was added dropwise. The mixture was stirred at rt for 24 h, then the solvent was washed twice with a 5% $NaHCO_3$ solution and finally once with brine. The collected organic layers, dried on anhydrous Na_2SO_4, were concentrated and the crude compound obtained after flash-column chromatography (eluent DCM:MeOH 95:5).

2-hydroxy-5-(3,5,7-trihydroxy-4-oxo-4H-chromen-2-yl)phenyl (E)-3-(benzo[d][1,3]dioxol-5-yl)acrylate **1E**: yellow resin, 32% yield. ^{1}H-NMR (DMSO d_6): δ 8.10-7.90 (m, 3H), 7.72 (d, 1H, J = 4.6 Hz), 7.66-7.59 (m, 1H), 7.52-7.41 (m, 2H), 7.35 (d, 1H, J = 4.6 Hz), 6.90 (dd, 2H, J = 3.0, 15.0 Hz), 6.10 (s, 2H). ^{13}C-NMR (DMSO d_6): δ 176.2, 166.5, 164.0, 162.0, 159.0, 152.2, 148.0 (x3C), 139.9, 136.4, 127.0, 126.1, 123.0, 122.4, 121.6, 116.1 (x2C), 115.3, 108.0, 105.9, 104.0, 100.2, 98.3, 94.1.

2-hydroxy-4-(3,5,7-trihydroxy-4-oxo-4H-chromen-2-yl)phenyl 5-(1,2-dithiolan-3-yl)pentanoate **1F**: Yellow resin, 46% yield. ^{1}H-NMR (DMSO d_6): δ 7.59 (s, 1H), 7.50-7.40 (m, 1H), 6.80-6.70 (m, 1H), 6.34 (s, 1H), 6.10 (s, 1H), 3.60-3.50 (m, 2H), 3.20-3.01 (m, 2H), 2.50-2.30 (m, 1H), 2.10-1.80 (m, 1H) 1.70-1.40 (m, 7H). ^{13}C-NMR (DMSO d_6): δ 176.1, 172.0, 166.4, 161.8, 158.8, 150.8, 146.9, 139.2, 136.5, 127.0, 124.0, 120.8, 114.3, 104.5, 98.3, 94.0, 61.4, 45.2, 43.3, 39.6, 38.2, 29.6, 24.6.

Procedure h): synthesis of 2-(3,4-diacetoxyphenyl)-4-oxo-4H-chromene-3,5,7-triyl triacetate **Que1**: Quercetin (1 equiv.), acetic anhydride (20 equiv.) and pyridine (15 mL) were stirred at reflux for 5 h. Then, a mixture of ice-water (50 g) was added. The resulting precipitate was filtered and washed with cold EtOAc to afford **Que1**. White solid, 79% yield. Spectroscopic data are in agreement with those reported. *(Mattarei et al., 2010)*

Procedure i): synthesis of 4-(3,5-diacetoxy-7-hydroxy-4-oxo-4H-chromen-2-yl)-1,2-phenylene diacetate **Que2**: A solution of imidazole (2 equiv.) in DCM (5 mL) was added dropwise to a solution of **Que1** (1 equiv.) in DCM (10 mL) at –15 °C in an ice/acetone bath. The resulting solution was allowed to warm to rt and stirred for 2 h. The reaction mixture was diluted in DCM (50 mL) and washed with 3 M aq. HCl (3 × 50 mL). The organic layer was then dried over Na_2SO_4, and filtered. The solvent was evaporated under reduced pressure. The resulting residue was purified through flash chromatography (eluent: $CHCl_3$/MeOH, 97:3). White solid, 87% yield. Spectroscopic data are in agreement with those reported. (*Mattarei et al., 2010*)

Procedure j): synthesis of 7-((5-(1,2-dithiolan-3-yl)pentanoyl)oxy)-2-(3,4-diacetoxyphenyl)-4-oxo-4H-chromene-3,5-diyl diacetate **Que3**: It was obtained by using the same procedure for compound **1F**. Yellow resin, 78% yield. ^{1}H-NMR ($CDCl_3$): δ 7.80-7.60 (m, 1H), 7.40-7.32 (m, 2H), 6.92-6.86 (m, 2H), 3.30-3.10 (m, 1H), 2.80-2.30 (m, 15H), 2.01-1.40 (m, 9H). ^{13}C-NMR ($CDCl_3$): δ 178.6, 169.3, 167.9 (x 3C), 167.8, 154.2, 150.3, 144.3, 126.4,

125.0, 124.0, 123.8, 122.3, 115.5, 114.1, 107.9, 56.2, 40.2, 38.5, 34.5, 33.7, 33.5, 28.6, 24.5, 24.3, 21.1, 21.0, 20.7, 20.6, 20.5.

Procedure k): synthesis of 2-(3,4-dihydroxyphenyl)-3,5-dihydroxy-4-oxo-4H-chromen-7-yl 5-(1,2-dithiolan-3-yl)pentanoate **3F**: **Que3** (1 equiv.) was added of CH_3CN (20 mL) and 6 N aq. HCl (10 mL). The resulting solution was stirred and refluxed for 1.5 h. Then EtOAc (100 mL) and water (100 mL) were added. The organic layer was washed with 3 M aq. HCl (3 × 100 mL), dried over Na_2SO_4 and filtered. The solvent was evaporated under reduced pressure. **3F** was obtained after crystallization of the residue with DCM. Yellow resin, 80% yield. ^{1}H-NMR (Acetone d_6): δ 12.30 (bs, OH-(C5), 1H), 9.80 (bs, OH-(C4'), 1H), 8.70 (bs, OH-(C3'), 1H), 8.40 (bs, OH-(C3), 1H), 7.83 (s, 1H), 7.70-7.50 (m, 1H), 7.01-6.90 (m, 1H), 6.51 (s, 1H), 6.28 (s, 1H), 3.60-3.50 (m, 2H), 3.20-3.01 (m, 2H), 2.50-2.30 (m, 1H), 2.10-1.80 (m, 1H) 1.70-1.40 (m, 7H). ^{13}C-NMR (Acetone d_6): δ 180.8, 169.2, 166.5, 161.9, 152.6, 151.2, 150.0, 146.9, 141.0, 136.0, 128.0, 125.7, 120.4, 120.0, 108.4, 103.4, 98.7, 61.4, 45.2, 43.3, 39.6, 38.2, 29.6.

Functional evaluation in KCl- and phenylephrine-induced contraction, K_{Ca}1.1 and Ca_V1.2 channel currents

The compounds were subjected to functional assays on rat tail artery myocytes – patch-clamp. As reported in Figure 18B, **1C** was able to activate K_{Ca}1.1 channel current (+119.8%) but at the high concentration of 100 μM, with an activation profile versus Ca_v1.2 channels of +41.1% (at 30 μM). This profile is in line with the little interaction profile demonstrated by docking simulations. **1E** demonstrated to be a suitable inhibitor of Ca_v1.2 channel current (-42.2%) although at high concentration of 100 μM, but no effect was registered in the case of K_{Ca}1.1 current. On the other hand, **1F** demonstrated to be a good activator of K_{Ca}1.1 current just at 30 μM, with no effect in the case of Ca_v1.2 current. **3F** demonstrated the best profile versus K_{Ca}1.1 currents at 10 μM with a +57.5% of activation rate. At the same concentration, **3F** was also able to activate Ca_v1.2 currents with a +72.0% of activation rate (EC_{50} = 2.7±0.4 μM). **3F** showed a profile, in terms of efficacy, essentially superimposable to that of Quercetin (Figure 18 C,F). For the other hybrids, in the essays that have been carried out, the same statement made above applies, with the exception of **1E** which loses the stimulatory activity on the Ca_v1.2 channels but at the same time also loses the vasodilatory activity (Figure 18 B). **1C** and **3F** stimulate the currents like Quercetin, while in **1E** this activity is lost and an inhibition of the same is observed. For this reason, the molecules were

assayed also in rat aorta rings demonstrating how **1C** is not more active than Quercetin. **3F**, which could be an H_2S donor, relaxed pre-contracted aorta rings with low potassium (K25), high potassium (K60) and phenylephrine (Phe) in a similar way to Quercetin (Figure 19). Only on the K60 there was a significantly higher activity at concentrations 30 and 100 µM, but this activity was not due to the release of H_2S, because in this case, on K25, where the potassium channels (activated by H_2S) play a more important role, should appear the effect. However, this effect may also be felt on $Ca_V1.2$ channels, or it may be due to the partially inhibitory action observed on these channels at 30 and 100 µM in electrophysiology experiments. All these data are summarized in Table 11.

Table 11. Effect of Quercetin derivatives on phenylephrine- or high K^+-induced contraction in rat aorta rings and on rat tail myocyte $K_{Ca}1.1$ and $Ca_V1.2$ channel currents; blue: weak inhibitor; red: inhibitor; green: stimulator.

	Endothelium-deprived rat aorta rings			**Rat tail artery myocytes**			
Drug	**KCl-induced contraction**		**Phenylephrine-induced contraction**	**$K_{Ca}1.1$ channel current (at 70 mV)**			**$Ca_V1.2$ (Ba^{2+}) channel current**
	25 mM K^+	**60 mM K^+**		**10 µM**	**30 µM**	**100 µM**	**100 µM (at 0 mV)**
Quercetin	**-73.1%**	**-62.6%**	**-79.8%**		**+120.9%**		**+126.8% (50 µM) (EC_{50}=8.1 µM)**
1C						**+119.8%**	**+41.1% (30 µM)**
1E	**-27.5%**	**-13.4%**	**-10.8%**				**-42.2% (100 µM)**
1F	**-74.9%**	**-68.3%**	**-67.9%**	**+53.4%**	**+158.7%**		
3F	**-73.1%**	**-83.1%**	**-81.4%**	**+57.5%**			**+72.0% (10 µM) (EC_{50}=2.7±0.4 µM)**

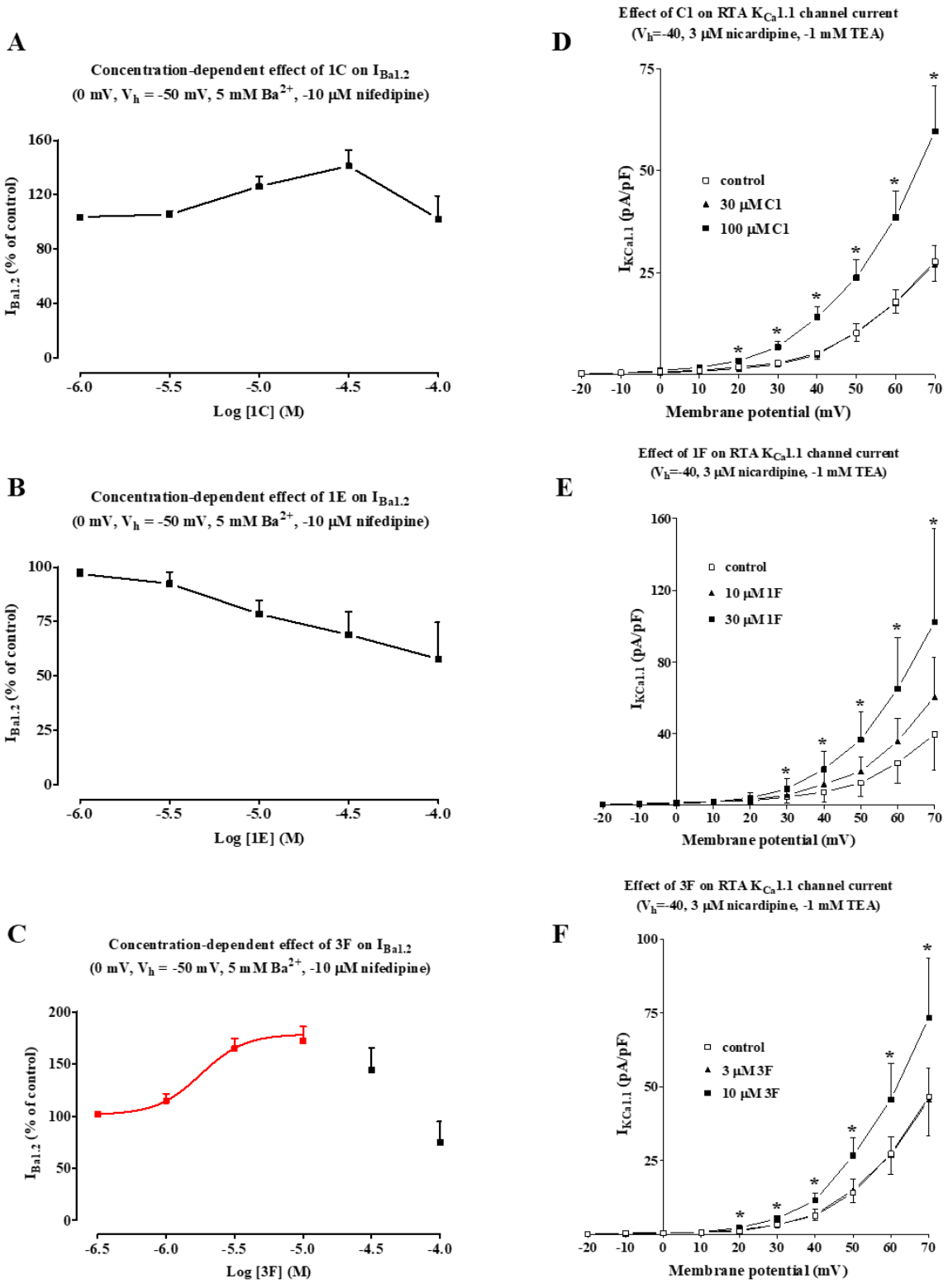

Figure 18. Functional profile of compounds on $K_{Ca}1.1$ and $Ca_V1.2$ channel currents

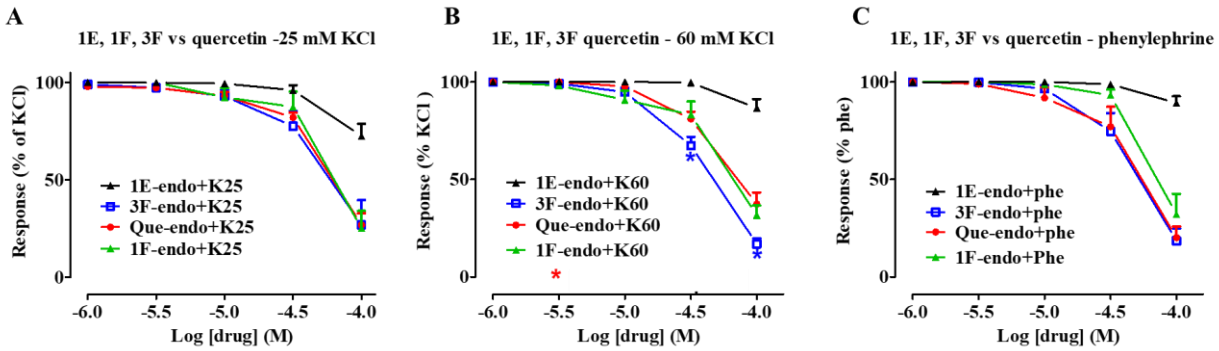

Figure 19. Effect of derivatives on rat aorta rings contracted with phenylephrine or high K^+.

Morin: a suitable scaffold for the investigation of new anti-hypertensive agents

Morin, also known as 2', 3, 4', 5, 7-pentahydroxyflavone, is a positional isomeric form of Quercetin, presenting a resorcinol moiety, a carbonyl group in position 4 and a difference in the ring B; the hydroxylation pattern of B-ring is meta substituted while in Quercetin is ortho-substituted. Morin is extracted from branches of *Morus alba L.* (white mulberry), but distributed ubiquitously in the family of Moraceae, in almond and sweet chestnut *(Venu Gopal, 2013)*. Morin produced several pharmacological activities, including free radical scavenging activity, xanthine oxidase inhibitor property, anti-inflammatory activity, protective effect of DNA from damage caused by free radical, prevention of low density lipoprotein oxidation and anticancer activity. Morin demonstrated also antitumoral, antibacterial, hypouricemic, and neuroprotective effects by modulating the activity of many enzymes *(Caselli et al., 2016)*. Regarding cardiovascular system, Morin exhibited protection in isoproterenol-induced myocardial infarction in rats, essentially mediated by antioxidant activity due to the hydroxyl groups. There was a dose-dependently improved hemodynamic profile, increased anti-oxidant levels, normalized myocardial architecture and reduced inflammatory markers and apoptosis, with a modulation of MAPK pathway *(Kumar Verma et al., 2019)*. In a *in vivo* study it was also demonstrated that Morin pretreatment (20, 40, and 80 mg/kg, respectively) daily for a period of 30 days decreased the activity of cardiac marker enzymes such as lactate dehydrogenase, creatine kinase, aspartate transaminase, calcium-dependent adenosine triphosphatase, sodium potassium-dependent adenosine triphosphatase, and magnesium-dependent adenosine triphosphatase *(Al-Numair et al., 2012)*. Morin was also able to inhibit *in vitro* LDL oxidation, demonstrating to prevent atherosclerosis *(Naderi et al., 2003)*. Furthermore, it was also able to reduce the tissue necrosis in post-ischemic and reperfused rabbit hearts, by reducing xanthine oxidase expression from the ischemic endothelium *(Wu et al., 1995)*. From the

medicinal chemist point of view, interestingly, Morin was found to be an agonist of the TRPV4 receptor, inducing endothelium-dependent relaxation of isolated rat mesenteric arteries in a concentration-dependent manner. Additionally, in hypertensive rats (hypertension induced by L-NAME), oral administration of Morin (50 mg/kg/day) decreased systolic blood pressure and improved the relaxation response of the arteries to acetylcholine *(Zhang et al., 2019)*. Regarding calcium channels, Morin was also useful in antagonizing $Ca_v1.2$ current stimulation induced by Quercetin or Myricetin, resulting a weak $Ca_v1.2$ inhibitor (E_{max} = 53.6 ± 8.9 % at 100 µM). Morin was found to interact with the channel through hydrophobic interactions mediated by Leu774, Phe1143, Met1188, Phe1191, Tyr1489, Phe1495, and hydrogen bonds with Tyr1489, Asn770 and π-π stacking with Phe1143, Phe1191 *(Saponara et al., 2011)*. In line with this, no interesting data were reported about the activation of $K_{Ca}1.1$ channel currents *(Fusi et al., 2020)*. Considering that some features in Morin structure are essential for $Ca_v1.2$ inhibition, the aim of this section was to synthesize a small library of derivatives, starting with the penta-acetylated one (**Morin-1**), in order to investigate if the typical dihydropyridine moieties (**Morin-3** and **Morin-4**) are useful to promote a better inhibition of $Ca_v1.2$ channel current from Morin.

Results and Discussion

Chemistry

Little information are present in literature regarding a suitable chemical approach to modify Morin, in order to develop hybrid compounds. So, starting from Morin, it was refluxed in acetic anhydride in order to obtain **Morin-1**, according with a published procedure *(Bhakuni et al., 2017)*. Then, it was selectively de-acetylated using imidazole in DCM to afford **Morin-2**, which was used for the formation of **Morin-3** in Schotten-Baumann conditions, with the corresponding acyl chloride; to obtain **Morin-4**, it was observed that the reaction of 3-nitrobenzoic acid, under Steglich conditions (CMC/HOBt) with **Morin-2**, afforded directly the de-acetylated compound.

Experimental part

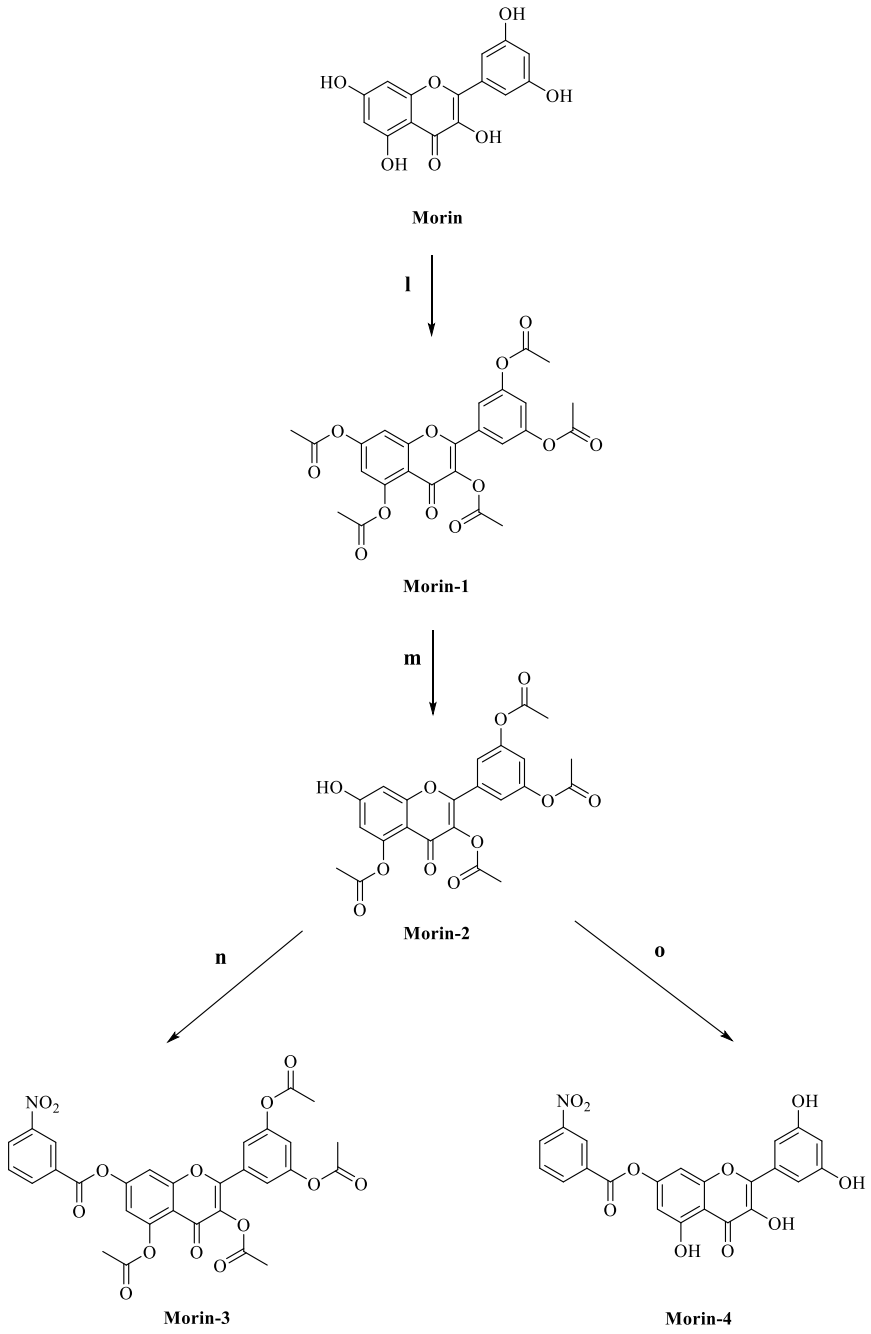

Scheme 4. Synthesis of Morin derivatives

Reagents and conditions: l) acetic anhydride, H_2SO_4, reflux, 24 h; m) imidazole, DCM, -15°C, then rt, 2 h; n) 3-nitrobenzoylchloride, Et_3N, DCM, 24 h, rt; o) 3-nitrobenzoic acid, HOBt, CMC, DCM, DMF, 0°C, 15 min, then rt, 24 h.

Procedure l): synthesis of 2-(2,4-diacetoxyphenyl)-4-oxo-4H-chromene-3,5,7-triyl triacetate **Morin-1**: Morin (1 equiv.), acetic anhydride (20 equiv.) and H_2SO_4 (2 drops) were stirred at reflux for 24 h. To the reaction a mixture of ice-water (50 g) was added. The resulting precipitate was filtered and washed with cold ethyl acetate to afford **Morin-1**. Brown solid, 89% yield. Spectroscopic data are in agreement with those reported *(Bhakuni et al., 2017)*.

Procedure m): synthesis of 5-(3,5-diacetoxy-7-hydroxy-4-oxo-4H-chromen-2-yl)-1,3-phenylene diacetate. **Morin-2**: a solution of imidazole (2 equiv.) in DCM (5 mL) was added dropwise to a solution of **Morin-1** (1 equiv.) in DCM (10 mL) at -15 °C in an ice/acetone bath. The resulting solution was allowed to warm to rt and stirred for 2 h. The reaction mixture was diluted in DCM (50 mL) and washed with 3 M aq. HCl (3×50 mL). The organic layer was then dried over Na_2SO_4, and filtered. The solvent was evaporated under reduced pressure. The resulting residue was purified through flash chromatography (eluent: $CHCl_3$/MeOH, 97:3). Light brown resin, 77% yield. ^{1}H-NMR ($CDCl_3$): δ 7.70 (d, 1H, *J* = 6.0 Hz), 7.20-7.10 (m, 2H), 6.76 (d, 1H, *J* = 4.0 Hz), 6.61 (d, 1H, *J* = 5.0 Hz), 2.34 (s, 3H), 2.25 (s, 3H), 2.22 (s, 3H), 1.25 (s, 3H). ^{13}C-NMR ($CDCl_3$): δ 176.0, 168.7, 168.6, 168.3, 167.7, 161.7, 156.3, 156.2, 154.8, 153.2, 151.6 (x 2C), 148.9, 133.0, 119.6, 117.4, 109.3, 105.7, 101.2, 29.7, 21.2, 21.0, 20.2.

Procedure n): synthesis of 5-(3,5-diacetoxy-7-((3-nitrobenzoyl)oxy)-4-oxo-4H-chromen-2-yl)-1,3-phenylene diacetate **Morin-3**: To a well strirred solution of 3-nitrobenzoylchloride in DCM, **Morin-2** was added; the mixture was stirred at rt for 24 h. After this time, the reaction was treated with $NaHCO_3$ until pH=7; then the mixture was partitioned between EtOAc and H_2O. The organic layer was dried over Na_2SO_4 and concentrated under reduced pressure. **Morin-3** was obtained after flash column chromatography (eluent EtOAc:*n*-hexane, 50:50). White resin, 75% yield. ^{1}H-NMR ($CDCl_3$): δ 9.09-9.00 (m, 1H), 8.60-8.50 (m, 3H), 7.80-7.70 (m, 3H), 7.60-7.55 (m, 1H), 7.20-7.10 (m, 1H), 2.34 (s, 3H), 2.25 (s, 3H), 2.22 (s, 3H), 1.25 (s, 3H). ^{13}C-NMR ($CDCl_3$): δ 170.2, 169.2, 169.1, 169.0, 168.0, 165.2, 158.1, 156.7, 153.3, 151.6 (x 2C), 151.5, 147.8, 136.4, 133.3, 131.2, 129.5, 129.1, 127.2, 123.9, 115.4 (x 2C), 114.5, 114.4, 108.6, 106.9, 20.3, 20.2, 20.1,19.9.

Procedure o): synthesis of 2-(3,5-dihydroxyphenyl)-3,5-dihydroxy-4-oxo-4H-chromen-7-yl 3-nitrobenzoate **Morin-4**: 3-nitrobenzoic acid (1 equiv.), **Morin-2** (1 equiv.), and HOBt (1.2 equiv.) in a solution DCM/DMF (3:1) (5 mL) were cooled at 0 °C and stirred under argon atmosphere for 15 min. Thereafter, a solution of CMC (1.5 equiv.) in DCM (3.5 mL) was added dropwise. The mixture was stirred at rt for 24 h, then the solvent was washed twice with a 5% $NaHCO_3$ solution and finally once with brine. The collected organic layers, dried on anhydrous Na_2SO_4, were concentrated and the crude compound obtained. White oil, 69% yield. ^{1}H-NMR ($CDCl_3$): 9.20 (s, 1H), 8.80-8.60 (m, 2H), 8.20-8.10 (m, 1H), 7.90-7.80 (m, 1H), 7.70-7.40 (m, 4H). ^{13}C-NMR ($CDCl_3$): 176.4,

161.0, 148.4, 143.4, 131.7, 130.2, 130.0, 129.0, 128.6, 128.5, 128.4, 126.5, 126.0, 125.7, 125.5, 124.3, 121.7, 119.7, 109.0, 107.2, 103.4, 102.1.

Functional evaluation in KCl- and phenylephrine-induced contraction, KCa1.1 and Cav1.2 channel currents

Firstly, the derivatives were assayed as suitable $Ca_v1.2$ channel blockers in Ba^{2+} currents, but as reported in Figure 20 A, all the compounds showed a comparable inhibition of the currents similar to the parent Morin, with the exception of **Morin-1**.

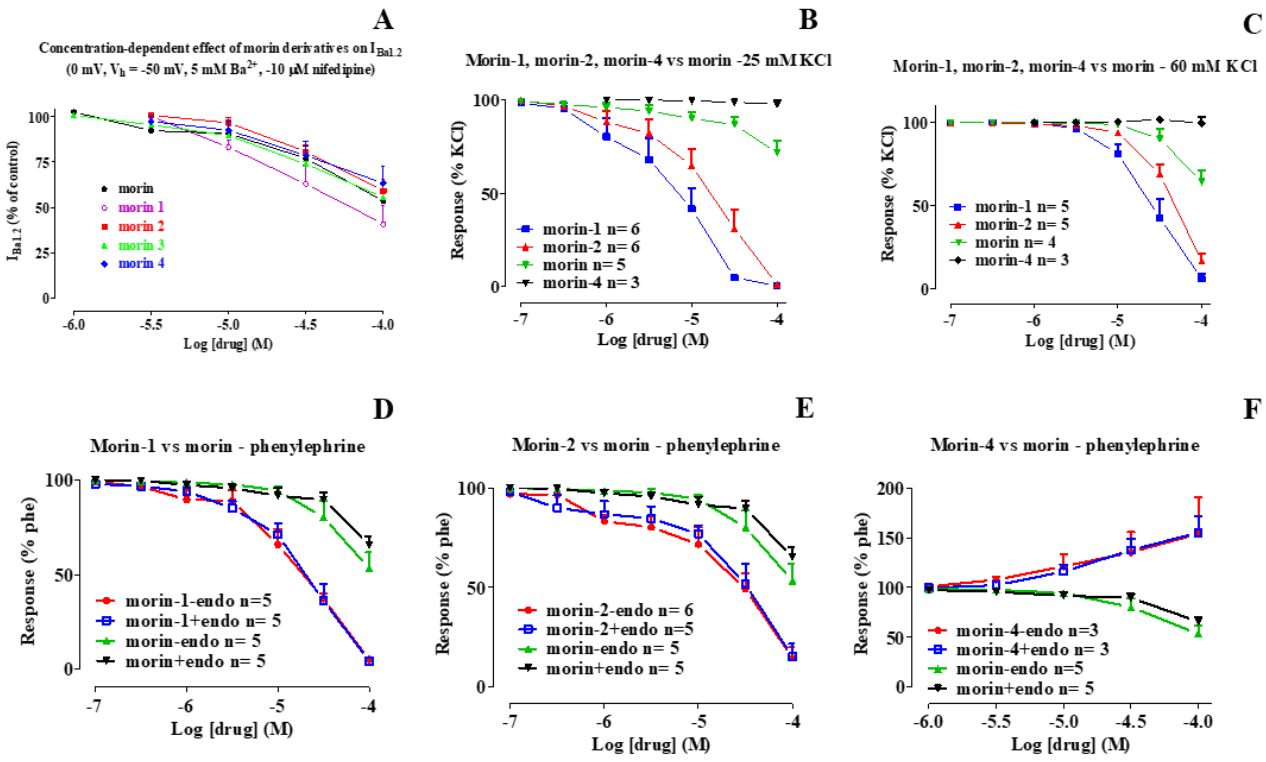

Figure 20. Evaluation of Morin derivatives on Cav1.2 channels and in rat aorta rings pre-contracted with KCl (25 mM and 60 mM) or phenylephrine

As reported in Figure 20 B-C, **Morin-1** and **Morin-2** were able to promote vasorelaxation in rat aorta rings pre-contracted with KCl, just at K25 and K60, with a high potency in the case of K25 for **Morin-1**. In all the cases, the two compounds resulted active respect to Morin, the parent compound. In line with these data, **Morin-1**, **Morin-2** and **Morin-4** have been evaluated also in rat aorta rings pre-contracted with phenylephrine in presence or absence of endothelium. **Morin-1** and **Morin-2** resulted active in promoting vasorelaxation in intact or denuded

rat aorta rings (Figure 20 D-E), with a potency higher than Morin. **Morin-4** resulted inactive compared to Morin (Figure 20F). Considering the results obtained, **Morin-1** was selected for further investigation about its mechanism of action in inducing vasorelaxation. It was found that **Morin-1** was an activator of the $K_{Ca}1.1$ channel current at 10 and 30 μM, with a good potency respect to the parent compound (Figure 21 A-B).

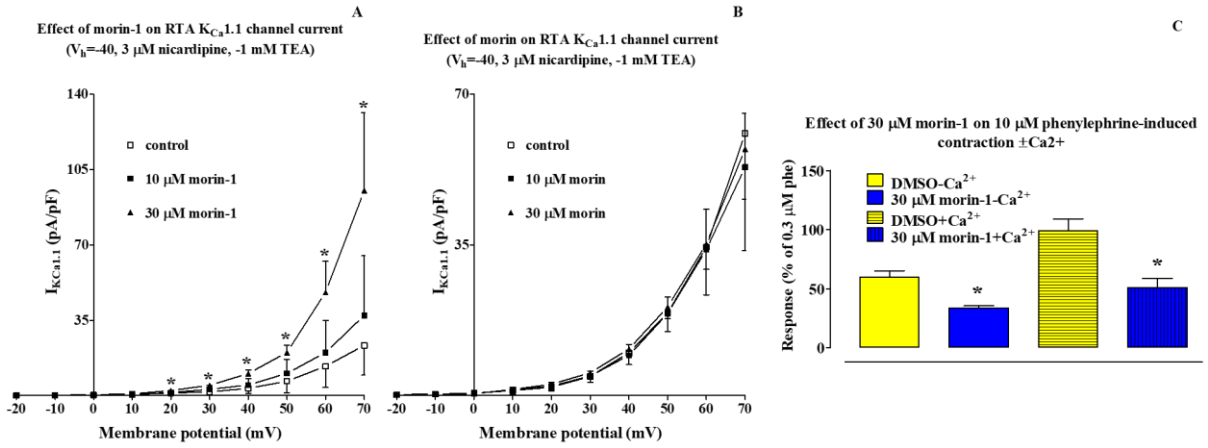

Figure 21. Morin-1 as a KCa1.1 channel activator and as Ca^{2+}-blocking agent from intracellular deposits

In another experiment, **Morin-1** was evaluated as a blocker for the release of Ca^{2+} from the intracellular departments. The picture reported in Figure 21C demonstrated how at the concentration of 30 μM, **Morin-1** was able to block the release of calcium from the intracellular deposits compared to DMSO, used as control. To conclude, **Morin-1** is a good activator of the $K_{Ca}1.1$ channels, a weak inhibitor of $Ca_v1.2$ channels and also antagonizes the release of Ca^{2+} from intracellular deposits.

Conclusions

This PhD thesis aims to investigate new potential tools for the treatment of metabolic disorders, including T2D and related complications, but also hypertension. The approaches used regard food and medicinal chemistry. In particular, starting from wine and wine pomace, it was demonstrated how grape represents a rich source of anti-inflammatory and vasodilating agents. In this field, starting from the ethnopharmacological relevance of Calabrian grapes/wines, autochthonous cultivars have been used. The red Magliocco Dolce, indigenously known as Arvino and the white berries of Mantonico and Pecorello were selected to perform the studies. Among the white berries, **PSS** resulted the most interesting vasodilating extract, able to foster NO release from the endothelium, also when embedded in the pectin matrix (**PSS pec**). These features were attributed to the complex chemical composition, which include known polyphenols able to promote vasodilatation such catechin and quercetin, but also to a diversified aminoacidic component including GABA, an endogenous vasodilator, reported to interfere with several vasoactive pathways. The study conducted with Magliocco Dolce aims to identify the most promising functional ingredient during the wine-making process. Among skins, seeds, must and wine, the best one was the red wine **LDC3**, able to promote a NO-dependent vasodilation. These findings highlighted the importance of diet in the management of a correct lifestyle, but also open the way for a new field in food chemistry and technology research. New functional food could be developed according to these starting ingredients. Furthermore, the **sgnss** extract (derived from Sangiovese seeds after wine-making) is able to increase the antioxidant and anti-inflammatory properties of kefir, an "elegant" and useful probiotic source, which is now becoming an important source of bioactive compounds.

Regarding the medicinal chemistry section, the starting point is represented by the couple metabolic disorders/polyphenols. In particular, a walk in the world of GPCRs and Cation channels was performed highlighting the suitable pharmacological targets to treat metabolic disorders such GPR40, GPR120, $K_{Ca}1.1$ and $Ca_v1.2$ channels. GPR40 was used as template for the development of insulin secretagogue agents, starting from the endogenous ligand OA. Two possible ligands were developed and assayed; the two compounds demonstrated to accommodate in the orthosteric GPR40 active site, opening the way for the development of new "non TAK 875-based" agonists. **AV1** demonstrated to be a full agonist while Quercetin-3-oleate, **AV2**, demonstrated to be a partial agonist. They were able to improve insulin secretion in GSIS conditions, and interestingly **AV2** was also able to promote wound healing targeting GPR40 *in vitro* and *in vivo*. In the context of wound healing, based on the efficacy of honeys in wound healing, which is attributed to Pinocembrin and its derivatives, the synthesis of new hybrid compounds was pursued. Pinocembrin was also speculated to be a GPR120 ligand, while the endogenous ligand DHA was evaluated as a wound healing agent *in vitro* and *in vivo*. The bio-catalytic combination of Pinocembrin with fatty acids furnished the compound **HW3**, interesting tool in wound healing

management, able to accommodate in the agonist site occupied by the known ligand TUG-891. These preliminary studies validated Pinocembrin as a good hit for the development of new GPR120 ligands.

Thereafter, a reliable approach was applied to find new interesting vasoactive agents, essentially starting from Quercetin and Morin, which were validated as $K_{Ca}1.1$ and $Ca_v1.2$ channel modulators. Quercetin was an activator of both the isoforms, and demonstrated a good potential as anti-hypertensive agent. Based on this, Quercetin is subjected to an intense metabolism both in foods and in aglyconic form. Twenty-four hybrids were designed and docked on $K_{Ca}1.1$ active site, furnishing lead compounds, which were further analysed *in vitro*. The most interesting compound **3F**, containing a thioctic moiety, was validated as a $K_{Ca}1.1$ modulator, with a limited effect on $Ca_v1.2$. Limited information are present about Morin and no derivatives have been reported. Only two compounds were synthesized, by using moieites of dihydropyridine drugs. The molecules demonstrated a limited efficacy as $Ca_v1.2$ blockers, but useful properties as KCa1.1 modulators and vasodilating agents in phenylephrine-induced contraction in rat aorta rings.

Further mechanistic and pharmacokinetic studies should clarify the efficacy of the synthesized molecules.

In conclusion, the aim of this PhD thesis was to furnish a plausible and innovative approach to fight T2DM and hypertension, that are the most present pathologies associated to metabolism.

Foods and new suitable drug candidates have been developed opening the way for translational applications.

References

- ✓ Adams, G.L.; Velazquez, F.; jayne, C.; Shah, U.; Miao, S.; Ashley, E.R.; Madeira, M.; Akiyama, T.E.; Di Salvo, J.; Suzuki, T.; Wang, N.; Truong, Q.; Gilbert, E.; Zhou, D.; Verras, A.; Kirkland, M.; Pachanski, M.; Powles, M.; Yin, W.; Ujjainwalla, F.; Venkatraman, S.; Edmondson, S.D. Discovery of chromane propionic acid analogues as selective agonists of GPR120 with in vivo activity in rodents. *ACS Med. Chem. Lett.* **2017**, 8(1), 96-101.
- ✓ Ahmed, Z.; Wang, Y.; Ahmad, A.; Khan, S.T.; Nisa, M.; Ahmad, H.; Afreen, A. Kefir and health: a contemporary perspective. *Crit. Rev. Food Sci. Nutr.* **2013**, *53*, 422-434.
- ✓ Aiello, F.; Armentano, B.; Polerà, N.; Carullo, G.; Loizzo, M.R.; Bonesi, M.; Cappello, M.S.; Capobianco, L.; Tundis, R. From vegetable waste to new agents for potential health applications: antioxidant properties and effects of extracts, fractions and pinocembrin from Glycyrrhiza glabra L. aerial parts on viability of five human cancer cell lines. *J. Agric. Food Chem.* **2017**, 65, 7944-7954.
- ✓ Aiello, F.; Badolato, M.; Pessina, F.; Sticozzi, C.; Maestrini, V.; Aldinucci, C.; Luongo, L.; Guida, F.; Ligresti, A.; Artese, A.; Allarà, M.; Costa, G.; Frosini, M.; Schiano Moriello, A.; De Petrocellis, L.; Valacchi, G.; Alcaro, S.; Maione, S.; Di Marzo, V.; Corelli, F.; Brizzi, A. Design and Synthesis of New Transient Receptor Potential Vanilloid Type-1 (TRPV1) Channel Modulators: Identification, Molecular Modeling Analysis, and Pharmacological Characterization of the N-(4-Hydroxy-3-methoxybenzyl)-4-(thiophen-2-yl)butanamide, a Small Molecule Endowed with Agonist TRPV1 Activity and Protective Effects against Oxidative Stress. *ACS Chem. Neurosci.* **2016**, *7*, 737-748.
- ✓ Al-Numair, K.S.; Chandramohan, G.; Alsaif, M.A. Pretreatment with morin, a flavonoid, ameliorates adenosine triphosphatases and glycoproteins in isoproterenol-induced myocardial infarction in rats. *J Nat Med* **2012**, *66*, 95-101.
- ✓ Alquier, T.; Peyot, M.; Latour, M.G.; Kebedel, M.; Sorensen, C.M.; Gesta, S.; Kahn, R.; Smith, R.D.; Jetton, T.L.; Metz, T.O.; Prentkil, M.; Poitout, V. Deletion of GPR40 impairs glucoseinduced insulin secretion in vivo in mice without affecting intracellular fuel metabolism in islets. *Diabetes* **2009**, *58*, 2607-2615.
- ✓ Arantes, E.L.; Dragano, N.; Ramalho, A.; Vitorino, D.; de-Souza, G.F.; Lima, M.H.M.; Velloso, L.A., Araújo, E.P. Topical docosahexaenoic acid (DHA) accelerates skin wound healing in rats and activates GPR120. *Biol Res Nurs* **2016**, 18(4), 411-419.
- ✓ Arumugam, S.; Thandavarayan, R.A.; Arozal, W.; Sari, F.R.; Giridharan, V.V.; Soetikno, V.; Palaniyandi, S.S.; Harima, M.; Suzuki, K.; Nagata, M.; Tagaki, R.; Kodama, M.; Watanabe, K. Quercetin offers cardioprotection against progression of experimental autoimmune myocarditis by suppression of oxidative and endoplasmic reticulum stress via endothelin-1/MAPK signalling. *Free Radic. Res.* **2012**, *46*, 154-163.
- ✓ Azevedo, C.M.G.; Watterson, K.R.; Wargent, E.T.; Hansen, S.V.F.; Hudson, B.D.; Kępczyńska, M.A.; Dunlop, J.; Shimpukade, B.; Christiansen, E.; Milligan, G.; Stocker, C.J.; Ulven, T. Non-acidic free fatty acid receptor 4 agonists with antidiabetic activity. *J. Med. Chem.* **2016**, 59, 8868-8878.
- ✓ Badolato, M.; Carullo, G.; Perri, M.; Cione, E.; Manetti, F.; Di Gioia, M.L.; Brizzi, A.; Caroleo, M.C.; Aiello, F. Quercetin/oleic acid-based G-protein-coupled receptor 40 ligands as new insulin secretion modulators. *Future Med. Chem.* **2017**, *9(11)*, 1873-1885.
- ✓ Barteková, M.; Čarnická, S.; Pancza, D.; Ondrejčáková, M.; Breier, A.; Ravingerová, T. Acute treatment with polyphenol quercetin improves postischemic recovery of isolated perfused rat hearts after global ischemia. *Can. J. Physiol. Pharmacol*. **2010**, *88*, 465-471.
- ✓ Beres, C.; Costa, G.N.S.; Cabezudo, I.; da Silva-James, N.K.; Teles, A.S.C.; Cruz, A.P.G.; Mellinger-Silva, C.; Tonon, R.V.; Cabral, L.M.C.; Freitas, S.L. Towards Integral Utilization of Grape Pomace From Winemaking Process: A Review. *Waste Manag* **2017**, *68*, 581-594.
- ✓ Bhakuni, G.S.; Bedi, O.; Bariwal, J.; Kumar, P. Hepatoprotective activity of morin and its semi-synthetic derivatives against alcohol induced hepatotoxicity in rats. *Indian J. Physiol. Pharmacol.* **2017**, *61(2)*, 175-190.
- ✓ Boulton, R.B.; Singleton, V.L.; Bisson, L.F.; Kunkee, R.E. Principles and Practices of Winemaking **2013**, Springer-Verlag, New York (USA).
- ✓ Bourrie, B.C.; Willing, B.P.; Cotter, P.D. The Microbiota and Health Promoting Characteristics of the Fermented Beverage Kefir. *Front. Microbiol.* **2016**, *7*, 1-17.
- ✓ Briscoe, C.P.; Tadayyon, M.; Andrews, J.L.; Benson, W.J.; Chambers, J.K.; Eilert, M.M.; Ellish, C.; Elshourbagy, N.; Goetz, A.S.; Minnick, D.T.; Murdock, P.R.; Sauls Jr, H.R.; Shabon, U.; Spinage, L.; Strum, J.C.; Szekeres, P.G.; Tan, K.B.; Way, J.M.; Ignar, D.M.; Wilson, S.; Muir, A. The orphan G protein-coupled receptor GPR40 is activated by Medium and Long-chain fatty acids. *J. Biol. Chem.* **2003**, *278*, 11303-11311.
- ✓ Cao, H.; Ou, J.; Chen, L.; Zhang, Y.; Szkudelski, T.; Delmas, D.; Daglia, M.; Xiao, J. Dietary polyphenols and type 2 diabetes: Human Study and Clinical Trial. *Crit Rev Food Sci Nutr* **2019**, *59(20)*, 3371-3379.
- ✓ Cardoso, C.R.; Favoreto Jr., S.; Oliveira, L.L.; Vancim, J.O.; Barban, G.B.; Ferraz, D.B.; Silva, J.S. Oleic acid modulation of the immune response in wound healing: a new approach for skin repair. *Immunobiology* **2011**, *216(3)*, 409-415.

- ✓ Carrera, C.; Ruiz-Rodríguez, A.; Palma, M.; Barroso, C.G. Ultrasound assisted extraction of phenolic compounds from grapes. *Anal Chim Acta* **2012**, *732*, 100-104.
- ✓ Carullo, G.; Ahmed, A.; Fusi, F.; Sciubba, F.; Di Cocco, M.E.; Restuccia, D.;Spizzirri, U.G.; Saponara, S.; Aiello, F. Vasorelaxant Effects Induced by Red Wine and Pomace Extracts of Magliocco Dolce cv. Pharmaceuticals **2020a**, 13, 87.
- ✓ Carullo, G.; Aiello, F. Quercetin-3-oleate. *Molbank* **2018**, M1006.
- ✓ Carullo, G.; Durante, M.; Sciubba, F.; Restuccia, D.; Spizzirri, U.G.; Ahmed, A.; Di Cocco, M.E.; Saponara, S.; Aiello, F.; Fusi; F. Vasoactivity of Mantonico and Pecorello grape pomaces on rat aorta rings: An insight into nutraceutical development. *J. Funct. Foods* **2019a**, *57*, 328-334.
- ✓ Carullo, G.; Governa, P.; Leo, A.; Gallelli, L.; Citraro, R.; Cione, E.; Caroleo, M.C.; Biagi, M.; Aiello, F.; Manetti, F. Quercetin-3-Oleate Contributes to Skin Wound Healing Targeting FFA1/GPR40. *ChemistrySelect* **2019c**, *4*, 8429-8433.
- ✓ Carullo, G.; Governa, P.; Spizzirri, U.G.; Biagi, M.; Sciubba, F.; Giorgi, G.; Loizzo, M.R.; Di Cocco, M.E.; Aiello, F.; Restuccia, D. Sangiovese cv Pomace Seeds Extract-Fortified Kefir Exerts Anti-Inflammatory Activity in an In Vitro Model of Intestinal Epithelium Using Caco-2 Cells. *Antioxidants* **2020b**, *9*, 54.
- ✓ Carullo, G.; Perri, M.; Manetti, F.; Aiello, F.; Caroleo, M.C.; Cione, E. Quercetin-3-oleoyl derivatives as new GPR40 agonists: Molecular docking studies and functional evaluation. *Bioorg. Med. Chem. Lett.* **2019b**, *29*, 1761-1764.
- ✓ Caselli, A.; Cirri, P.; Santi, A.; Paoli, P. Morin: A Promising Natural Drug. *Curr. Med. Chem.* **2016**, *23*, 774-791.
- ✓ Chao, C.; Lii, C.; Ye, S.; Li, C.; Lu, C.; Lin, A.; Liu, K.; Chen, H. Docosahexaenoic acid inhibits vascular endothelial growth factor (VEGF)-induced cell migration via the GPR120/PP2A/ERK1/2/eNOS signaling pathway in human umbilical vein endothelial cells. *J. Agric. Food Chem.* **2014**, 62, 4152-4158.
- ✓ Chen, T.; Ning, M.; Ye, Y.; Wang, K.; Leng, Y.; Shen, J. Design, synthesis and structure−activity relationship studies of GPR40 agonists containing amide linker. *Eur J Med Chem* **2018**, *152*, 175-194.
- ✓ Chinthakunta, N.; Cheemanapalll, S.; Chinthakunta; S.; Anuradha, C.M.; Kumar Chitta, S. A new insight into identification of in silico analysis of natural compounds targeting GPR120. *Netw Model Anal Health Inform Bioinform* **2018**, 7, 8.
- ✓ Christiansen, E.; Hansen, S.V.F.; Urban, C.; Hudson, B.D.; Wargent, E.T.; Grundmann, M.; Jenkins, L.; Zaibi, M.; Stocker, C.J.; Ullrich, S.; Kostenis, E.; Kassack, M.U.; Milligan, G.; Cawthorne, M.A.; Ulven, T. Discovery of TUG-770: A Highly Potent Free Fatty Acid Receptor 1 (FFA1/GPR40) Agonist for Treatment of Type 2 Diabetes. *ACS Med. Chem. Lett.* **2013**, *4*, 441-445.
- ✓ Cirillo, G.; Puoci, F.; Iemma, F.; Curcio, M.; Parisi, O.I.; Spizzirri, U.G.; Altimari, I.; Picci, N. Starch-quercetin conjugate by radical grafting: synthesis and biological characterization. *Pharm. Dev. Technol.* **2012**, *17*, 466-476.
- ✓ Cocetta, V.; Catanzaro, D.; Borgonetti, V.; Ragazzi, E.; Giron, M.C.; Governa, P.; Carnevali, I.; Montopoli, M.; Biagi, M. A Fixed Combination of Probiotics and Herbal Extracts Attenuates Intestinal Barrier Dysfunction from Inflammatory Stress in an In vitro Model Using Caco-2 Cells. *Recent Pat Food Nutr Agric* **2019**, *10*, 62-69.
- ✓ Coda, R.; Larena, A.; Trani, A.; Gobbetti, M.; Cagno, R.D. Yogurt-like beverages made of a mixture of cereals, soy and grape must: microbiology, texture, nutritional and sensory properties. *Int J Food Microbiol* **2012**, *155*, 120-127.
- ✓ D'Andrea, G. Quercetin: a flavonol with multifaceted therapeutic applications? *Fitoterapia* **2015**, *106*, 256-271.
- ✓ de Oliveira, L.M.; de Oliveira, T.S.; Menezes da Costa, R.; de Souza Gil, E.; Alves Costa, E.; de Cassia Aleixo Tostes Passaglia, R.; Paranaíba Filgueira, F.; Ghedini, P.C. The vasorelaxant effect of gallic acid involves endothelium-dependent and-independent mechanisms. *Vasc. Pharmacol.* **2016**, *81*, 69-74.
- ✓ Detremmerie, C.M.; Chen, Z.; Li, Z.; Alkharfy, K.M.; Leung, S.W.; Xu, A.; Gao, Y.; Vanhoutte, P.M. Endothelium-dependent contractions of isolated arteries to thymoquinone require biased activity of soluble guanylyl cyclase with subsequent cyclic IMP production. *J. Pharmacol. Exp. Ther.* **2016**, *358(3)*, 558-568.
- ✓ Dias, K.S.T.; de Paula, C.T.; dos Santos, T.; Souza, I.N.O.; Boni, M.S.; Guimarães, M.J.R.; da Silva, F.M.R.; Castro, N.G.; Neves, G.A.; Veloso, C.C.; Coelho, M.M.; Souza F. de Melo, I.; Giusti, F.C.V.; Giusti-Paiva, A.; da Silva, M.L.; Dardenne, L.E.; Guedes, I.A.; Pruccoli, L.; Morroni, F.; Tarozzi, A.; Viegas Jr., C. Design, synthesis and evaluation of novel feruloyl-donepezil hybrids as potential multitarget drugs for the treatment of Alzheimer's disease. *Eur. J. Med. Chem.* **2017**, *130*, 440-457.
- ✓ Eichhorn, B.; Dobrev, D. Vascular large conductance calcium-activated potassium channels: functional role and therapeutic potential, *Naunyn Schmiedebergs Arch. Pharmacol.* **2007**, *376*, 145-155.
- ✓ Feng, X.; Leng, J.; Xie, Z.; Li, S.; Zhao, W.; Tang, Q. GPR40: A therapeutic target for mediating insulin secretion (Review). *Int J Mol Med.* **2012**, *30*, 1261-1266.
- ✓ Fontana, A.R.; Antoniolli, A.; Bottini, R. Grape pomace as a sustainable source of bioactive compounds: extraction, characterization, and biotechnological applications of phenolics. *J. Agric. Food Chem.* **2013**, *61*, 8987-9003.

- ✓ Fransen, P.; Van Hove, C.E.; Leloup, A.J.; Martinet, W.; De Meyer, G.R.; Lemmens, K.; Bult, H.; Schrijvers, D.M. Dissecting out the complex Ca2+-mediated phenylephrine induced contractions of mouse aortic segments. *PLoS One* **2015**, *10(3)*, e0121634.
- ✓ Frattaruolo, L.; Carullo, G.; Brindisi, M.; Mazzotta, S.; Bellissimo, L.; Rago, V.; Curcio, R.; Dolce, V.; Aiello, F.; Cappello, A.R. Antioxidant and anti-inflammatory activities of flavanones from Glycyrrhiza glabra L. (licorice) leaf phytocomplexes: identification of licoflavanone as a modulator of NF-kB/MAPK pathway. *Antioxidants* **2019**, 8, 186.
- ✓ Fuentes, E.; Palomo, I. Mechanisms of endothelial cell protection by hydroxycinnamic acids. *Vasc. Pharmacol.* **2014**, *63*, 155-161.
- ✓ Fujita, T.; Matsuoka, T.; Honda, T.; Kabashima, K.; Hirata, T.; Narumiya, S. A GPR40 Agonist GW9508 Suppresses CCL5, CCL17, and CXCL10 Induction in Keratinocytes and Attenuates Cutaneous Immune Inflammation. *J Invest Dermatol* **2011**, *131(8)*, 1660-1667.
- ✓ Fusi F.; Saponara S.; Pessina F.; Gorelli B.; Sgaragli G. Effects of quercetin and rutin on vascular preparations. A comparison between mechanical and electrophysiological phenomena. *Eur. J. Nutr*. **2003**, *42*, 10-17.
- ✓ Fusi, F.; Durante, M.; Spiga, O.; Trezza, A.; Frosini, M.; Floriddia, E.; Teodori, E.; Dei, S.; Saponara, S. *In vitro* and *in silico* analysis of the vascular effects of asymmetrical N,N-bis(alkanol)amine aryl esters, novel multidrug resistance-reverting agents. *Naunyn Schmiedebergs Arch Pharmacol* **2016a**, *389*, 1033-1043.
- ✓ Fusi, F.; Durante, M.; Sticozzi, C.; Frosini, M.; Perrone, M.G.; Colabufo, N.A.; Saponara, S. Vascular toxicity risk assessment of MC18 and MC70, novel potential diagnostic tools for *in vivo* PET studies. *Basic Clin Pharmacol Toxicol* **2018**, *120(5)*, 434-441.
- ✓ Fusi, F.; Manetti, F.; Durante, M.; Sgaragli, G.; Saponara, S. The vasodilator papaverine stimulates L-type Ca^{2+} current in rat tail artery myocytes via a PKA-dependent mechanism. *Vascul. Pharmacol.* **2016b**, *76*, 53-61.
- ✓ Fusi, F.; Saponara, S.; Pessina, F.; Gorelli, B.; Sgaragli, G. Effects of quercetin and rutin on vascular preparations: a comparison between mechanical and electrophysiological phenomena. *Eur J Nutr* **2003**, *42(1)*, 10-17.
- ✓ Fusi, F.; Trezza, A.; Tramaglino, M.; Sgaragli, G.; Saponara, S.; Spiga, O. The beneficial health effects of flavonoids on the cardiovascular system: Focus on K+ channels. *Pharmacol. Res.* **2020**, *152*, 104625.
- ✓ Gao, X.; Li, B. Chemical and microbiological characteristics of kefir grains and their fermented dairy products: A review. *Cogent Food Agric.* **2016**, *2*, 1272152.
- ✓ Gharras, H.E. Polyphenols: food sources, properties and applications – a review. *Int. J. Food Sci. Technol.* **2009**, *44*, 2512-2518.
- ✓ Ghayur, M.N.; Khan, H.; Hassan Gilani, A. Antispasmodic, bronchodilator and vasodilator activities of (+)-catechin, a naturally occurring flavonoid. *Arch. Pharmacal Res.* **2007**, *30(8)*, 970-975.
- ✓ Giorgetti, L.; Giorgi, G.; Cherubini, E.; Gervasi, P.G.; Della Croce, C.M.; Longo, V.; Bellani, L. Screening and identification of major phytochemical compounds in seeds, sprouts and leaves of Tuscan black kale Brassica oleracea (L.) ssp acephala (DC) var. sabellica L. *Nat Prod Res* **2018**, *32(14)*, 1617-1626.
- ✓ Golden, S.H.; Robinson, K.A.; Saldanha, I.; Anton, B., Ladenson, P.W. Prevalence and Incidence of Endocrine and Metabolic Disorders in the United States: A Comprehensive Review. *J Clin Endocrinol Metab* **2009**, *94(6)*, 1853-187.
- ✓ Gonçalves, G.A.; Soares, A.A.; Correa, R.C.G.; Barros, L.; Haminiuk, C.W.I.; Peralta, R.M.; Ferreira, I.C.F.R.; Bracht, A. Merlot grape pomace hydroalcoholic extract improves the oxidative and inflammatory states of rats with adjuvant-induced arthritis. *J Funct Foods* **2017**, *33*, 408-418.
- ✓ Governa, P.; Carullo, G.; Biagi, M.; Rago, V.; Aiello, F. Evaluation of the in vitro wound-healing activity of calabrian honeys. *Antioxidants* **2019**, 8, 36.
- ✓ Governa, P.; Marchi, M.; Cocetta, V.; De Leo, B.; Saunders, P.T.K.; Catanzaro, D.; Miraldi, E.; Montopoli, M.; Biagi, M. Effects of Boswellia serrata Roxb . and Curcuma longa L . in an In Vitro Intestinal Inflammation Model Using Immune Cells and Caco-2. *Pharmaceuticals* **2018**, *11*, 126.
- ✓ Gujral, N.; Won Suh, J.; Sunwoo, H.H. Effect of anti-gliadin IgY antibody on epithelial intestinal integrity and inflammatory response induced by gliadin. *BMC Immunology* **2015**, *16*, 41.
- ✓ Guo, D.; Li, D.; Ning, M.; Dang, X.; Zhang, L.; Zeng, L.; Hu, Y.; Leng, Y. Yhhu4488, a novel GPr40 agonist, promotes GLP-1 secretion and exerts anti-diabetic effect in rodent models. *Biochem Biophys Res Commun* **2015**, *466*, 740-747.
- ✓ Hamdouchi, C.; Maiti, P.; Warshawsky, A.M.; DeBaillie, A.C.; Otto, K.A.; Wilbur, K.L.; Kahl, S.D.; Patel Lewis, A.; Cardona, G.R.; Zink, R.W.; Chen, K.; CR, S.; Lineswala, J.P.; Neathery, G.L.; Bouaichi, C.; Diseroad, B.A.; Campbell, A.N.; Sweetana, S.A.; Adams, L.A.; Cabrera, O.; Ma, X.; Yumibe, N.P.; Montrose-Rafizadeh, C.; Chen, Y.; Reifel Miller, A. Discovery of LY3104607: A Potent and Selective G Protein-Coupled Receptor 40 (GPR40) Agonist with Optimized Pharmacokinetic Properties to Support Once Daily Oral Treatment in Patients with Type 2 Diabetes Mellitus. *J. Med. Chem.* **2018**, *61*, 934-945.
- ✓ Hayakawa, K.; Kimura, M.; Kamata, K. K. Mechanism underlying gammaaminobutyric acid-induced antihypertensive effect in spontaneously hypertensive rats. *Eur. J Pharmacol.* **2002**, *438(1-2)*, 107-113.

- ✓ Heiss, E.H.; Dirsch, V.M. Regulation of eNOS enzyme activity by posttranslational modification. *Curr. Pharm. Des.* **2014**, *20(22)*, 3503-3513.
- ✓ Houze, J.B.; Zhu, L.; Sun, Y.; Akerman, M.; Qiu, W.; Zhang, A.J.; Sharma, R.; Schmitt, M.; Wang, Y.; Liu, J.; Liu, J.; Medina, J.C.; Reagan, J.D.; Luo, J.; Tonn, G.; Zhang, J.; Lu, J.Y.; Chen, M.; Lopez, E.; Nguyen, K.; Yang, L.; Tang, L.; Tian, H.; Shuttleworth, S.J.; Lin, D.C. AMG837: a potent, orally bioavailable GPR40 agonist. *Bioorg Med Chem Lett* **2012**, *22(2)*, 1267-1270.
- ✓ Huang, W.F.; Ouyang, S.; Li, S.Y.; Lin, Y.F.; Ouyang, H.; Zhang, H.; Lu, C.J. Effect of quercetin on colon contractility and L-type Ca(2+) channels in colon smooth muscle of guinea-pig. *Sheng Li Xue Bao* **2009**, *61*, 567-576.
- ✓ Hubatsch, I.; Ragnarsson, E.G.E.; Artursson, P. Determination of drug permeability and prediction of drug absorption in Caco-2 monolayers. *Nature Protocols* **2007**, *2*, 2111.
- ✓ Iozzi, D.; Schubert, R.; Kalenchuk, V.U.; Neri, A.; Sgaragli, G.; Fusi, F.; Saponara, S. Quercetin Relaxes Rat Tail Main Artery Partly via a PKG-mediated Stimulation of KCa 1.1 Channels. *Acta Physiol (Oxf)* **2013**, *208(4)*, 329-339.
- ✓ Jiménez, R.; Duarte, J.; Perez-Vizcaino, F. Epicatechin: endothelial function and blood pressure. *J Agric Food Chem* **2012**, *60*, 8823-8830.
- ✓ Katsimardou, A.; Imprialos, K.; Stavropoulos, K.; Sachinidis, A.; Doumas, M.; Athyros, V. Hypertension in Metabolic Syndrome: Novel Insights. *Curr Hypertens Rev* **2019**, *15*, 1-7.
- ✓ Komprda, T. Effect of n-3 long-chain polyunsaturated fatty acids on wound healing using animal models – a review. *Acta Vet. Brno* **2018**, 87, 309-320.
- ✓ Krasavin, M.; Lukin, A.; Zhurilo, N.; Kovalenko, A.; Zahanich, I.; Zozulya, S.; Moore, D.; Tikhonova, I.G. Novel free fatty acid receptor 1 (GPR40) agonists based on 1,3,4-thiadiazole-2-carboxamide scaffold. *Bioorganic Med Chem* **2016**, *24*, 2954-2963.
- ✓ Kumar Verma, V.; Malik, S.; Narayanan, S.P.; Mutneja, E.; Kumar Sahu, A.; Bhatia, J.; Singh Arya, D. Role of MAPK/NF-κB pathway in cardioprotective effect of Morin in isoproterenol induced myocardial injury in rats. *Mol. Biol. Rep.* **2019**, *46*, 1139-1148.
- ✓ Kumar, M.; Kasala, E.R.; Bodduluru, L.N.; Kumar, V.; Lahkar, M. Molecular and biochemical evidence on the protective effects of quercetin in isoproterenol-induced acute myocardial injury in rats. *J. Biochem. Mol. Toxicol.* **2017**, *31*, e21832.
- ✓ Leal, J.; Teixeira-Santos, L.; Pinho, D.; Afonso, J.; Carvalho, J.; de Lourdes Bastos, M.; Albino-Teixeira, A.; Fraga, S.; Sousa, T. L-proline supplementation improves nitric oxide bioavailability and counteracts the blood pressure rise induced by angiotensin II in rats. *Nitric Oxide* **2019**, *82*, 1-11.
- ✓ Li, A.; Li, Y.; Du, L. Biological characteristics and agonists of GPR120 (FFAR4) receptor: the present status of research. *Future Med. Chem.* **2015**, 7(11), 1457-1468.
- ✓ Li, N.; Shi, Z.; Tang, Y.; Yang, J.; Duan, J. An efficient partial synthesis of 4'-O-methylquercetin via regioselective protection and alkylation of quercetin. *Beilstein J. Org. Chem.* **2009**, *5*, 60.
- ✓ Li, Z.; Xu, W.; Huang, W.; Qian, H. Free Fatty Acid Receptor 1 (FFAR1) as an Emerging Therapeutic Target for Type 2 Diabetes Mellitus: Recent Progress and Prevailing Challenges. *Med Res Rev.* **2018**, *38(2)*, 381-425.
- ✓ Liu, M.; Saeki, M.; Matsunobu, T.; Okuno, T.; Koga, T.; Sugimoto, Y.; Yokoyama, C.; Nakamizo, S.; Kabashima, K.; Narumiya, S.; Shimizu, T.; Yokomizo, T. 12-hydroxyheptadecatrienoic acid promotes epidermal wound healing by accelerating keratinocyte migration via the BLT2 receptor. *J. Exp. Med.* **2014**, *211(6)*, 1063-1078.
- ✓ Liu, Z.; Hopkins, M.M.; Zhang, Z.; Quisenberry, C.B.; Fix, L.C.; Galvan, B.M.; Meier, K.E. Omega-3 fatty acids and other FFA4 agonists inhibit growth factor signaling in human prostate cancer cells. *J Pharmacol Exp Ther.* **2015**, 352(2), 380-394.
- ✓ Lodi, F.; Jimenez, R.; Moreno, L.; Kroon, P.A.; Needs, P.W.; Hughes, D.A.; Santos-Buelga, C.; Gonzalez-Paramas, A.; Cogolludo, A.; Lopez-Sepulveda, R.; Duarte, J.; Perez-Vizcaino, F. Glucuronidated and sulfated metabolites of the flavonoid quercetin prevent endothelial dysfunction but lack direct vasorelaxant effects in rat aorta. *Atherosclerosis* **2009**, *204*, 34-39.
- ✓ Loh, Y.C.; Tan, C.S.; Ch'ng, Y.S.; Yeap, Z.Q.; Ng, C.H.; Yam, M.F. Overview of the microenvironment of vasculature in vascular tone regulation. *Int J Mol Sci* **2018**, *19(1)*, 120.
- ✓ Lucarini, M.; Durazzo, A.; Romani, A.; Campo, M.; Lombardi-Boccia, G.; Cecchini, F. Bio-based compounds from grape seeds: a biorefinery approach. *Molecules* **2018**, *23*, 1888.
- ✓ Malishevskaia, I.V.; Ilashchuk, T.A.; Okipniak, I.V. Therapeutic efficacy of quercetin in patients with ischemic heart disease with underlying metabolic syndrome. *Georg. Med. News* **2013**, *225*, 67-71.
- ✓ Mattarei, A.; Biasutto, L.; Rastrelli, F.; Garbisa, S.; Marotta, E.; Zoratti, M.; Paradisi, C. Regioselective O-Derivatization of Quercetin via Ester Intermediates. An Improved Synthesis of Rhamnetin and Development of a New Mitochondriotropic Derivative. *Molecules* **2010**, *15*, 4722-4736.
- ✓ Mazzotta, S.; Brizzi, A.; Manetti, F.; Borgonetti, V.; Pessina, F.; Governa, P.; Carullo, G.; Aiello, F. ACS MED CHEM LETT 2020.

- ✓ Meegalla, S.K.; Huang, H.; Martin, T.; Xu, J.; Zhao, S.; Liu, J.; Hall, M.; Gunnet, J.; Wang, Y.; Rady, B.; Silva, J.; Otieno, M.; Arnoult, E.; Lee, S.P.; Pocai, A.; Player, M.R. Discovery of a novel potent GPR40 full agonist. *Bioorg Med Chem Lett* **2018**, *28*, 720-726.
- ✓ Miller, K.V.; Block, D.E. A review of wine fermentation process modelling. *J. Food Eng.* **2020**, *273*, 109783.
- ✓ Milligan, G.; Alvarez-Curto, E.; Hudson, B.D.; Prihandoko, R.; Tobin, A.B. FFA4/GPR120: pharmacology and therapeutic opportunities. *Trends Pharmacol Sci* **2017**, 38(9), 809-821.
- ✓ Mukhopadhyay, P.; Prajapati, A.K. Quercetin in anti-diabetic research and strategies for improved quercetin bioavailability using
- ✓ Naderi, G.A.; Asgary, S.; Sarraf-Zadegan, N.; Shirvany, H. Anti-oxidant effect of flavonoids on the susceptibility of LDL oxidation. *Mol Cell Biochem* **2003**, *246*, 193-196.
- ✓ Natoli, M.; Nicolosi, G.; Piattelli, M. Regioselective Alcoholysis of Flavonoid Acetates with Lipase in an Organic Solvent. *J. Org. Chem.* **1992**, *57*, 5776-5778.
- ✓ Negoro, N.; Sasaki, S.; Mikami, S.; Ito, M.; Suzuki, M.; Tsujihata, Y.; Ito, R.; Harada, A.; Takeuchi, K.; Suzuki, N.; Miyazaki, J.; Santou, T.; Odani, T.; Kanzaki, N.; Funami, M.; Tanaka, T.; Kogame, A.; Matsunaga, S.; Yasuma, T.; Momose, Y. Discovery of TAK-875: A Potent, Selective, and Orally Bioavailable GPR40 Agonist. *ACS Med. Chem. Lett.* **2010**, *1*, 290-294.
- ✓ Oh, S.Y.; Lee, S.J.; Jung, Y.H.; Lee, H.J.; Han, H.J. Arachidonic acid promotes skin wound healing through induction of human MSC migration by MT3-MMP-mediated fibronectin degradation. *Cell Death Dis.* **2015**, *6*, e1750.
- ✓ Olmo, I.; Teuber, S.; Larrazabal, C.; Alarcon, P.; Raipane, F.; Burgos, R.A.; Hidalgo, M.A. Docosahexaenoic acid and TUG-891 activate free fatty acid-4 receptor in bovine neutrophils. *Vet Immunol Immunopathol* **2019**, 209, 53-60.
- ✓ Olokoba, A.B.; Obateru, O.A.; Olokoba, L.B. Type 2 Diabetes Mellitus: A Review of Current Trends. *Oman Med. J.* **2012**, *27(4)*, 269-273.
- ✓ Perez-Martinez, P.; Garcia-Rios, A.; Delgado-Lista, J.; Perez-Jimenez, F.; Lopez-Miranda, J. Mediterranean diet rich in olive oil and obesity, metabolic syndrome and diabetes mellitus. *Curr. Pharm. Des.* **2011**, *17(8)*, 769-777.
- ✓ Polerà, N.; Badolato, M.; Perri, F.; Carullo, G.; Aiello, F. Quercetin and its Natural Sources in Wound Healing Management. *Curr Med Chem* **2019**, DOI: https://doi.org/10.2174/0929867325666180713150626.
  polymer-based carriers – a review. *RSC Adv.* **2015**, *5*, 97547-97562.
- ✓ Rayasam, G.V.; Tulasi, V.K.; Sundaram, S.; Singh, W.; Kant, R.; Davis, J.A.; Saini, K.S.; Ray, A. Identification of Berberine as a Novel Agonist of Fatty Acid Receptor GPR40. *Phytother. Res.* **2010**, *24*, 1260-1263.
- ✓ Restuccia, D.; Sicari, V.; Pellicanò, T.M.; Spizzirri, U.G.; Loizzo, M.R. The impact of cultivar on polyphenol and biogenic amine profiles in Calabrian red grapes during winemaking. *Food Res Int.* **2017**, *102*, 303-312.
- ✓ Restuccia, D.; Spizzirri, U.G.; Chiricosta, S.; Puoci, F.; Altimari, I.; Picci, N. Antioxidant properties of extravirgin olive oil from cerasuola cv olive fruit: Effect of stone removal. *Int. J Food Sci* **2011**, *23*, 62-71.
- ✓ Ridner, G.; Bartoov-Shifman, R.; Zalogin, T.; Avnit-Sagi, T.; Sharivkin, R.; Kantorovich, L.; Weiss, S.; Walker, M.D. Regulation of the GPR40 locus: towards a molecular understanding. *Biochem Soc Trans* **2008**, *36(3)*, 360-362.
- ✓ Rodrigues, D.A.; de Sena M. Pinheiro, P.; Ferreira, T.T.S.C.; Thota, S.; Fraga, C.A.M. Structural Basis for the Agonist Action at Free Fatty Acid Receptor 1 (FFA1R or GPR40). *Chem Biol Drug Des* **2018**, *91(3)*, 668-680.
- ✓ Saik, A.Y.H.; Lim, Y.Y.; Stanslas, J.; Choo, W.M. Enzymatic synthesis of quercetin oleate esters using Candida antarctica lipase B. *Biotechnol. Lett.* **2017**, *39*, 297-304.
- ✓ Sambuy, Y.; De Angelis, I.; Ranaldi, G.; Scarino, M.L.; Stammati, A.; Zucco, F. The Caco-2 cell line as a model of the intestinal barrier: influence of cell and culture-related factors on Caco-2 cell functional characteristics. *Cell Biol Toxicol* **2005**, *21*, 1-26.
- ✓ Saponara, S.; Carosati, E.; Mugnai, P.; Sgaragli, G.; Fusi, F. The flavonoid scaffold as a template for the design of modulators of the vascular $Ca_v1.2$ channels. *Br. J. Pharmacol.* **2011**, *164*, 1684-1697.
- ✓ Saponara, S.; Durante, M.; Spiga, O.; Mugnai, P.; Sgaragli, G.; Huong, T.T.; Khanh, P.N.; Son, N.T.; Cuong, N.M.; Fusi, F. Functional, electrophysiological and molecular docking analysis of the modulation of $Ca_v1.2$ channels in rat vascular myocytes by murrayafoline A. *Br. J. Pharmacol.* **2016**, *173(2)*, 292-304.
- ✓ Saponara, S.; Sgaragli, G.; Fusi, F. Quercetin as a novel activator of L-type Ca^{2+} channels in rat tail artery smooth muscle cells. *Br. J. Pharmacol.* **2002**, *135*, 1819-1827.
- ✓ Sciubba, F.; Di Cocco, M.E.; Gianferri, R.; Impellizzeri, D.; Mannina, L.; De Salvador, F.R.; Venditti, A.; Delfini, M. Metabolic profile of different Italian cultivars of hazelnut (*Corylus avellana*) by nuclear magnetic resonance spectroscopy. *Nat Prod Res* **2014**, *28*, 1075-1081.
- ✓ Sebastiani, G.; Ceccarelli, E.; Castagna, M.G.; Dotta, F. G-protein-coupled receptors (GPCRs) in the treatment of diabetes: Current view and future perspectives. *Best Pract Res Clin Endocrinol Metab.* **2018**, 32(2), 201-213.
- ✓ Shapiro, H.; Shachar, S.; Sekler, I.; Hershfinkel, M.; Walker, M.D. Role of GPR40 in fatty acid action on the beta cell line INS-1E. *Biochem Biophys Res Commun* **2005**, *335(1)*, 97-104.

- ✓ Shebeko, S.K.; Zupanets, I.A.; Popov, O.S.; Tarasenko, O.O.; Shalamay, A.S. Chapter 27 - Effects of Quercetin and Its Combinations on Health Polyphenols: Mechanisms of Action in Human Health and Disease (Second Edition) **2018**, 373-394.
- ✓ Song, T.; Yang, Y.; Zhou, Y.; Wei, H.; Peng, J. GPR120: a critical role in adipogenesis, inflammation, and energy metabolism in adipose tissue. *Cell Mol Life Sci.* **2017**, 74(15), 2723-2733.
- ✓ Spizzirri, U.G.; Altimari, I.; Puoci, F.; Parisi, O.I.; Iemma, F.; Picci, N. Innovative antioxidant thermos-responsive hydrogels by radical grafting of catechin on inulin chain. *Carbohydr Pol* **2011**, *84*, 517-523.
- ✓ Suri, S.; Liu, X.H.; Rayment, S.; Hughes, D.A.; Kroon, P.A.; Needs, P.W.; Taylor, M.A.; Tribolo, S.; Wilson, V.G. Quercetin and its major metabolites selectively modulate cyclic GMP-dependent relaxations and associated tolerance in pig isolated coronary artery. *Br J Pharmacol* **2010**, *159*, 566-575.
- ✓ Tabasco, R.; Sánchez-Patán, F.; Monagas, M.; Bartolomé, B.; Moreno-Arribas, M.V.; Peláez, C.; Requena, T. Effect of grape polyphenols on lactic acid bacteria and bifidobacteria growth: Resistance and metabolism. *Food Microbiol* **2011**, *28*, 1345-1352.
- ✓ Tian, C.; Hao, L.; Yi, W.; Ding, S.; Xu, F. Polyphenols, Oxidative Stress, and Metabolic Syndrome. *Oxid Med Cell Longev* **2020**, *2020*, 7398453.
- ✓ Tsioutsiou, E. E.; Giachetti, D.; Miraldi, E.; Governa, P.; Magnano, A. R.; Biagi, M. Phytotherapy and Skin Wound Healing. *Acta Vulnologica* **2016**, *14* (3), 126–139.
- ✓ Tsukahara, T.; Hamouda, N.; Utsuni, D.; Matsumoto, K.; Amagase, K.; Kato, S. G Protein-Coupled Receptor 35 Contributes to Mucosal Repair in Mice via Migration of Colonic Epithelial Cells. *Pharmacol Res.* **2017**, *123*, 27-39.
- ✓ Vaisali, C.; Belur, P.D.; Iyyaswami, R. Lipase mediated synthesis of rutin fatty ester: Study of its process parameters and solvent polarity. *Food Chem.* **2017**, *232*, 278-285.
- ✓ Vanhoutte, P.M.; Zhao, Y.; Xu, A.; Leung, S.W. Thirty years of saying NO: Sources, fate, actions, and misfortunes of the endothelium-derived vasodilator mediator. *Circulation Research* **2016**, *119(2)*, 375-396.
- ✓ Venu Gopal, J. Morin Hydrate: Botanical origin, pharmacological activity and its applications: A mini-review. *Pharmacogn. Rev.* **2013**, *5*, 123-126.
- ✓ Vidau, C.; Brunet, J.; Badiou, A.; Belzunces, L.P. Phenylpyrazole insecticides induce cytotoxicity by altering mechanisms involved in cellular energy supply in the human epithelial cell model Caco-2. *Toxicol in Vitro* **2009**, *23*, 589-597.
- ✓ Vinayagam, R.; Xu, B. Antidiabetic properties of dietary flavonoids: a cellular mechanism review. *Nutr. Metab.* **2015**, *12*, 60.
- ✓ Wach, A.; Pyrzy´nska, K.; Biesaga, M. Quercetin content in some food and herbal samples. *Food Chem.* **2007**, *100(2)*, 699-704.
- ✓ Watson, S. J.; Brown, A. J.; Holliday, N. D. Differential signaling by splice variants of the human free fatty acid receptor GPR120. *Mol. Pharmacol.* **2012**, 81, 631-642.
- ✓ Weiß, K.T.; Fante, M.; Köhl, G.; Schreml, J.; Haubner, F.; Kreutz, M.; Haverkampf, S.; Berneburg, M.; Schreml, S. Proton-sensing G Protein-Coupled Receptors as Regulators of Cell Proliferation and Migration During Tumor Growth and Wound Healing. *Exp. Dermatol.* **2017**, *26*, 127-132.
- ✓ Wright, J.M.; Musini, V.M.; Gill, R. First-line drugs for hypertension. *Cochrane Database of Systematic Reviews* **2018**, *4*, CD001841.
- ✓ Wu, T.W.; Fung, K.P.; Zeng, L.H.; Wu, J.; Hempel, A.; Grey, A.A.; Camerman, N. Molecular properties and myocardial salvage effects of morin hydrate. *Biochem Pharmacol* **1995**, *49*, 537-543.
- ✓ Yabuki, C.; Komatsu, H.; Tsujihata, Y.; Maeda, R.; Ito, R.; Matsuda Nagasumi, K.; Sakuma, K.; Miyawaki, K.; Kikuchi, N.; Takeuchi, K.; Habata, Y.; Mori, M. A Novel Antidiabetic Drug, Fasiglifam/TAK-875, Acts as an Ago-Allosteric Modulator of FFAR1. *PLoS One* **2013**, *8(10)*, e76280.
- ✓ Yang, K.; Chan, C.B. Epicatechin potentiation of glucose-stimulated insulin secretion in INS-1 cells is not dependent on its antioxidant activity. *Acta Pharmacol. Sin.* **2018**, *39*, 893-902.
- ✓ Yu, J.; Ahmedna, M. Functional components of grape pomace: their composition, biological properties and potential applications. *Int J Food Sci Tech* **2013**, *48*, 221-223.
- ✓ Zhang, B.; Chen, T.; Chen, Z.; Wang, M.; Zheng, D.; Wu, J.; Jiang, X.; Li, X. Synthesis and anti-hyperglycemic activity of hesperidin derivatives. *Bioorg. Med. Chem. Lett.* **2012**, *22(23)*, 7194-7197.
- ✓ Zhang, H.T.; Wang, Y.; Deng, X.L.; Dong, M.Q.; Zhao, L.M.; Wang, Y.W. Daidzein relaxes rat cerebral basilar artery via activation of large-conductance Ca2+-activated K+ channels in vascular smooth muscle cells. *Eur. J. Pharmacol.* **2010**, *630*, 100-106.
- ✓ Zhang, X.; Mao, A.; Xiao, W.; Zhang, P.; Han, X.; Zhou, T.; Chen, Y.; Jin, J.; Ma, X. Morin induces endothelium-dependent relaxation by activating TRPV4 channels in rat mesenteric arteries. *Eur. J. Pharmacol.* **2019**, *859*, 172561.
- ✓ Zhao, H.; Qiao, J.; Zhang, S.; Zhang, H.; Lei, X.; Wang, X.; Deng, Z.; Ning, L.; Cao, Y.; Guo, Y.; Liu, S.; Duan, E. GPR39 marks specific cells within the sebaceous gland and contributes to skin wound healing. *Sci Rep* **2015**, *5*, 7913.

✓ Zhao, Y.; Vanhoutte, P.M.; Leung, S.W.S. Vascular nitric oxide: Beyond eNOS. *J. Pharmacol. Sci* **2015**, *129(2)*, 83-94.

APPENDIX 1

Table S1. ^{1}H NMR resonance assignment of the extract samples.

Compound	Assignment[a]	^{1}H (ppm)	Multiplicity[b]	Sample
Amino acids				
Valine	α -CH β-CH **γ-CH_3** γ'-CH_3	3,62 2,29 **1,05** 1,00	m m **d** d	2,4,6
Isoleucine	α -CH β-CH γ-CH γ'-CH **δ-CH_3** δ'-CH_3	3,69 1,99 1,25 1,49 **1,01** 0,95	m m m m **d** t	2,4,6
Alanine	α-CH **β-CH_3**	3,77 **1,49**	q **d**	1,2,3,4,5,6
GABA	α-CH_2 β-CH_2 **γ-CH_2**	2,35 1,91 **3,02**	t m **t**	1,2,3,4
Glutamate	α-CH β-CH_2 γ-CH_2	α-CH β-CH_2 **γ-CH_2**	3,74 2,08 **2,36**	2
Glutamine	α-CH β-CH_2 γ-CH_2	α-CH β-CH_2 **γ-CH_2**	3,76 2,11 **2,45**	2
Tyrosine	C2,6H-ring **C3,5H-ring**	6,88 **7,18**	m **m**	4
Phenylalanine	C2,6H-ring CH-4 ring **C3,5H-ring**	7,33 7,39 **7,42**	m m **m**	2,4,6
Tryptophan	CH-2 ring CH-4 ring CH-5 ring **CH-6 ring** CH-7 ring	7,31 7,27 7,19 **7,72** 7,53	s d m **m** d	2,4,6
Organic Acids				
Lactic acid	α-CH **β-CH**	4,12 **1,37**	q **d**	2,3,4
Quinic Acid	**CH_2-1** CH-2 CH-3 CH-4 CH_2-5	**1,89, 2,09** 4,02 3,55 4,15 2,00, 2,06	**dd** m m m dd	1,2,3,4
Succinic acid	**α,β-CH_2**	**2,41**	**s**	2,3,4,6
Malic acid	**α –CH** β-CH_2 β'-CH_2	**4,28** 2,34 2,65	**dd** dd dd	1,2,3,4
Fumaric acid	**α,β-CH=CH**	**6,51**	**s**	1,2

p-Coumaric acid	**α –CH** β-CH CH-2,6 CH-3,5	**6,36** 7,49 6,80 7,51	**d** d m m	2
Gallic acid	**CH-2,6**	**7.05**	**s**	1,2,3,4,5,6
Caffeic acid	**α –CH** β-CH CH-2 CH-5 CH-6	**6,42** 7,42 7.22 6.96 7.14	**d** d d d dd	2
Formic acid	**CH**	**8,46**	**s**	1,2,3,4,5,6
Carbohydrates				
α-Glucose	**CH-1** CH-2 CH-3 CH-4 CH-5 CH_2-6	**5,23** 3,55 3,72 3,42 3,84 3,73 – 3,90	**d** m m m m m	1,2,3,4,5,6
β-Glucose	CH-1 **CH-2** CH-3 CH-4 CH-5 CH_2-6	4,65 **3,24** 3,50 3,42 3,48 3,74 – 3,91	d **dd** m m m m	1,2,3,4,5,6
Sucrose	**GLC CH-1** CH-2 CH-3 CH-4 CH-5 CH2-6 FRU CH_2-1’ CH-3’ CH-4’ CH-5’ CH_2-6	**5,42** 3,59 3,79 3,48 3,85 3,82 3,69 4,22 4,06 3,90 3,82	**d** m m m m m m d m m m	1,6
Fructose	CH_2-1 **CH-3** CH-4 CH-5 CH_2-6	3,69 **4,20** 4,06 3,90 3,82	m **d** m m m	2,3,5,6
Miscellaneous Compounds				
2,3-butanediol	**CH_3**-1 CH-2 CH-3 CH_3-4	**1,16** 3,65 3,74 1,17	**d** m m d	2,3,6
Catechin	CH-6 **CH-8** CH-2’ CH-5’ CH-6’ CH-2’’ CH-3’’ CH2-4’’	6,12 **6,14** 6,95 6,75 6,68 4,56 3,97 2,49, 2,82	d **d** d d dd d m dd	2,3,5,6
Quercetin-3-O-	CH-6	6,20	d	1,2,3

Galactoside	CH-8 CH-2' CH-5' CH-6' **CH-1"** CH-2" CH-3" CH-4" CH-5" CH2-6"	6,41 7,69 6,91 7,55 **5,48** 3,80 3,87 3,98 4,08 3,73	d d d dd **d** m m m m m	
Nicotinamide riboside	**C2H Nam** C4H Nam C5H Nam C6H Nam	**9,61** 8,89 8,31 9,34	**s** m m m	1,2,3,4,5,6

[a] specific resonance signal used for quantization are reported in bold

[b] s: singlet; d: doublet; dd: double doublet; t: triplet; q: quartet; m: multiplet

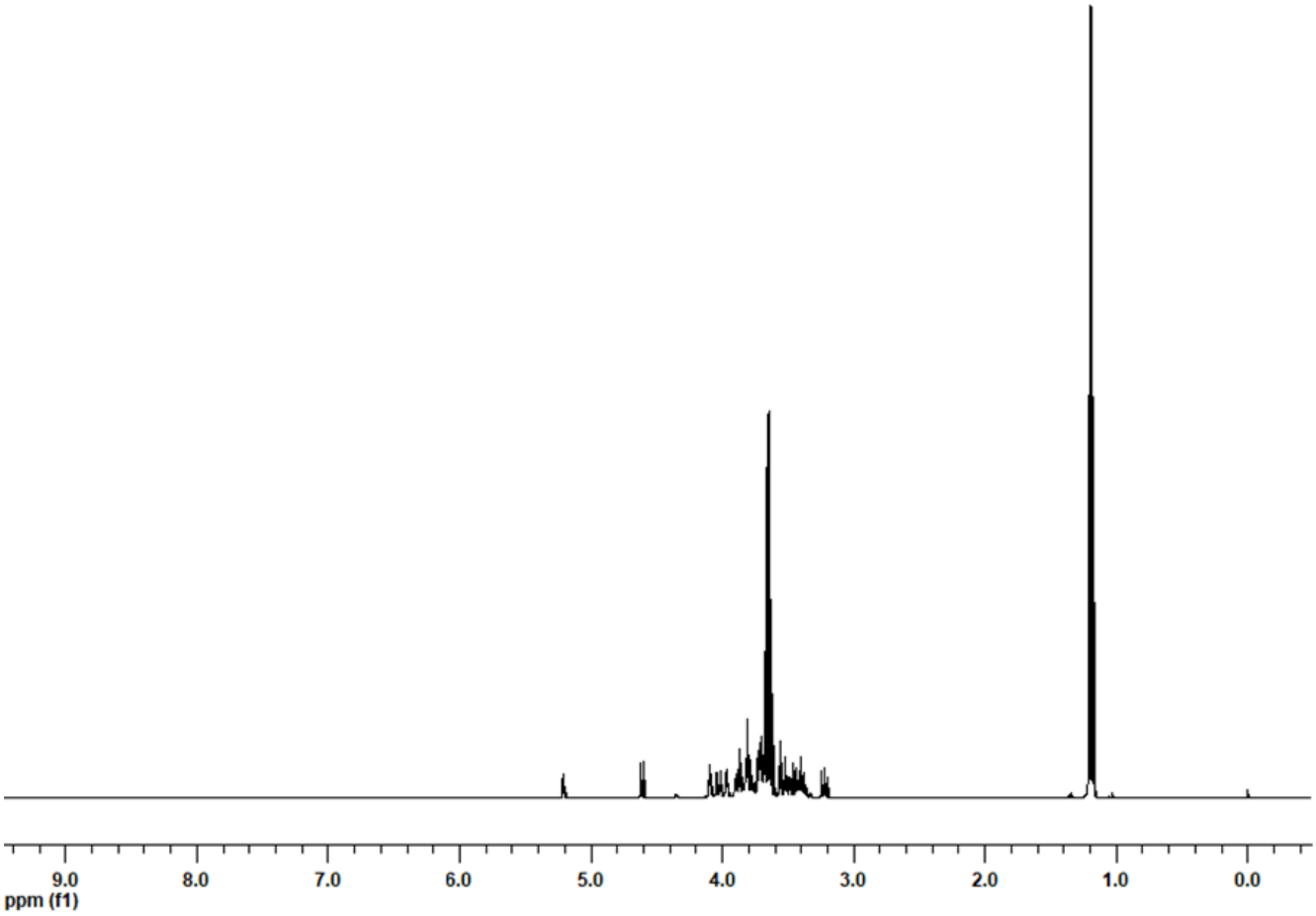

Figure S1: 1D ^{1}H NMR spectrum of **LDC1**

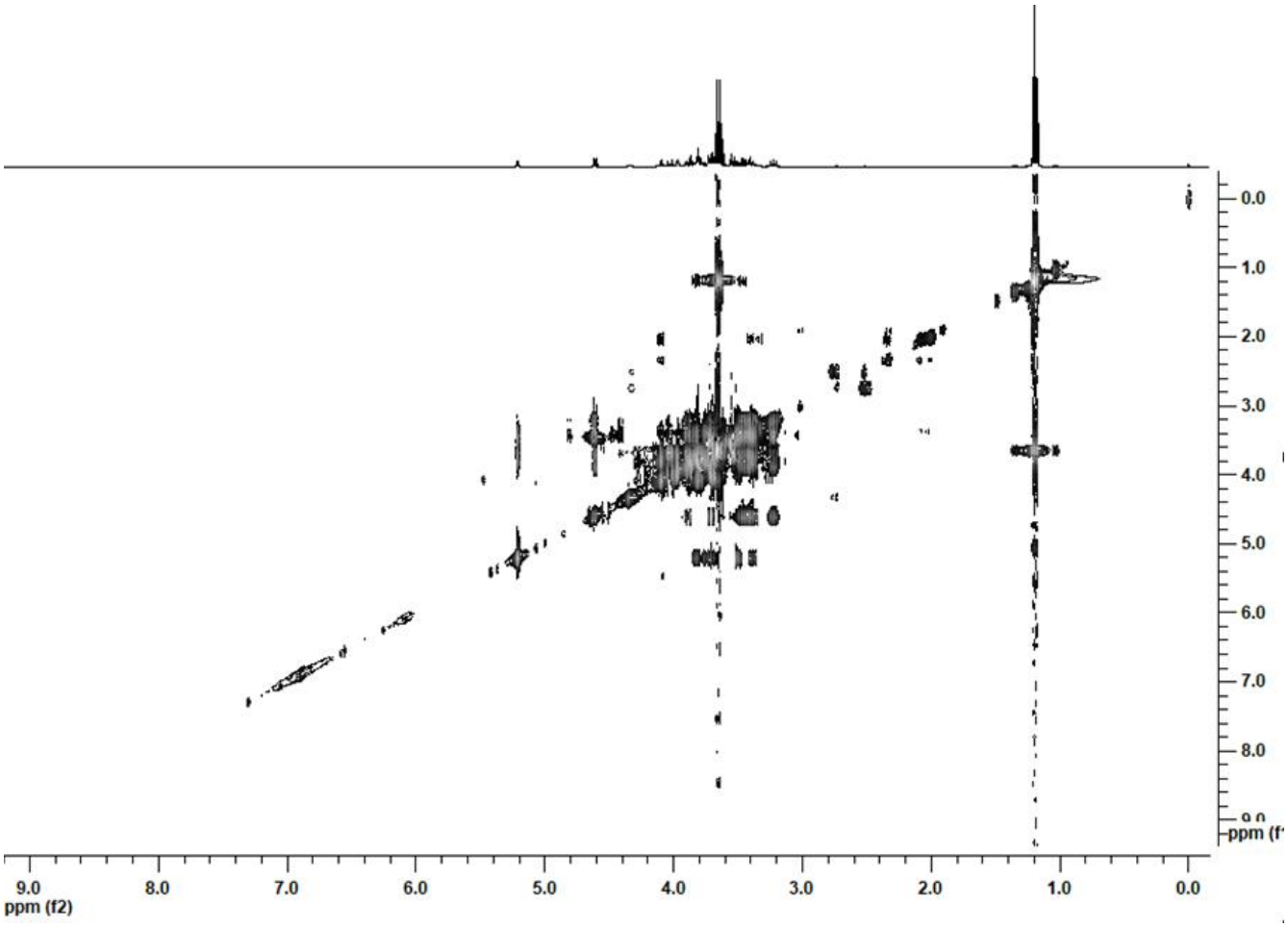

Figure S2: ^{1}H-^{1}H TOCSY NMR spectrum of **LDC1**

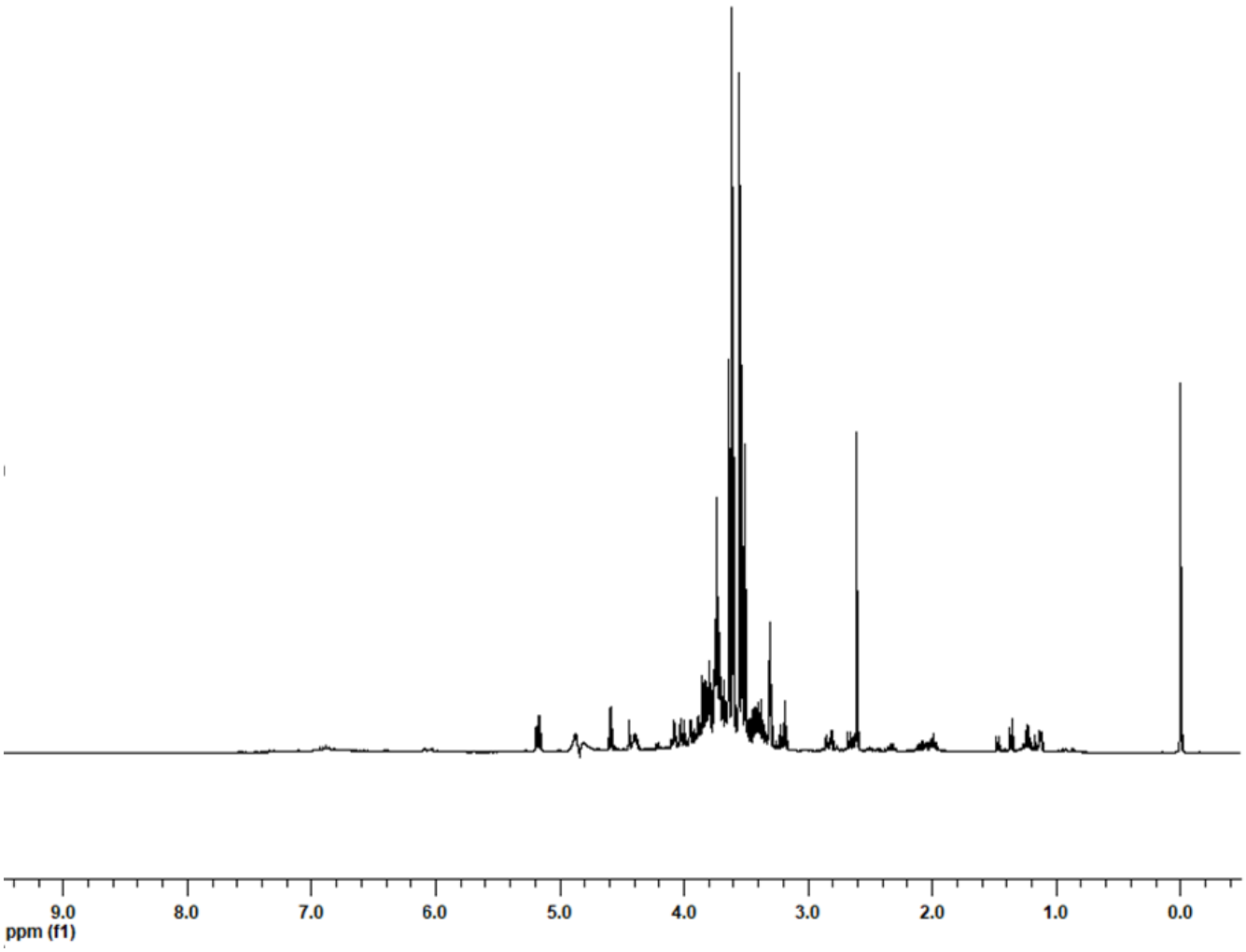

Figure S3: 1D ^{1}H NMR spectrum of **LDC2**

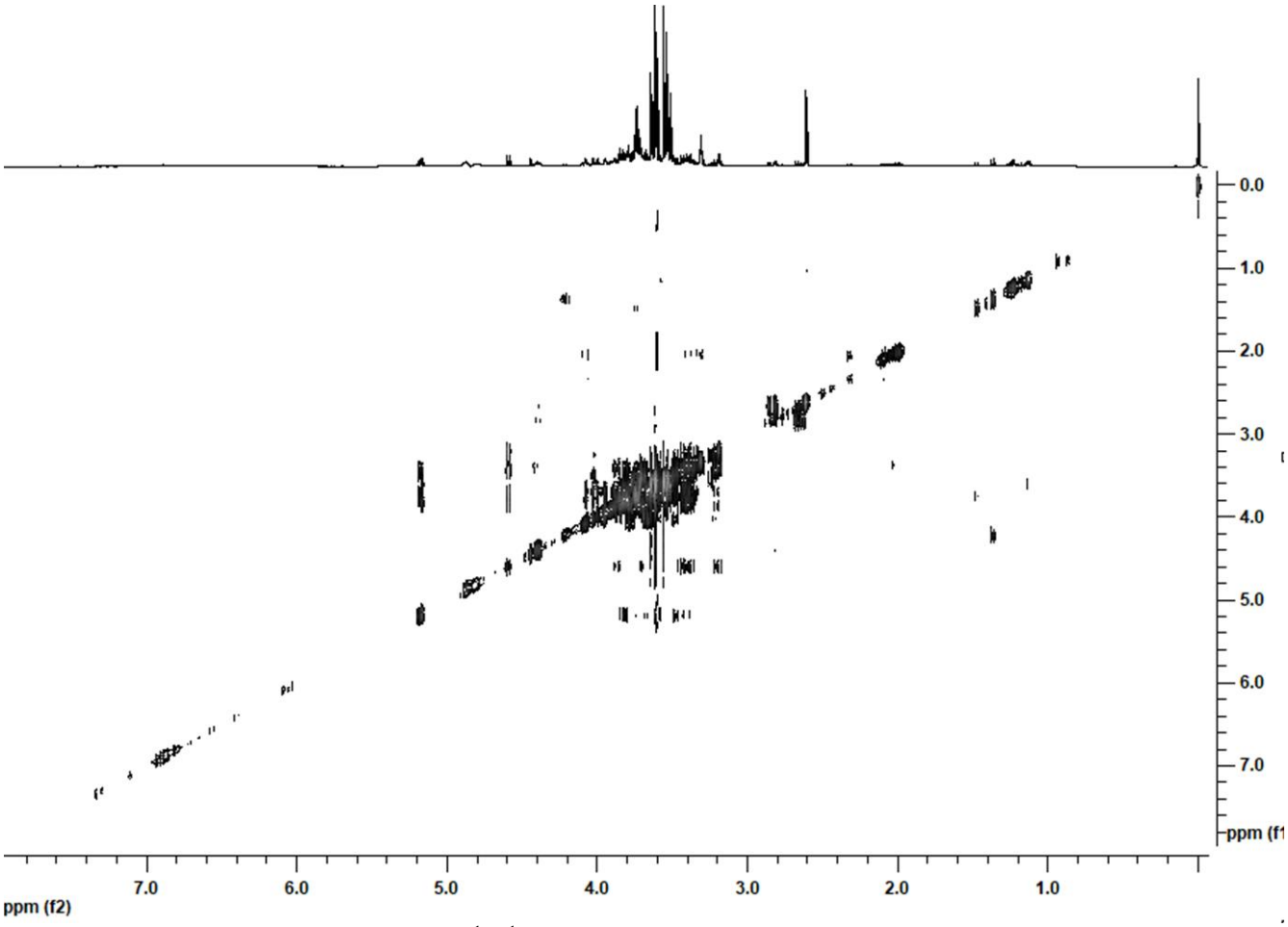

Figure S4: ^{1}H-^{1}H TOCSY NMR spectrum of **LDC2**

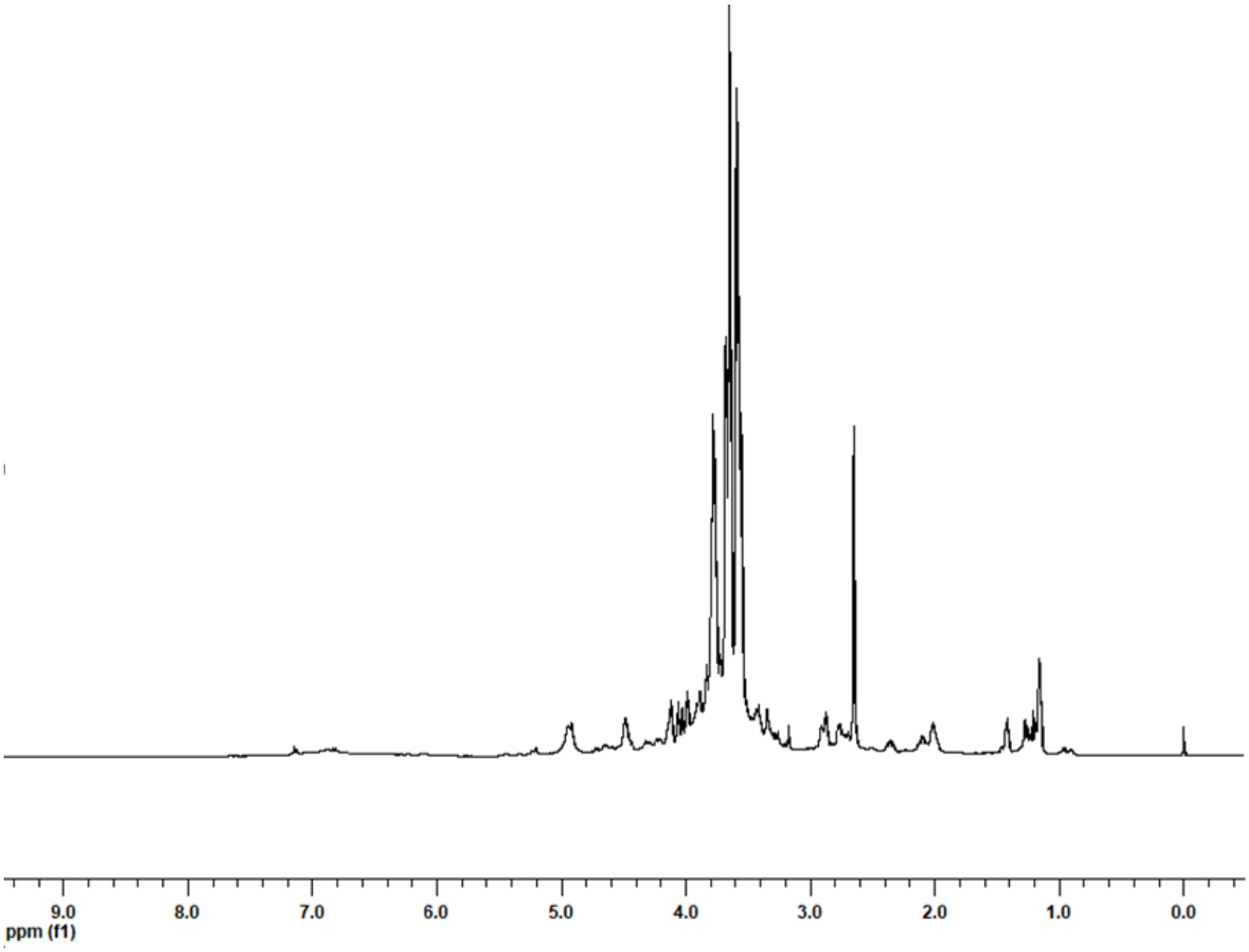

Figure S5: 1D ^{1}H NMR spectrum of **LDC3**

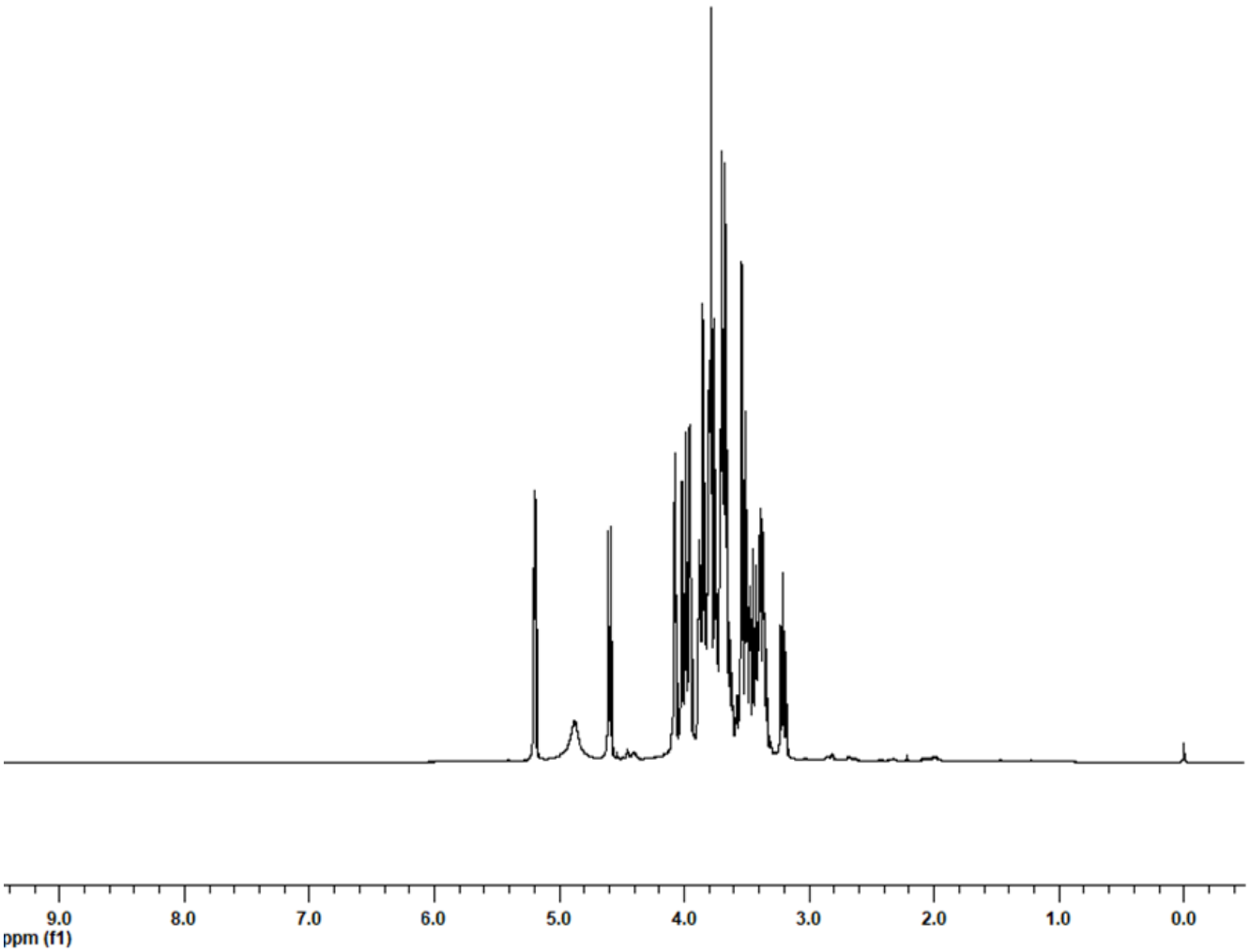

Figure S6: 1D ^{1}H NMR spectrum of **LDC4**

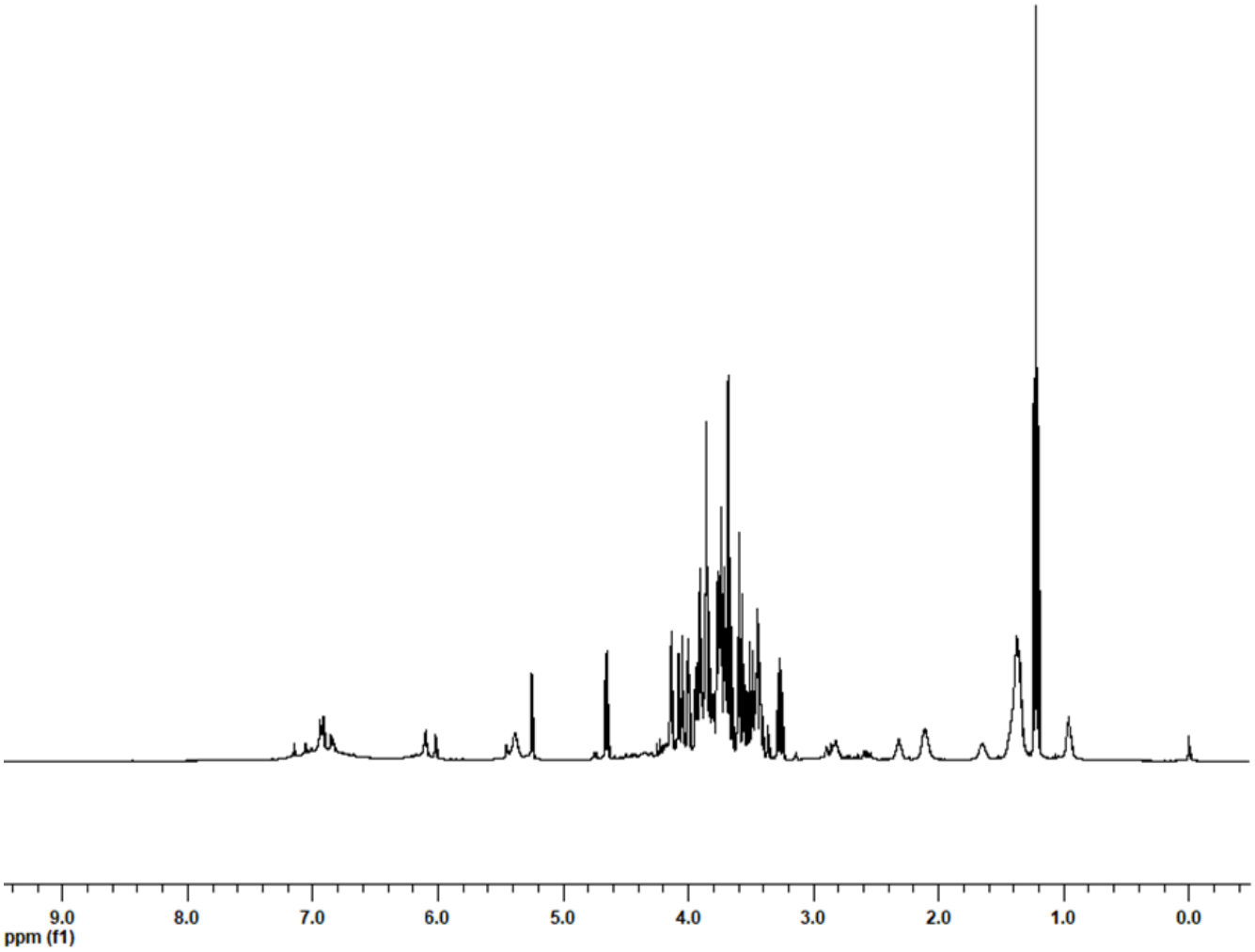

Figure S7: 1D ^{1}H NMR spectrum of **LDC5**

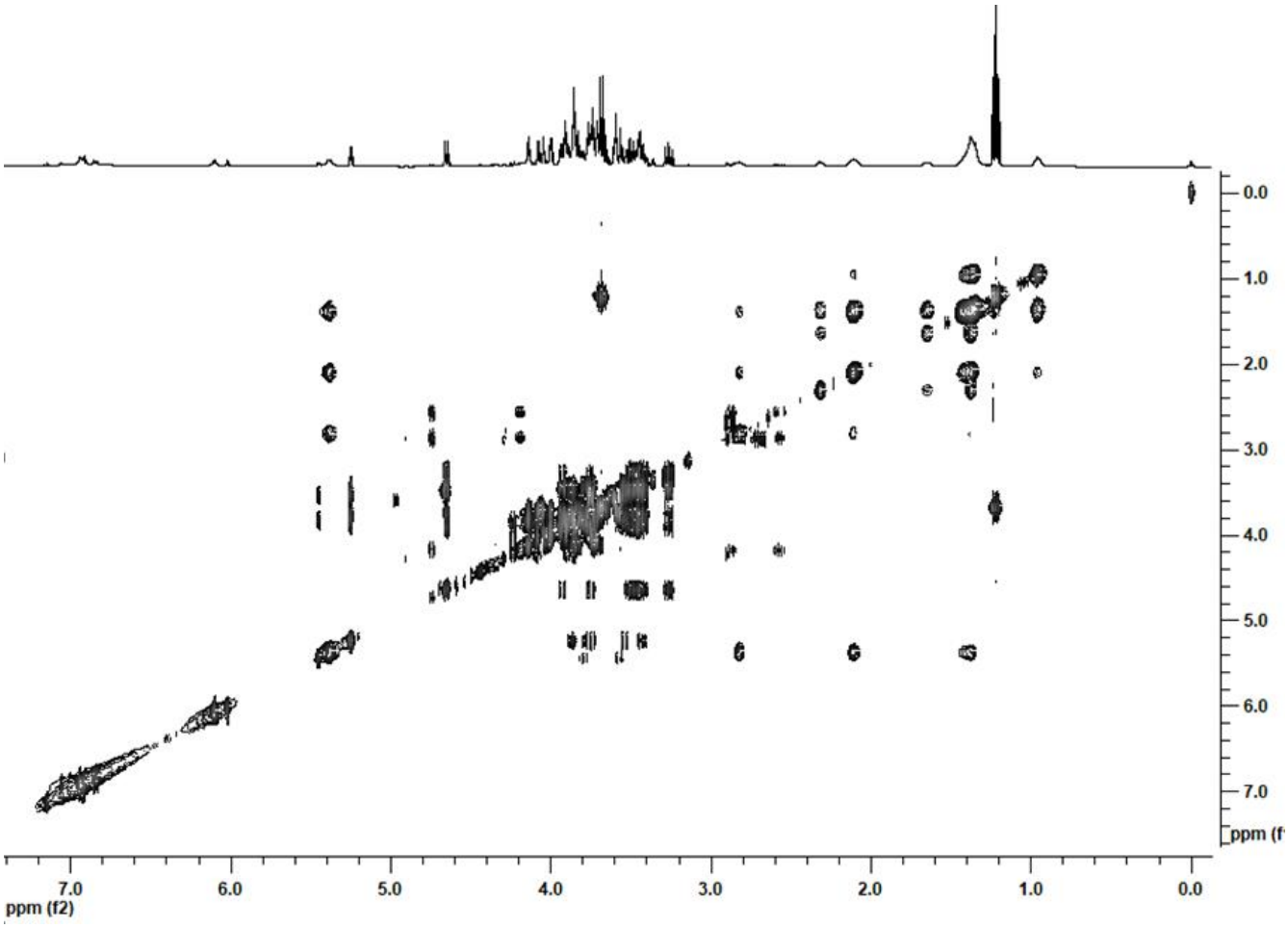

Figure S8: ^{1}H-^{1}H TOCSY NMR spectrum of **LDC5**

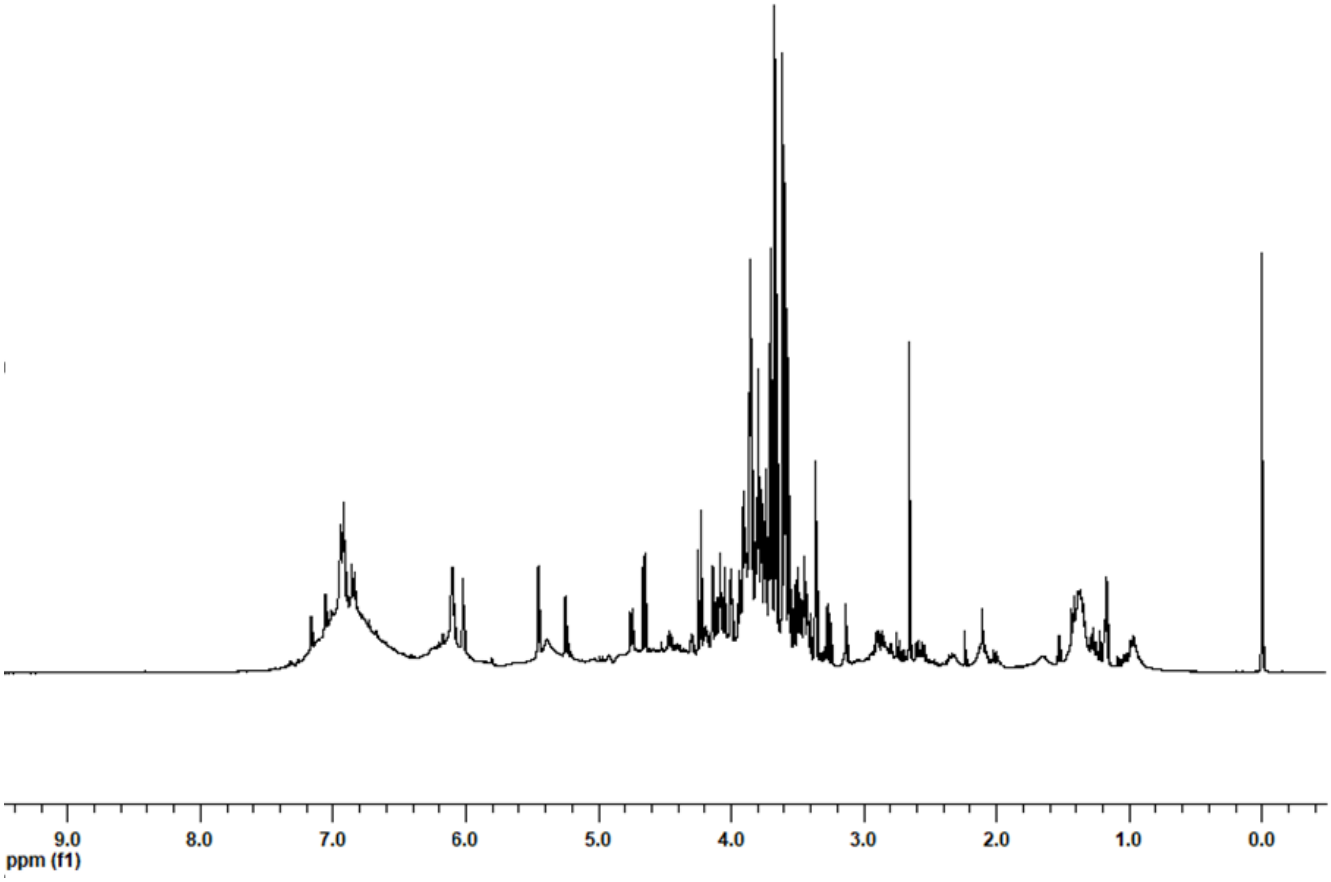

Figure S9: 1D ^{1}H NMR spectrum of **LDC6**